공학박사 학위논문

Relocation of clustered seismic events on the Korean Peninsular using double-difference technique and cross-correlation

이중차기법과 상호상관을 이용한

한반도 군집지진 발생 위치 재결정

2016년 8월

서울대학교 대학원

협동과정 계산과학전공

손 민 경

Abstract

Earthquake location is one of the starting points for earthquake research. This study relocated seismic events in and around the Korean Peninsula using the cross-correlation and the double-difference of travel time residual for surface wave. The analyzed events were from the Baekryeong Island earthquake sequence, the Boryeong offshore earthquake sequence, the earthquake swarm around Gyeongju, and the seismic events in the Dogye area. During the course of the analysis based on waveform similarity, unreported events were newly detected and waveforms were classified. Epicentral area size shrank by a factor of hundreds after relocation, and the spatial distribution of relocated epicenters coincided with the locations of clusters classified according to waveform similarity. When examining each of the four regions, 24 unreported fore- and aftershocks were newly detected, and 55 relocated epicenters were in accordance with the result of waveform classification for the Baekryeong Island earthquake sequence. For the Boryeong offshore earthquake sequence, it was confirmed that 149 relocated epicenters form a clear lineament that proceeded northeast during a two- months period. The segment that could cause the largest event in the sequence was identified, and the L_g-P_g time increase with increasing epicentral distance validated the relocation result. Around the city of Gyeongju, 70 earthquakes with similar waveforms were newly detected from the continuous data recorded during a two- year period. Relocated epicenters including catalogued and detected events were concentrated east of the Yeonil Tectonic Line. The fault plane

solution derived from first motions for the largest event displayed the same trend as the tectonic line. For the seismic events in the Dogye mining area, six event groups were identified by relocation and waveform classification. Additionally, more than 44,000 events were newly detected by waveform cross-correlation from the continuous data recorded during one year, and the signals produced by mining activities were distinguished.

Keywords: earthquake relocation, double-difference, Boryeong Offshore, Baekryeong Island, Gyeongju, Dogye mine

Student Number: 2011-30135

Contents

List of Tables

List of Figures

1. Introduction

Earthquake location is one of the starting points for earthquake research including earthquake physics, fault orientations and Earth's deformation. Historical seismicity of the Korean Peninsula is low to moderate (Lee and Yang, 2006), and only a few moderate-sized earthquakes have been recorded since most of the seismic stations were installed in 1990s (Kang and Shin, 2006). Interpreting earthquakes with small to medium size has difficulty because epicenters of these earthquakes are not clearly associated with major faults or boundaries of major geological units. Improving earthquake location accuracy has been an important and challenging goal in seismology for the past few decades (Jordan and Sverdrup; 1981; Lienert et al., 1986; Kennett and Engdahl, 1991; Lahr et al., 1994). In contrast to catalogues located one-at-a-time by phase picks, many studies show that the seismicity tightens around mapped faults by locating groups of events all together and use of waveform (Got, 1994; Shearer, 1997; Rubin et al., 1998; Waldhasuer and Ellsworth, 2000; Hauksson and Shearer, 2005; Richards et al., 2006). Double-difference algorithm (Waldhauser and Ellsworth, 2000) is widely used in relocation of seismic events (Miller et al., 2004; Segall et al., 2006; Julian et al., 2010; Keranen et al., 2014). When with an event cluster having similar waveforms, the double-difference technique is effectively utilized because using travel-time differences of neighboring events observed at common stations (Richards et al., 2006).

This study analyzed seismic events clustering in offshore and inland of South Korea as follows: the Baekryeong Island earthquake sequence, the Boryeong Offshore earthquake sequence, the earthquake swarm around the city of Gyounju, and seismic events in the Dogye mining area. The seismic events were detected and classified according to waveform similarity and their epicenters are relocated by the double-difference technique, expecting that newly identified features increase our understating of seismogenic structures in the studied regions.

1.1. Seismic events in and around the Korean Peninsula

Seismic events in and around South Korea were examined in their locations to identify clusters. The number of events over M_L 2.0 that have occurred in and around South Korea (34 ~ 38 °N, 124 ~ 130 °E) is 1024 according to the event catalogue of Korea Institute of Geoscience and Mineral Resources (KIGAM) from January 2009 to March 2016. Epicenters of the 1024 events are shown in Figure 1.1: a circle is the epicenter position of the event catalogue, and a radius of circle is proportional to the value of the local magnitude. Some clusters of events are visible with naked eyes in Figure 1.1. The bivariate Gaussian kernel density estimation was carried out for epicenters expressed in longitude and latitude to quantitatively confirm spatial clusters about the 1024 events. The kernel density map was computed with bandwidth of 0.1° in both latitude and longitude. The result in Figure 1.2 shows some clusters where earthquakes crowded. This study takes four event clusters marked by the capital letters A, B, C and D in Figure 1.2: A for the Baekryeong Island earthquake sequence, B for the Boryoeng offshore earthquake sequence, C for the earthquake swarm around the city of Gyeongju, and D for seismic events in the Dogye mining area.

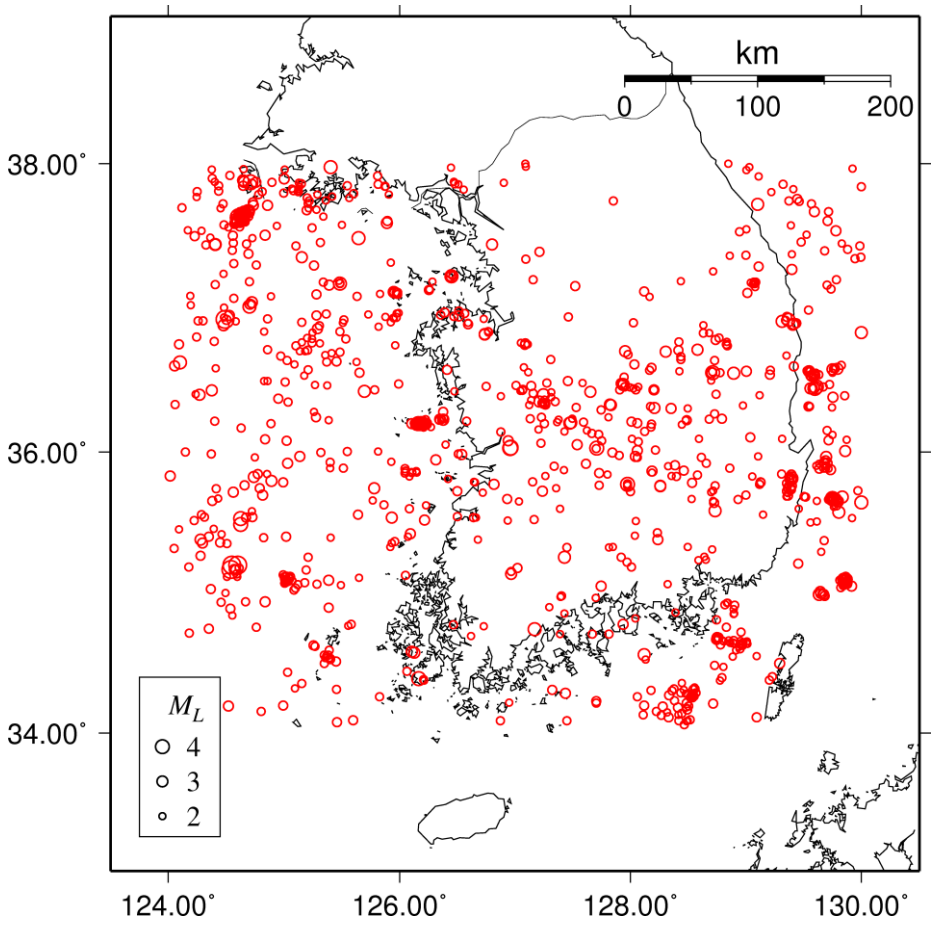

Figure 1.1. Epicenters of 1024 events (M_L>2) that occurred in and around South Korea (34 ~ 38°N 124 ~ 130°E) from January 2009 to March 2016: a circle is the epicenter position of the event catalogue, and a radius of circle is proportional to the value of the local magnitude.

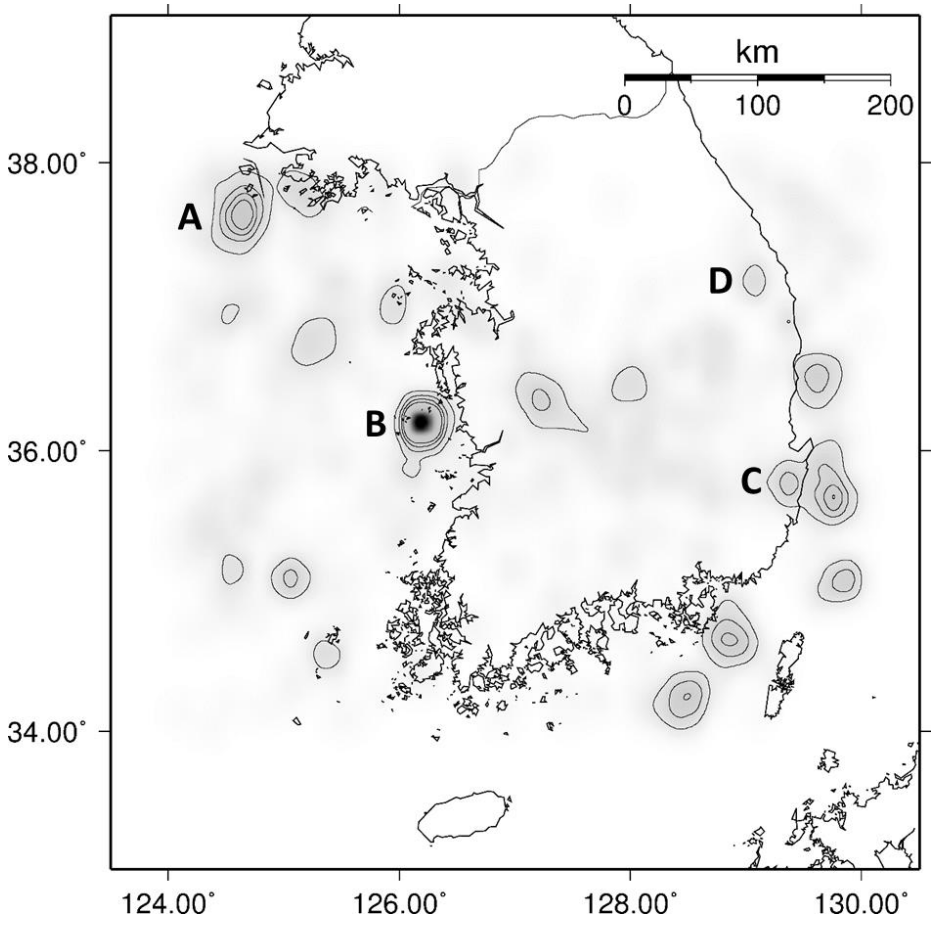

Figure 1.2. Epicenter clusters defined by the kernel density estimation with bandwidths of 0.1° in both latitude and longitude: the capital letters A, B, C, and D represent the Bakeryoeng Island earthquake sequence, the Boryeong offshore earthquake sequence, the earthquake swarm around the city of Gyeongju, and seismic events in the Dogye mining area, respectively.

1.2. Earthquake relocation using double-difference technique

Earthquake location considering travel-time differences has been studied over the past few decades (Jordan and Sverdrup, 1981; Got et al., 1994; Shearer, 1998). Waldhauser and Ellsworth (2000) also used travel-time differences, proposing the double-difference of residual between observed and modeled travel-times among neighboring events observed at a common station. The followings shows derivations of the double difference technique for hypocenter relocation as stated in Waldhauser and Ellsworth (2000). Geiger (1910) linearized the nonlinear relationship between travel-time and event location using Taylor series expansion. Thus the travel-time residual, r, for an event i becomes linearly related to perturbations, $\Delta\mathbf{p}$, to parameters describing hypocenters for each station k:

$$\frac{\partial t_k^i}{\partial \mathbf{p}} \Delta \mathbf{p}^i = r_k^i, \tag{1}$$

where $\Delta\mathbf{p}^i = \left(\Delta x^i, \Delta y^i, \Delta z^i, \Delta \tau^i\right)$ with the origin time τ of event i, and the residual, $r_k^i = \left(t^{obs} - t^{cal}\right)_k^i$ with the observed travel-time t^{obs} and calculated travel-time t^{cal}. To combine Eq. (1) and the travel-time difference between events i and j observed at station k expressed as $t_k^{i,obs} - t_k^{j,obs}$, $t_k^{j,obs}$ is subtracted from each side of the residual. Then, $t_k^{j,cal}$ is added to each side of the residual to utilize $r_k^j = t_k^{j,obs} - t_k^{j,cal}$ as

bellows:

$$
\begin{aligned}
r_k^i - t_k^{j,obs} &= \left(t^{obs} - t^{cal}\right)_k^i - t_k^{j,obs} \\
r_k^i - t_k^{j,obs} + t_k^{j,cal} &= \left(t^{obs} - t^{cal}\right)_k^i - t_k^{j,obs} + t_k^{j,cal} \\
r_k^i - r_k^j &= \left(t^{obs} - t^{cal}\right)_k^i - \left(t^{obs} - t^{cal}\right)_k^j,
\end{aligned}
\tag{2}
$$

and then, the double-difference $r_k^i - r_k^j$ can be expressed directly with the travel-time difference $t_k^{i,obs} - t_k^{j,obs}$ as bellows:

$$
\begin{aligned}
dr_k^{i,j} &= r_k^i - r_k^j \\
&= \left(t^{obs} - t^{cal}\right)_k^i - \left(t^{obs} - t^{cal}\right)_k^j \\
&= \left(t_k^i - t_k^j\right)^{obs} - \left(t_k^i - t_k^j\right)^{cal},
\end{aligned}
\tag{3}
$$

or be written out using Eq. (1) as following:

$$
\frac{\partial t_k^i}{\partial \mathbf{p}} \Delta \mathbf{p}^i - \frac{\partial t_k^j}{\partial \mathbf{p}} \Delta \mathbf{p}^j = dr_k^{i,j}. \tag{4}
$$

The partial derivatives in the left side of Eq. (4) can be calculated from travel-time equation, and the double-difference in the right side of Eq. (4) are the subtraction between the observed travel-time difference $\left(t_k^i - t_k^j\right)^{obs}$ and modeled travel-time difference $\left(t_k^i - t_k^j\right)^{cal}$. Finally, Eq. (4) with all event pairs for every station can form a system of linear equations.

Waldhauser (2001) distributed HypoDD a program package for hypocenter relocation using the double-difference technique described above, and HypoDD have become one of the most widely used method as follows. Miller et al. (2004) found correlation between a high-pressure source and aftershocks using precise hypocenter locations. Segall et al. (2006) located earthquakes and revealed swarms of earthquakes triggered by silent slips on Kilauea volcano, Hawaii. Julian et al. (2010) imaged hydraulic fractures at the Coso geothermal field in eastern California, by obtaining relative hypocenter locations. Keranen et al. (2014) verified that earthquake swarms in Oklahoma occurred within disposal formations of gas production, and suggested that disposal wells be responsible. About earthquakes of South Korea, Kang and Shin (2006b) located hypocenters of an earthquake swarm at offshore of Uljin, East Sea. They used time differences computed from manual picking, instead of cross-correlation, because of poor waveform similarity between events. Kim et al. (2010) successfully relocated the Odaesan earthquake sequence with HypoDD. For the focal depth, however, they accepted only a relative depth of the relocated hypocenters, because HypoDD does not guarantee precise results for non-well-linked events. For the one sequence displaying high waveform similarity and relatively good azimuthal coverage, they could observe relocation results forming a linear pattern and spatio-temporal migration of events.

The double-difference technique is appropriate for densely distributed events only a few km apart when local stations separated from the epicenters by several tens of kilometers are used (Richards et

al., 2006). The seismic stations in and around the Korean peninsula, however, are sparsely distributed compared to what Richards et al. (2006) mentioned. In addition, the Korean peninsula has low to moderate earthquakes so body wave used for hypocenter relocation often remain with unclear phase. To overcome these constraints, this study employed travel-time difference of surface wave instead of body wave. Schaff and Richards (2004a) mentioned three advantages of surface wave in location: (1) surface wave is commonly the largest-amplitude regional wave, which may give high signal-to-noise ratio; (2) surface wave propagates more slowly than does body-wave, which results in smaller uncertainty in distance; and (3) surface wave travels horizontally in the crust, which reduce the number of unknown parameters especially regarding depth. This study adapted the double difference technique of Schaff and Richards (2004a) and relocated only epicenters precisely.

2. Theory and Methods

Earthquakes that are close together spatially and have similar rupture mechanisms produce similar waveforms at common stations (Poupinet et al., 1984). Waveform similarity is quantifiable with waveform cross-correlation. This study employed cross-correlation for a time window including surface wave to perform three tasks: (1) arrival-time differences for neighboring earthquakes observed at common stations were measured by cross-correlation, and were employed as inputs for the double-difference technique after Waldhauser and Ellsworth (2000), Schaff and Richards, (2004a, b), Hauksson and Shearer, (2005), and Shelly et al., (2006); (2) new events corresponding to a template event were detected by cross-correlation from continuous seismic records based on the method of Schaff and Richards (2004a), Gibbons and Ringdal, (2006, 2007), Kim (2013). This detection technique was applied to search fore and aftershocks of the Baekryeong Island earthquake, events with similar waveforms on the Yeonil tectonic line, and seismic events in the Dogye mining area; (3) seismic events was grouped by dendrogram (hierarchical cluster tree) derived from correlation coefficients among event pairs as stated by Rowe et al. (2002), Wolfe et al. (2004), Lin et al. (2007), Buurman and West, (2010), and West, (2013). For every case in this study, clusters classified according to waveform similarity corresponded well to distribution of relocated epicenters.

2.1. Epicenter relocation using double-difference technique with cross-correlation for surface wave

The double-difference equation for hypocenters proposed by Waldhauser and Ellsworth (2000) can be expressed in Cartesian coordinate space as following,

$$\begin{aligned}&\frac{\partial t_k^i}{\partial x}\Delta x^i + \frac{\partial t_k^i}{\partial y}\Delta y^i + \frac{\partial t_k^i}{\partial z}\Delta z^i + \Delta\tau^i \\ &-\left(\frac{\partial t_k^j}{\partial x}\Delta x^j + \frac{\partial t_k^j}{\partial y}\Delta y^j + \frac{\partial t_k^j}{\partial z}\Delta z^i + \Delta\tau^j\right) = dr_k^{ij},\end{aligned} \tag{1}$$

for travel-times t observed at station k of events i and j with respect to their locations (x, y, z) and origin times τ. Schaff and Richards (2004a) proposed the double-difference for epicenter relocation using L_g phase that this study called EpiDD. Because surface wave including L_g phase travels horizontally in the crust, solving Eq. (1) leaves the local map coordinates x and y, along with the origin time τ,

$$\frac{\partial t_k^i}{\partial x}\Delta x^i + \frac{\partial t_k^i}{\partial y}\Delta y^i + \Delta\tau^i - \left(\frac{\partial t_k^j}{\partial x}\Delta x^j + \frac{\partial t_k^j}{\partial y}\Delta y^j + \Delta\tau^j\right) = dr_k^{ij}. \tag{2}$$

The double-difference dr is defined as bellows:

$$\begin{aligned}dr_k^{ij} &= \left(t^{obs} - t^{cal}\right)_k^i - \left(t^{obs} - t^{cal}\right)_k^j \\ &= \left(t^i - t^j\right)_k^{obs} - \left(t^i - t^j\right)_k^{cal},\end{aligned} \tag{3}$$

in which the subscripts ‘ *obs* ’ and ‘ *cal* ’ mean ‘observed’ and ‘calculated,’ respectively. Waveform cross- correlation was used to measure the observed travel-time difference $\left(t^i - t^j\right)^{obs}$ between i and j events. L_g wave traveling horizontally in the crust allows us to express the partial derivatives analytically with a Cartesian coordinate system as follows:

$$
\begin{aligned}
t &= \frac{D}{V} \\
D &= \sqrt{\left(x - x_s\right)^2 + \left(y - y_s\right)^2} \\
\frac{\partial t}{\partial x} &= \frac{x - x_s}{V\sqrt{\left(x - x_s\right)^2 + \left(y - y_s\right)^2}} \\
\frac{\partial t}{\partial y} &= \frac{y - y_s}{V\sqrt{\left(x - x_s\right)^2 + \left(y - y_s\right)^2}}
\end{aligned}
\qquad (4)
$$

in which D is the epicentral distance to the station, x_s and y_s are station coordinates. Schaff and Richards (2004a) employed V as a group velocity of 3.3 km/s, and expected that using the group velocity of the major energy packet will result in reflecting an epicentral location for the centroid of moment release. We have also V = 3.5 km/s as a constant for the every partial derivatives. No significant differences could be found in the pattern formed from relative location of relocated epicenters depending on the value of V. To include surface wave, a time-window is set to have a length of an average speed 3.5 km/s for each station. Figure 2.1 explains seismic events i and j depicted by stars, and station k located at $\left(x_s, y_s\right)$. The observed

travel-time difference $\left(t^i - t^j\right)_k^{obs}$ is a time lag corresponding to the maximum correlation coefficient as shown in Figure 2.2. Eq. (2) can be combined from all epicenter pairs for a station, and for all stations to form a system of linear equations of the form as following,

$$\mathbf{Gm=d}, \tag{5}$$

where **G** is a matrix of size *M* (the number of travel-time difference observation that is equal to residual pairs)$\times 3 \times N$ (the number of events) containing the partial derivatives, **d** is the input vector composed of double-differences, **m** is a vector of length *3N*, $\left[\Delta x, \Delta y, \Delta \tau\right]^T$. Eq. (6) displays components of the matrix in Eq. (5). Capital alphabets are used for stations in Eq. (6) instead of integers for easy recognition.

$$
\begin{bmatrix}
\frac{\partial t_A^1}{\partial x_A^1} & & & & \\
\frac{\partial t_A^1}{\partial y_A^1} & \cdots & & & \\
\frac{\partial t_A^1}{\partial \tau_A^1} & & & & \\
-\frac{\partial t_A^2}{\partial x_A^1} & & & & \\
-\frac{\partial t_A^2}{\partial y_A^1} & \cdots & & & \\
-\frac{\partial t_A^2}{\partial \tau_A^1} & & & & \\
 & \ddots & & & \\
 & & \frac{\partial t_{N-1}^{n-1}}{\partial x_{N-1}^{n-1}} & & \\
 & \cdots & \frac{\partial t_{N-1}^{n-1}}{\partial y_{N-1}^{n-1}} & & \\
 & & \frac{\partial t_{N-1}^{n-1}}{\partial \tau_{N-1}^{n-1}} & & \\
 & & -\frac{\partial t_N^n}{\partial x_N^n} & & \\
 & \cdots & -\frac{\partial t_N^n}{\partial y_N^n} & & \\
 & & -\frac{\partial t_N^n}{\partial_N^n} & &
\end{bmatrix}^T
\begin{bmatrix}
\Delta x^1 \\ \Delta y^1 \\ \Delta \tau^1 \\ \Delta x^2 \\ \Delta y^2 \\ \Delta \tau^2 \\ \vdots \\ \Delta x^{n-1} \\ \Delta y^{n-1} \\ \Delta \tau^{n-1} \\ \Delta x^n \\ \Delta y^n \\ \Delta \tau^n
\end{bmatrix}
=
\begin{bmatrix}
dr_A^1 - dr_A^2 \\ \vdots \\ dr_N^1 - dr_N^2 \\ dr_A^1 - dr_A^3 \\ \vdots \\ dr_k^{i,j} \\ \vdots \\ dr_N^{n-2} - dr_N^n \\ dr_A^{n-1} - dr_A^n \\ \vdots \\ dr_N^{n-1} - dr_N^n
\end{bmatrix}
\tag{6}
$$

The matrix **G** is highly sparse as each equation links together only two events, i.e., of the $3N$ columns in each of the M rows of **G**, only six have nonzero elements. One of the best ways to regularize ill-conditioned systems is pre-filtering the data by only including events that are well linked to other events. This study programmed EpiDD by modifying HypoDD (Waldhauser, 2001), a program package for hypocenter relocation using double-difference technique. EpiDD applied a constraint for a solution constructed by conjugate gradients and used damping factor to regularize of ill-conditioned system as Waldhauser and Ellsworth (2000) did. Finally, the conjugate gradient algorithm LSQR of Paige and Saunders (1982) also employed by HypoDD solves the solution of EpiDD.

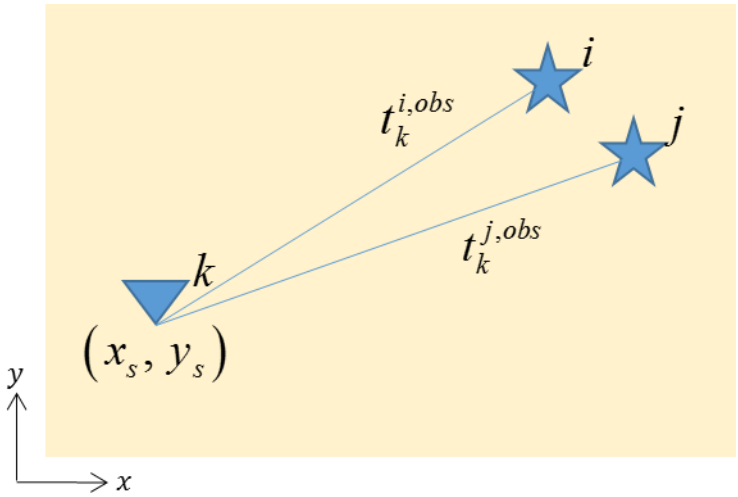

Figure 2.1. Illustration of symbols and indices in the double-difference technique of epicenter relocation: $t_k^{i,obs}$ and $t_k^{j,obs}$ observed at the common station k located at (x_s, y_s) depicted by an inverted triangle are travel times starting from epicenters i and j depicted by solid stars, respectively.

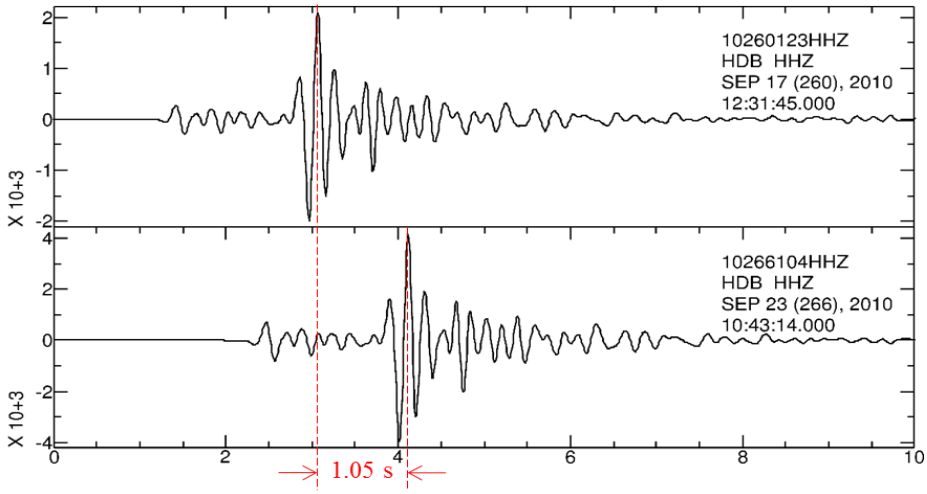

(a)

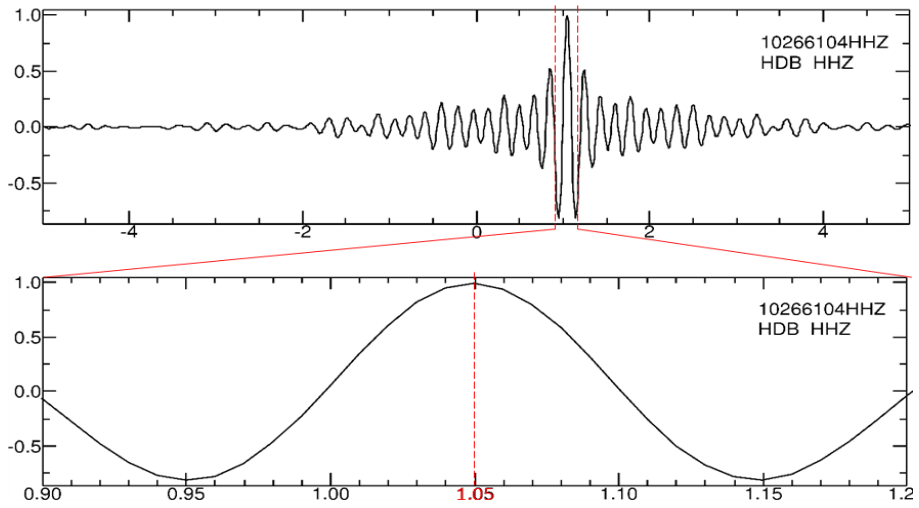

(b)

Figure 2.2. Measurement of travel-time difference by cross-correlation: (a) two similar traces of which time-difference is 1.05 s, (b) cross-correlation results showing the maximum coefficient (dashed line) corresponding the time difference 1.05 s

2.2. Hierarchical clustering with dendrogram derived from cross-correlation coefficients of waveforms

Hierarchical clustering with cross-correlation can identify sets of similar earthquakes without prior knowledge of event location or developing a master event. Many studies have used cross-correlation to group waveforms of seismic events: Harris (1991) compared waveforms of un-located explosions in a quarry; Riviere-Barbier and Grant (1993) identified and located closely spaced mining events. The hierarchical clustering have been applied to seismic events in and around volcanoes (Rowe et al., 2002; Wolfe et al., 2004; Deshon et al., 2007; Buurman and West, 2010; West, 2013; Kasatkina et al., 2014).

A common methodology for hierarchical clustering assigns events into clusters based on their average cross-correlation coefficient with all other events in the cluster. In Figures 2.3, an example is shown for hierarchical clustering using 27 waveforms parts of seismic events described in Chapter 7. The 27 traces were band-pass filtered between 1.2 and 5 Hz. Each trace was cross-correlated against each other trace, storing the maximum normalized cross-correlation coefficient and its associated lag time. In the course of selection for event pairs with high cross-correlation coefficients, similar waveforms will be placed closer together and dissimilar waveforms will be placed farther apart. This process creates a dendrogram (hierarchical cluster tree). The dendrogram shown in Figure 2.3a describes how waveforms are linked together and combined into larger clusters. There are four clusters with the branch cut of 0.8 in Figure 2.3a. Waveform similarity in each

cluster can be found in traces shown in Figure 2.3b. The choice of 0.8 as the clustering threshold is arbitrary. A higher threshold result in more clusters composed of traces that are more similar. In this case, the number of traces for each cluster becomes smaller. A lower threshold is more inclusive of events that differ slightly. As shown in Figure 2.3b, the 27 waveforms sorted into four clusters with distinct waveform similarity. Figure 2.4 displays two matrix for cross-correlation coefficients that is the basis for hierarchical clustering. Event numbers of Figure 2.4a were aligned with origin times from the catalogue, and Event number of Figure 2.4b were aligned with hierarchical clustering results. Four clusters are clearly observed in Figure 2.4b.

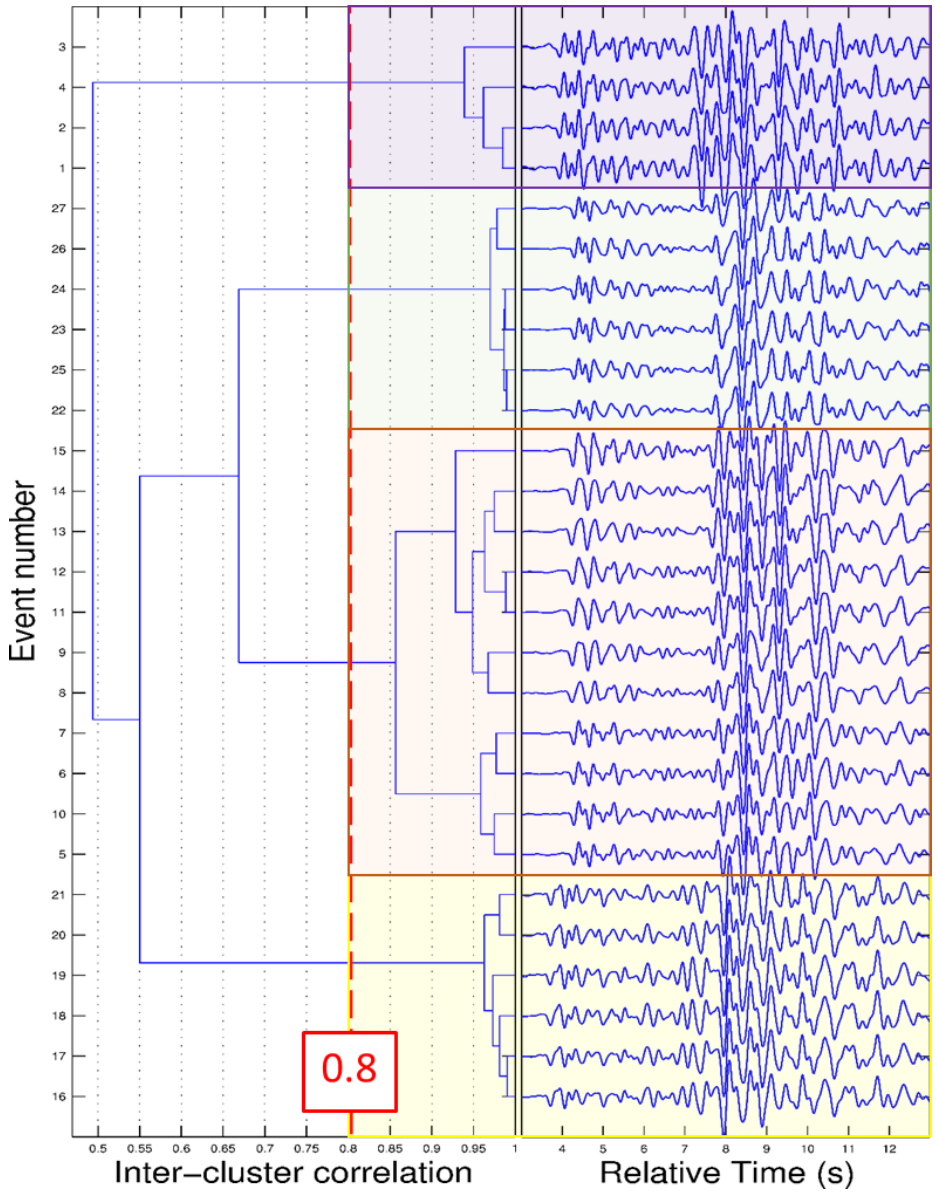

(a) (b)

Figure 2.3. An example for hierarchical clustering for 27 waveforms: (a) dendrogram (hierarchical cluster tree) showing four clusters with the branch cut of 0.8; (b) waveforms aligned after the clustering

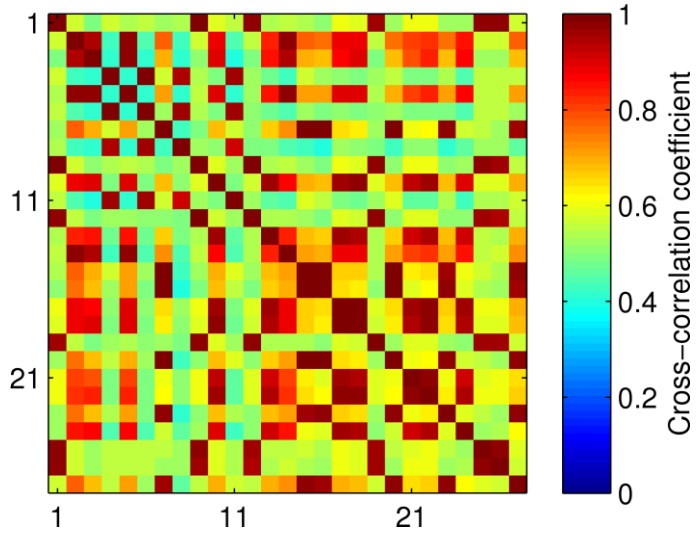

(a)

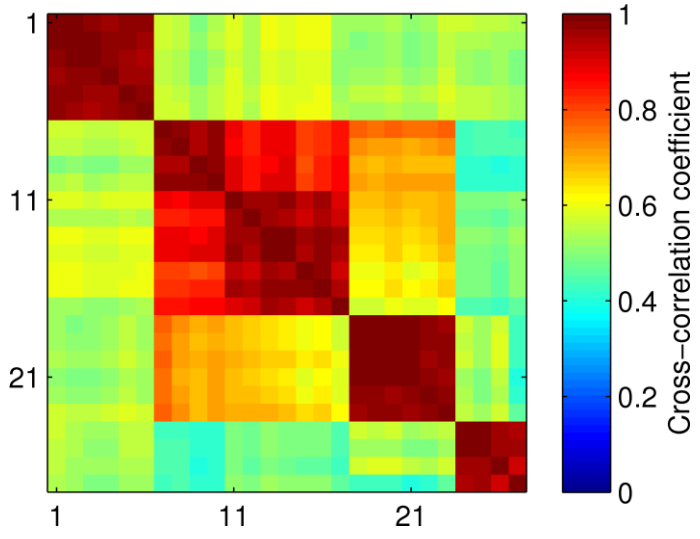

(b)

Figure 2.4. Matrix for the maximum cross-correlation coefficients among 27 waveforms: (a) event numbers were ordered in origin times from catalogue, (b) event numbers were ordered in waveform similarity defined by hierarchical clustering.

2.3. Event detection through waveform cross-correlation between catalogued events and continuous record

New events corresponding to a waveform template can be detected from continuous seismic records by cross-correlation. Detection using cross-correlation also known as matched filter has been used for both man-made and natural seismicity: Gibbons and Ringdal (2006, 2007) succeeded to detect low magnitude earthquakes at regional distances; Obara (2002) and Shelly et al. (2007) recognized non-volcanic tremor and low-frequency earthquakes in subduction zone of southwest Japan; Schaff and Waldhauser (2010) studied performance of a correlation detector; Shelly et al. (2013) researched a fluid-driven earthquakes swarm detected by cross-correlation. Seismic event detection using cross-correlation was illustrated in Figure 2.5. A seismic waveform as a template slides along incoming waveform as shown in Figure 2.5a. Cross-correlation trace in Figure 2.5b measures the waveform similarity between the template and incoming data from the same station. Three peaks in Figure 2.6b indicate the time when the events detected as a similar event with the template recorded. The three detected events are founded from continuous data as shown in Figure 2.5c.

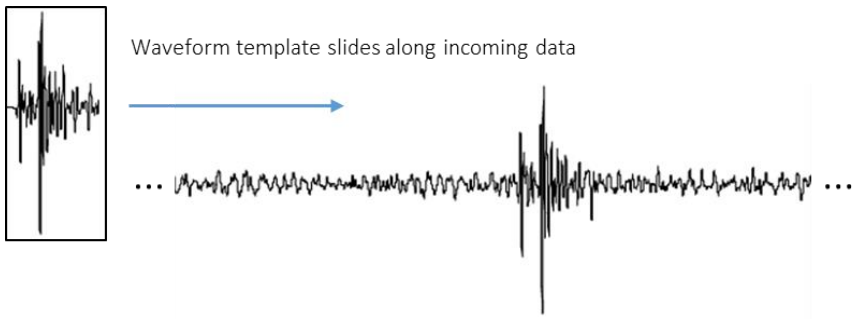

(a)

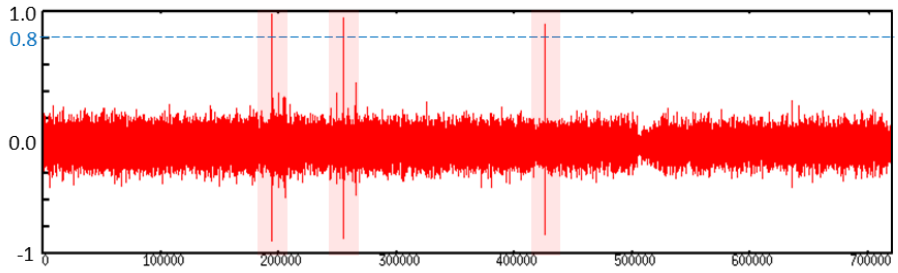

(b)

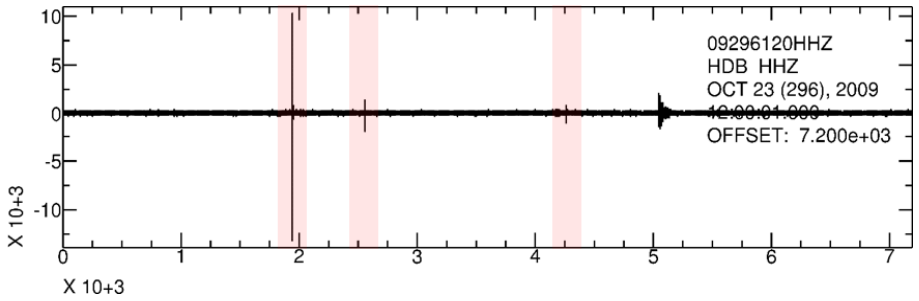

(c)

Figure 2.5. Detection of seismic events using waveform cross-correlation: (a) cross-correlation between a template and continuous data, (b) cross-correlation result showing three peaks, (c) three detected events in continuous data.

3. Application

Seismic events in clusters at the four regions marked by capital letters A, B, C and D in Figure 1.2 were analyzed: A for the Baekryeong Island earthquake sequence, B for the Boryoeng offshore earthquake sequence, the earthquake swarm around the city of Gyeongju, and D for the seismic events in the Dogye mining area. The Baekryeong Island earthquake sequence and the Boryeong Offshore earthquake sequence occurred at the Yellow sea west of the Korean Peninsula in 2013. The Baekryeong sequence showed the typical foreshock-mainshock-aftershock sequence during two weeks. The Boryeong sequence, in comparison, showed the consecutive occurrence of more than a hundred earthquakes over two months without an obvious mainshock. The city of Gyeongju, on the other hand, is located in the inland part of southeast Korea where the Quaternary faults are extensively observed. The catalogue has reported intermittent occurrences of earthquakes around the Gyeongju over the past few years. Lastly, seismic events in the Dogye a major coal mining area of the country were analyzed. The Dogye mining area is where some ground subsidence were reported (Ko et al., 2000). The catalogue listed seismic events of which source are not specified.

3.1. Baekryeong Island earthquake sequence

The M_w 4.9 earthquake occurred 37 km south of Baekryoeng Island in the Yellow Sea on May 17, 2013. The Korea Institute of Geoscience and Mineral Resources (KIGAM) and the U.S. Geological Survey (USGS) reported the epicenter at 37.6283°N, 124.6148°E and 37.633°N, 124.580°E, respectively. A dozen small foreshocks preceded the earthquake. More events occurred over a 2-week period after the mainshock. These events showing the typical foreshock-mainshock-aftershock sequence was named as the Baekryoeng Island earthquake sequence. The sequence includes 39 fore- and aftershocks (M_L 1.5 ~ 4.0) that occurred near Baekryeong Island (37.5-37.8°N, 124.5-124.8°E) on May 14 to 26. The KIGAM catalogue reported these 40 events. Figure 3.1 shows epicenters of the 40 events form the catalogue and six seismic stations used in relocation (DACB, BRD, YPD, DEI, GBI, and RCN). Stations are located east of the epicenters, except station RCN. To increase an azimuthal coverage data from station RCN was employed though station RCN is located ~210 km west. Figure 3.2a presents the occurrence history of the 40 catalogued events with their local magnitudes. Figure 3.2b is the histogram for the depth reported by the catalogue. For 13 events, the catalogue failed to determine depths as shown by dark grey in Figure 3.2b.

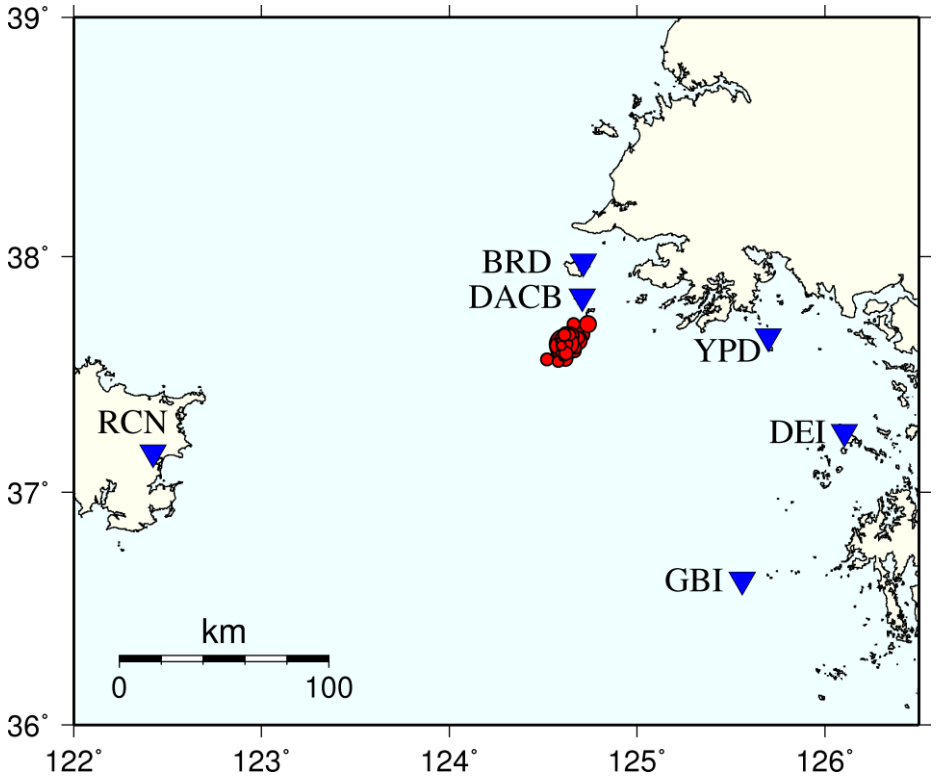

Figure 3.1. Map for the 40 catalogued events of the Baekryeong Island earthquake sequence. Circles represent the location of 40 epicenters from catalogue. Inverted triangles are seismic stations used in epicenter relocation.

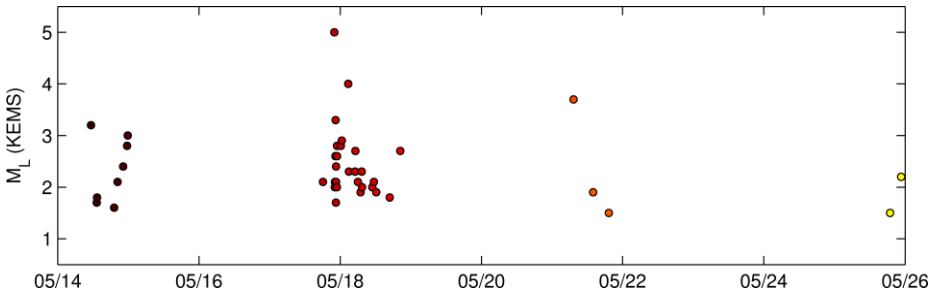

(a)

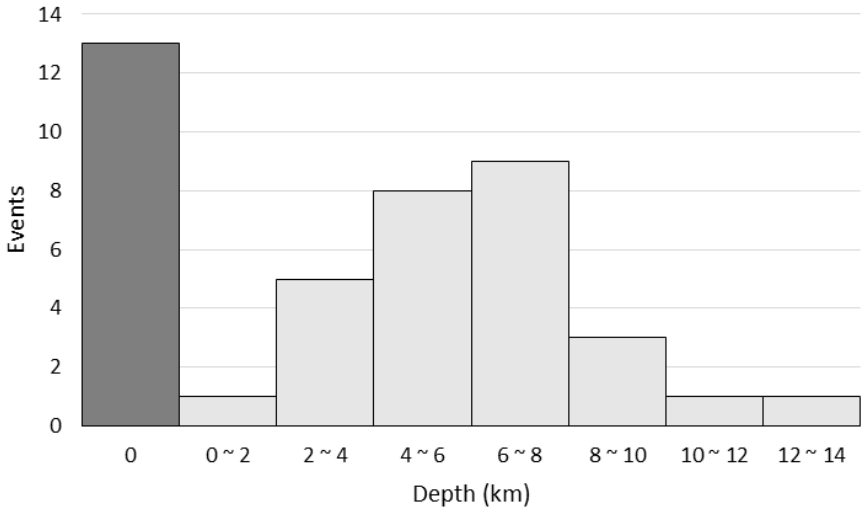

(b)

Figure 3.2. Statistics for the 40 catalogued events of the Baekryeong Island earthquake sequence: (a) occurrence history with their local magnitudes, (b) histogram for their depths from the catalogue. The catalogue reported that most earthquakes occurred at 18 May in 2013, and failed to define depths of 13 events depicted by a dark grey bar representing a depth of 0 km.

3.1.1. Detection of fore and aftershocks

During the same period, 31 events were newly detected by waveform cross-correlation of continuous data from station BRD. Events reported on the KIGAM catalogue was employed as a template with a window length of 10 s after the first P arrival. Seismogram of station BRD about 37 km away were used after filtered from 1 to 3 Hz, and the detection criteria was CC (correlation coefficient) $\geq$ 0.7. Figure 3.3 shows the waveforms of 69 events recorded at station DACB, the closest to the general epicenter. The waveforms are for a vertical velocity component with a sampling rate of 100 Hz, and are band-pass filtered between 1 and 4 Hz. Waveforms in Figure 3.3a are aligned by catalogue origin time, except the waveforms of 29 events newly detected by cross-correlation. Waveforms in Figure 3.3b were aligned using cross-correlation for a time window including surface wave. The waveforms were shifted by up to 2.47 s from the catalogue origin time. Because the waveforms of the 69 events were similar as shown in Figure 3.3b, we infer that the events must have occurred near one another sharing a similar focal mechanism. Figure 3.4 is the occurrence histogram for catalogued and newly detected events. As shown in Figure 3.4, the detection succeeded to detect foreshocks and aftershocks that occurred at May 18 when most catalogued events including the mainshock recorded.

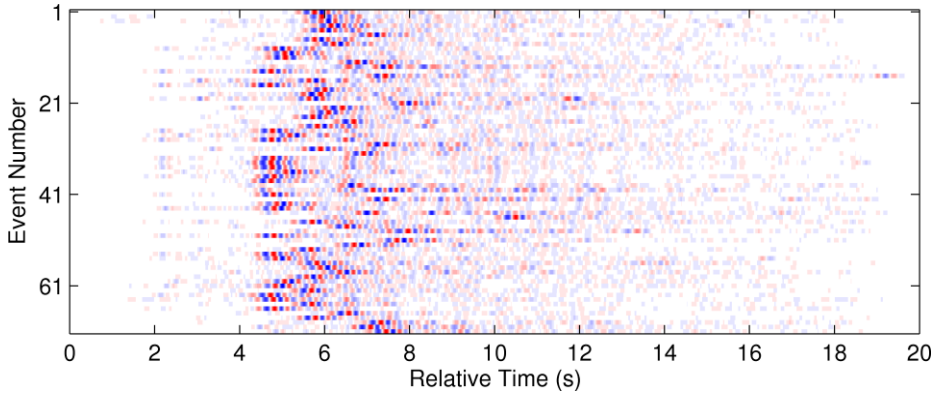

(a)

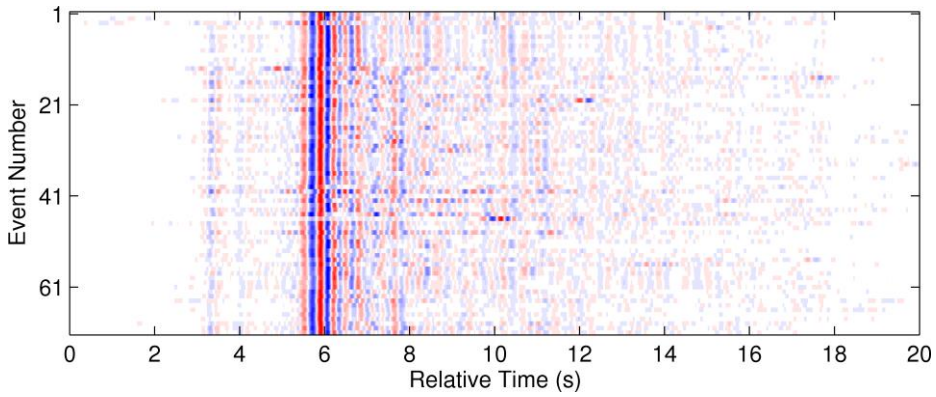

(b)

Figure 3.3. Waveforms of the Baekryeong Island earthquake sequence recorded at station DACB: (a) aligned by the catalogue origin time of 40 events (or waveform cross-correlation for 29 newly detected events), and (b) alignment using waveform cross-correlation for a time window including surface wave. Each trace was shaded with blue = -1 and red = +1 amplitude. Events are ordered from earliest to latest, and the event number increases with the origin time.

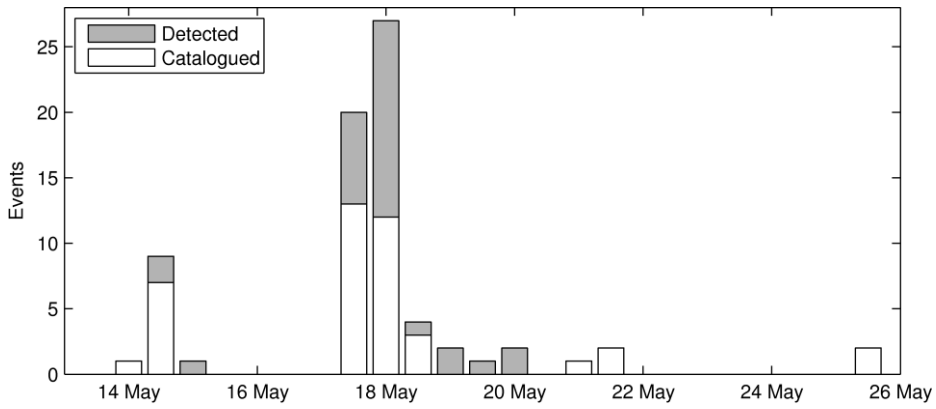

Figure 3.4. Occurrence histogram for 31 newly detected events represented (grey bar) and 40 catalogued events (white bar). The bin width is 12-hour, and the mainshock occurred on 17 May. The detection succeeded to find 4 foreshocks and 25 aftershocks that were not reported on the catalogue.

3.1.2. Epicenter relocation

Of the Baekryeong Island earthquake sequence, we relocated 55 events that occurred after May 17 because we could not acquire the data from station RCN before May 17. Figures 3.5a and b show epicenters of the Baekryeong sequence from the KIGAM catalogue and relocation results of EpiDD, respectively. To the newly detected events, we assigned randomly perturbed initial location within a 5 km radius from the general epicenter for the 31 events reported on the catalogue. Epicenters relocated by EpiDD exhibited tighter spatial clustering of seismicity than did the KIGAM catalogue as shown in Figures 3.5a and b. Figure 3.5c shows relocation results on an enlarged map and the fault-plane solution of the mainshock (M_w 4.9) quoted from Son et al. (2015a). In Figure 3.5c, the east-west strike of the fault plane solution for the mainshock seems relevant to relocated epicenters. The location mainshock, however, is about 1 km away from a possible rupture plane. It is inferred that the mainshock may have a greater depth than other events. The rupture plane dipping southward may be one answer, although the fault plane with the east-west strike in Figure 3.5c dips in opposite directions. In Figure 3.5c, circle color indicates time evolution after the first event of the sequence, and the gradation of black in the background presents the density of earthquakes. All of the events occurred late is located in the northwestern section of the rupture region as shown in Figure 3.5c. Thus, it can be inferred that the Baekryeong sequence progressed toward west.

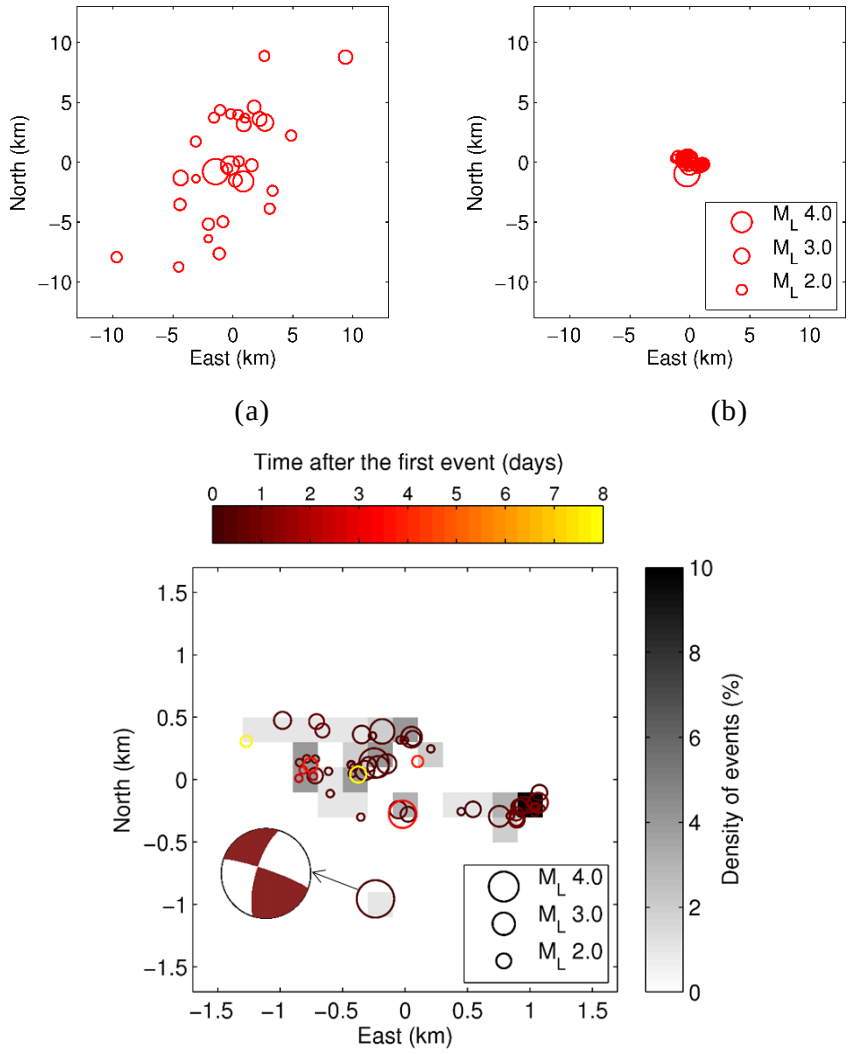

Figure 3.5. Epicenters of the Baekryeong Island earthquake sequence: (a) the catalogue (31 events), (b) EpiDD (including 24 newly detected events), and (c) the result from EpiDD on an enlarged map and the fault-plane solution of the mainshock (M_w 4.9)

3.1.3. Hierarchical clustering of waveforms

The Baekryeong Island earthquake sequence was classified into two clusters: Cluster A with 21 events and Cluster B with 17 events. The clustering analysis was performed with dendrogram derived from the maximum correlation coefficients representing the similarity of 55 events among coda of surface wave recorded at station DACB. Figure 3.6a shows distinct differences in waveforms between two clusters for coda of surface wave (5 ~ 10 s) recorded at station DACB, and Figure 3.6b is the correlation matrix of the two clusters. Figure 3.6c shows the two clusters separated in map view: most events of Cluster A (blue circles) were west of the mainshock, and all 17 events of Cluster B (pink circles) were located east of the mainshock. The spatial distribution of relocated epicenters reflected the location of the two clusters classified according to waveform similarity, whereas the temporal order of occurrence seemed irrelevant to the two clusters. The east-west strike of the fault-plane solution for the mainshock (M_w 4.9) in Figure 3.6c may be associated with the relocated epicenters for Clusters A and B distributed horizontally.

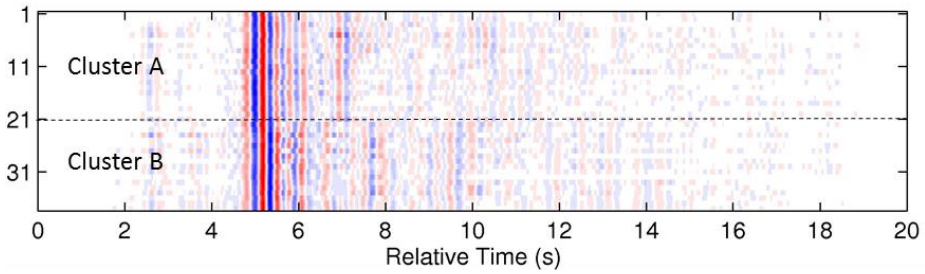

(a)

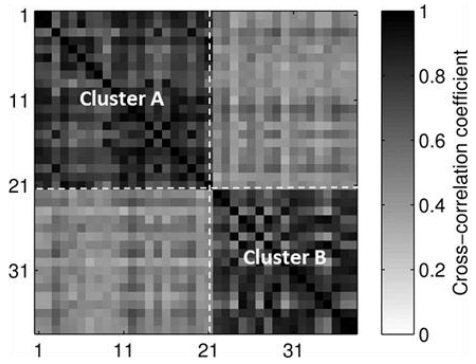

(b)

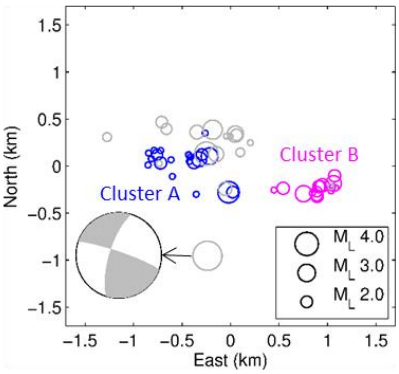

(c)

Figure 3.6. Clusters of the Baekryeong Island earthquake sequence: (a) waveforms of Clusters A and B, (b) correlation matrix for surface wave form data of station DACB , and (c) fault-plane solution for the mainshock (M_w 4.9) and location of epicenters for cluster A (blue), Cluster B (pink) and the others (grey)

3.2. Boryeong offshore earthquake sequence

From June 3 to August 4 in 2013, 160 earthquakes that occurred at the Boryeong offshore (36.0–36.4º N, 126.0–126.4º E) of the Yellow Sea were reported in the KIGAM catalogue. No obvious mainshock was recorded in the Boryeong offshore earthquake sequence of which the largest magnitude was 3.8 in local magnitude. The consecutive occurrence of more than 100 earthquakes over a period of months is abnormal seismicity for Korea. Of the 160 events, we analyzed 149 recorded by station PORA, the closest station to the epicenter cluster 38 km away. Local magnitudes for the analyzed events range from 1.3 to 3.8.

The epicenters of 149 events and the locations of the 11 seismic stations used (PORA, ANM, HSB, BUY, SES2, GUS, NPR, PUA, SMKB, WID, and GBI) are shown in Figure 3.7. Stations are located in the interior of the Korean Peninsula, except for station GBI. The azimuthal gap of stations exceeded 130°. Figure 3.8a shows the occurrence history of the Boryeong offshore earthquake sequence with local magnitudes ranging from 1.3 to 3.8. Figure 3.8b is the histogram for the depth reported by the catalogue. For 64 events, the catalogue failed to determine depths as shown by dark grey in Figure 3.8b. Figure 3.9 shows the waveforms of 149 events recorded at station PORA. Each trace was shaded with blue = -1 and red = +1 amplitude. Events are ordered from earliest to latest, and the event number increases with the origin time. Waveforms in Figure 3.9a are aligned by catalogued origin times. Waveforms of Figure 3.9b are aligned using cross-correlation for

a time window including surface wave. The waveforms were shifted up to 2.91 s from the catalogue origin time. It is confirmed that waveforms of 149 events are highly similar, as shown in Figure 3.9b, and inferred that to display such waveform similarity, the events must have occurred in close proximity and have the same mechanism. The uneven alignment shown in Figure 3.9a suggests uncertainty in the catalogue location.

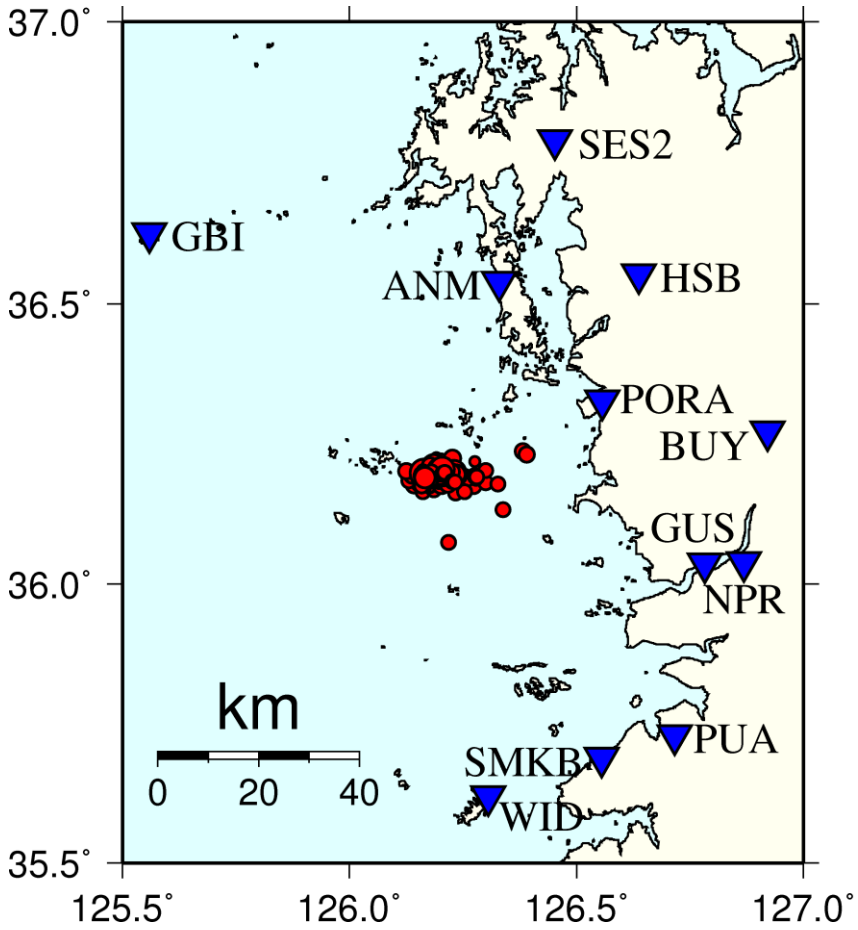

Figure 3.7. Map for the Boryeong offshore earthquake sequence: Circles represent the location of 160 epicenters from catalogue. Inverted triangles are seismic stations used in epicenter relocation.

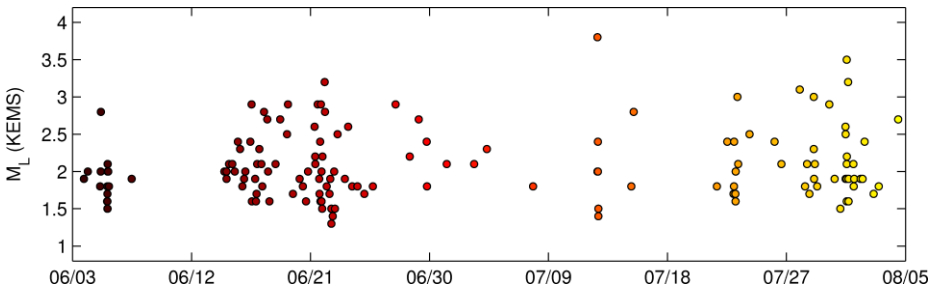

(a)

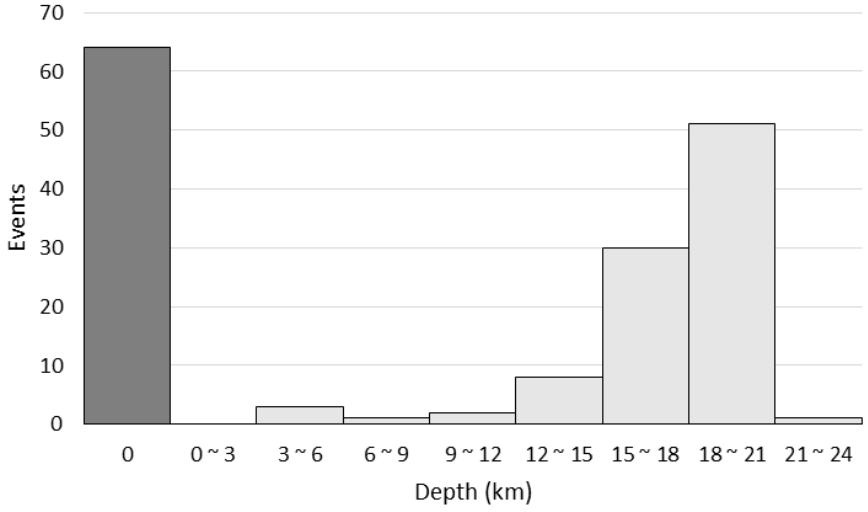

(b)

Figure 3.8. Statistics for the Boryeong offshore earthquake sequence: (a) occurrence history with their local magnitudes, (b) histogram for their depths from catalogue. The catalogue failed to define depths of 64 events depicted by a dark grey bar for a depth of 0 km.

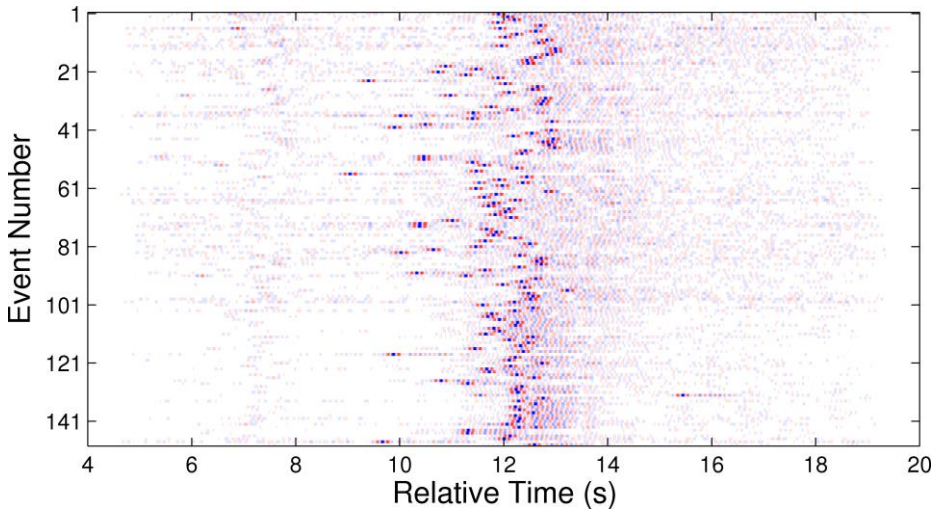

(a)

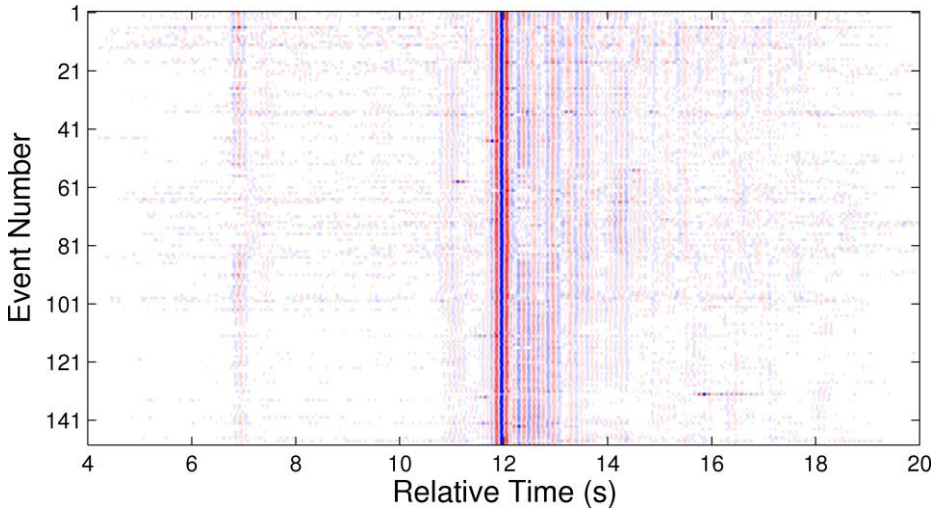

(b)

Figure 3.9. Waveforms for 149 events of the Boryeong offshore earthquake sequence recorded at station PORA: (a) aligned by catalogue origin time, and (b) aligned by waveform cross-correlation for surface wave. . Each trace was shaded with blue = -1 and red = +1 amplitude.

3.2.1. Epicenter relocation

Figures 3.10a and b display 149 epicenters of the Boryeong offshore earthquake sequence form the KIGAM catalogue and relocation results, respectively. As shown in Figures 3.10a and b, epicenters relocated by EpiDD exhibit much tighter spatial clustering of seismicity than do those from the routinely generated catalogue. Figure 3.10c shows relocation results on an enlarged map and the fault-plane solution of the largest event (M_L 3.8) quoted from Son et al. (2015a). The relocated epicenters form a significantly linear pattern with a length of 700 m in map view that strikes northeast-southwest. The fault-plane solution in Figure 3.10c corresponds well to the strike of the linear pattern consisting of relocated epicenters. Compared with the epicenters of the sequence on the catalogue in Figure 3.10a, the relocated epicenters reflect a seismogenic zone and are suggestive of a fault. In Figure 3.10c, circle color indicates the time evolution for 63 days after the first event of the sequence, and the gradation of black in the background indicates the density of earthquakes. As shown in Figure 3.10c, the sequence started with an event of M_L 1.9 at the southwestern part of the map. An intermediate period of the sequence (events colored in red) was concentrated in northeast from the early part of the sequence. After the middle of the sequence ended, the largest event took place where most events occurred. The sequence continued to progress toward the northeast, and then diffused in seismicity, as shown by the yellow circles, form the end of July.

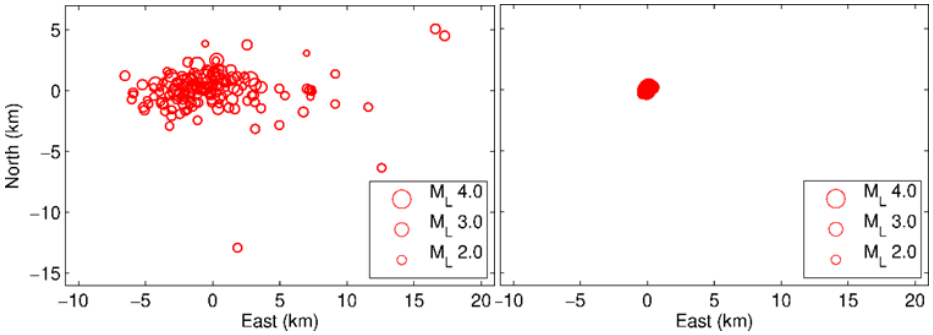

(a) (b)

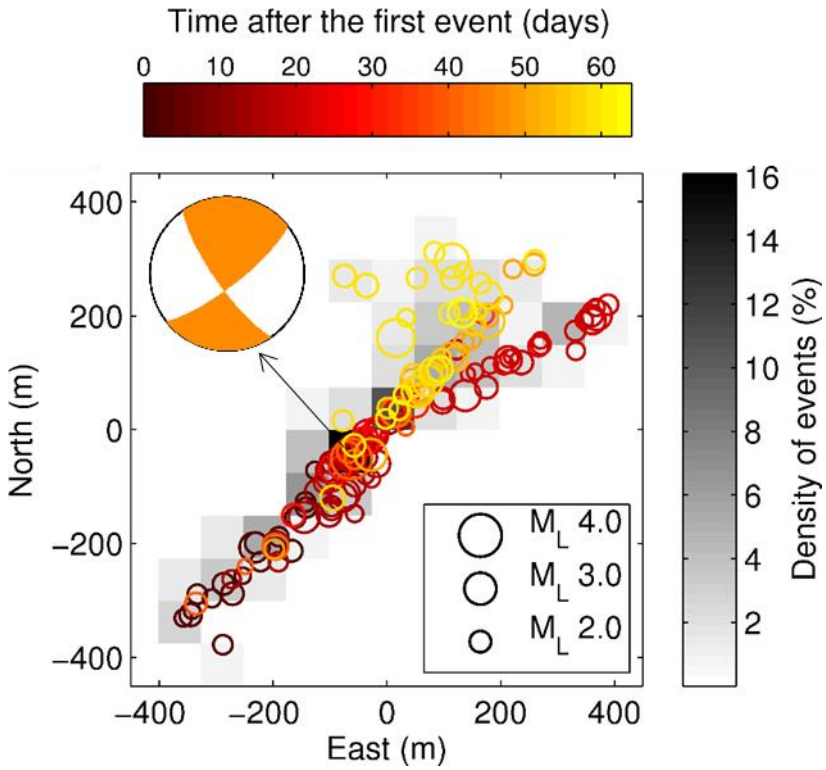

(c)

Figure 3.10. Epicenters of the Boryeong offshore earthquake sequence: (a) the catalogue, (b) relocation results, and (c) results on an enlarged map and the fault-plane solution for the largest of the sequence (M_L 3.8)

Figure 3.11 confirms the successful performance of the relocation results. In Figure 3.11, seismograms of 77 events with local magnitudes greater than 2.0 are aligned in order of epicentral distance from station PORA based on relocated epicenters. The waveforms band-pass filtered between 1 and 6 Hz and amplitude normalized are for vertical velocity component with a sampling rate of 100 Hz. The difference between L_g-phase and *P*-phase arrival time increases as epicentral distance increase. The move-out of P-phase represented by the red dashed line is clearly visible.

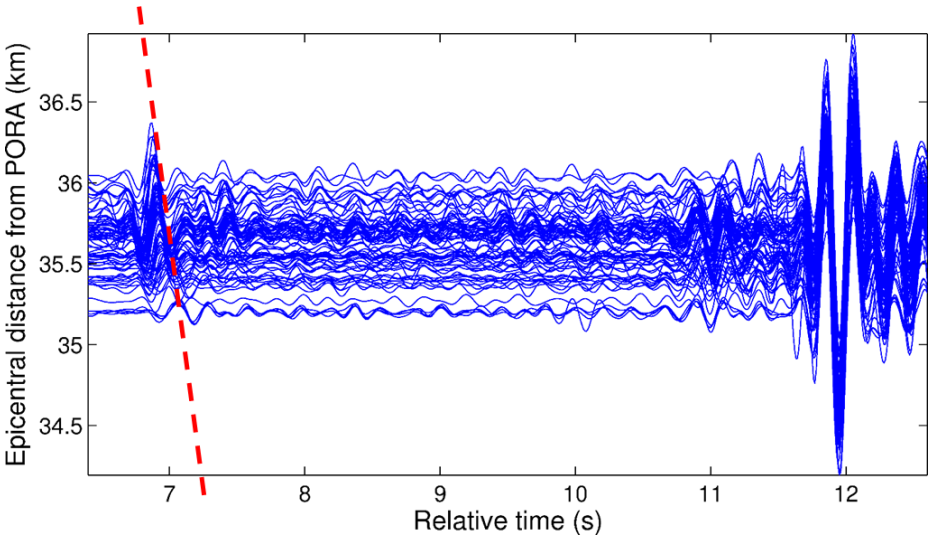

Figure 3.11. Seismograms of events with local magnitudes larger than 2.0 arranged in order of epicentral distances from station PORA (the closest station): Seismograms align on their surface wave. The move-out of P_g arrivals for events is clearly visible. The L_g-P_g time for each trace increases with increasing epicentral distance.

3.2.2. Hierarchical clustering of waveforms

In Figures 3.9b, it can be observed that the amplitudes of events in an intermediate period of the sequence (with event numbers from 60 to 80 in Figure 3.9b) differ from the amplitudes of other events, especially for the coda of surface wave after 12 s. Events of the Boryeong offshore earthquake sequence were sorted into four clusters: Cluster A with 53 events, Cluster B with 41 events, Cluster C with 18 events, and Cluster D with 9 events. The clustering analysis employed the dendrogram derived from the maximum correlation coefficients representing the similarity of 149 events among period from body-phase to coda of surface wave recorded at station PORA. The four clusters can be observed in Figure 3.12 with the branch cut of 0.875. Figure 3.12 shows the occurrence histogram for the four clusters over a 63-day period and traces of the four clusters. Events of Cluster A are concentrated in the early part, bur occurred during the entire sequence including the largest event (M_L 3.8) of the sequence. The occurrence of Cluster B is mainly in the end part of the sequence. Events of Cluster C occurred only from 21 to 25 June, and the eight events of Cluster D are in the starting part of the sequence. Figure 3.13 shows the four clusters distinctly separated in the map view: relocated epicenters in Clusters A, B, and C formed a line striking northeast-southwest. Excluded events are depicted as gray circles. The four clusters classified according to waveform similarity corresponded well to the spatial distribution of relocated epicenters.

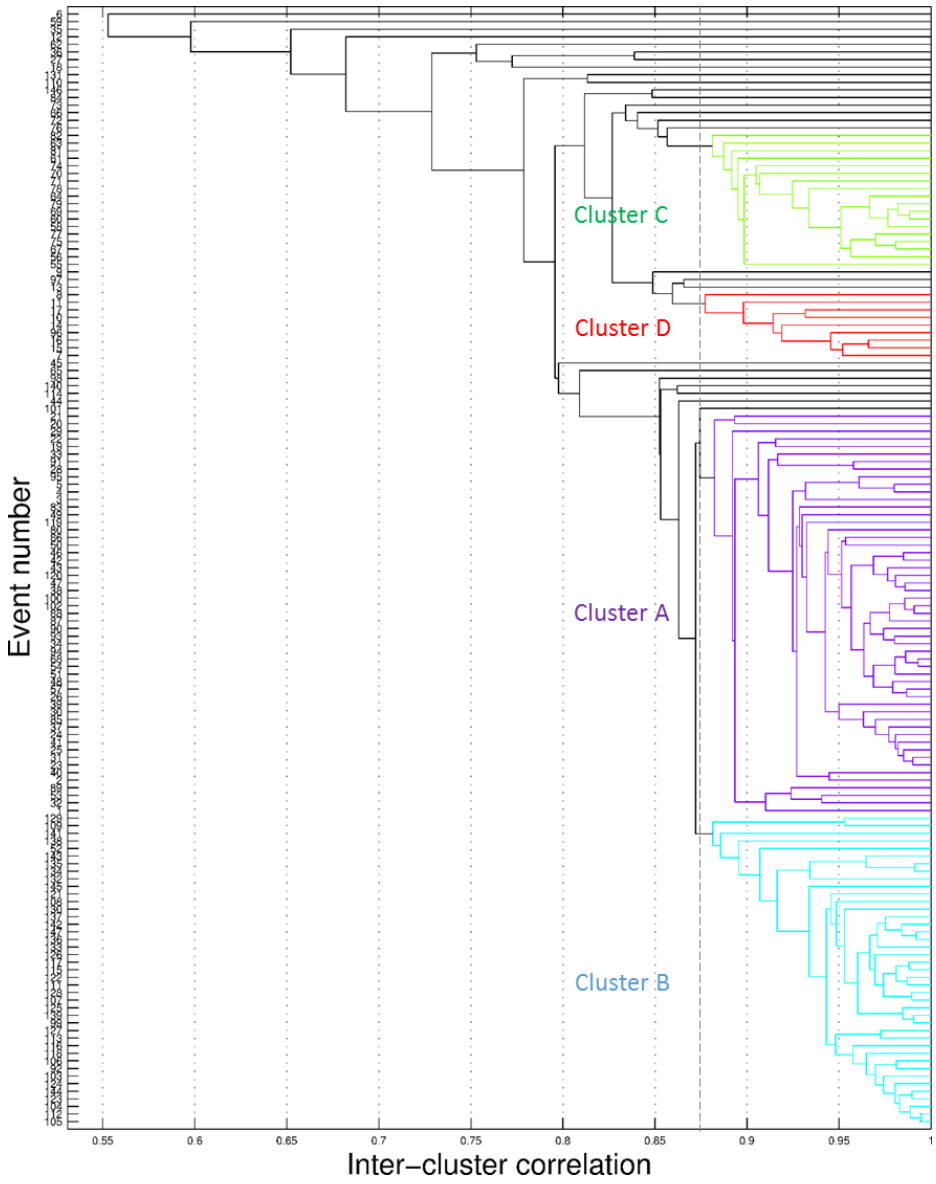

Figure 3.12. Hierarchical clustering result for the Boryeong Offshore earthquake sequence: The dendrogram (hierarchical cluster tree) with branch cut of 0.875 shows four clusters: Cluster A with 53 events, Cluster B with 41 events, Cluster C with 18 events, and Cluster D with nine events

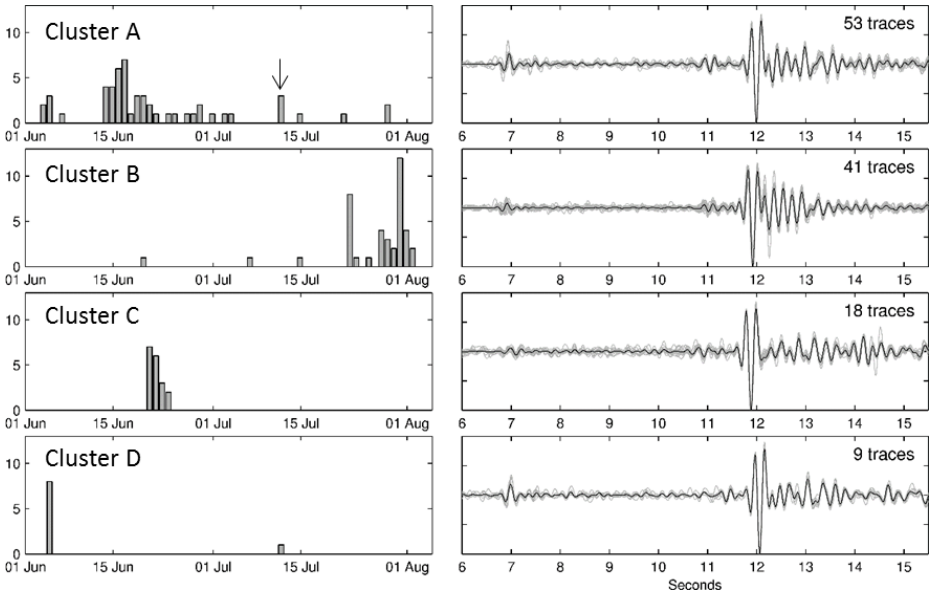

Figure 3.13. Occurrence histograms and traces of event clusters in the Boryeong Offshore earthquake sequence: Events of Cluster A occurred during the entire sequence, and were concentrated in the early to middle part. The arrow in Cluster A indicates the largest event (M_L 3.8) of the sequence. The occurrence of Cluster B was mainly in the end part of the sequence. Events of Cluster C occurred only from 21 to 25 June, and the eight events of Cluster D are in the starting part of the sequence.

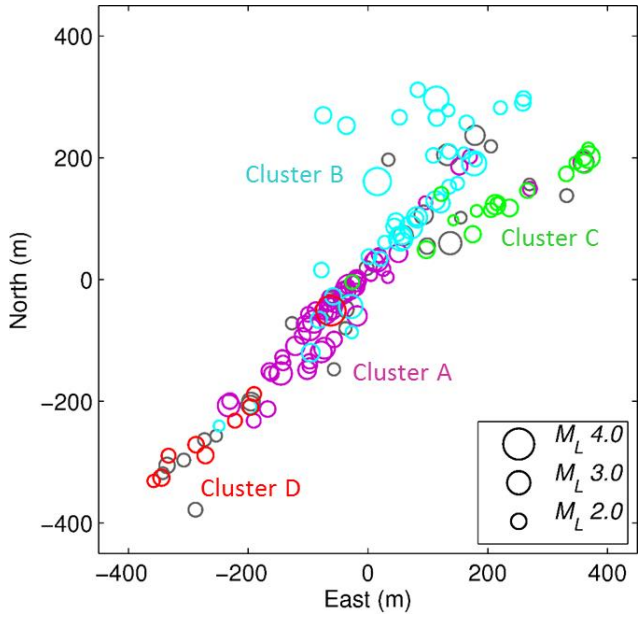

Figure 3.14. Epicenters of four clusters in the Boryeong Offshore earthquake sequence: Cluster A (magenta), Cluster B (cyan), Cluster C (light green), and Cluter D (red) are distinctly separated in map view, which means that the four clusters classified according to waveform similarity corresponds well to the spatial distribution of relocation result.

3.2.3. Spatiotemporal evolution of epicenters

To examine spatiotemporal progression in detail, the coordinates of relocated epicenters were transformed to coordinate system for the slope direction (the strike direction) and its orthogonal direction. The slope direction was estimated by linear regression for the coordinate of epicenters in latitude and longitude. Figure 3.11a and b display values for the strike direction and for the direction orthogonal to the strike direction with time after the first event, respectively. Circles are epicenters of the Boryeong sequence, and their radiuses are proportional to magnitudes. The four clusters also are represented by colors: Cluster A (magenta), Cluster B (cyan), Cluster C (light green), and Cluter D (red). As shown in Figure 3.11a, the early part of the sequence (Cluster D) that occurred within five days after the first event moved on southwest 300 m making the first segment: The sequence held off until ten days after the first event, and then developed intensively the second segment in northeast area during eight days. Jumping to northeast 17 days after the first event Cluster B occurred. The Boryeong sequence, then, became relatively silent for a month from 20 days to 50 days after the first event. At this lull, the largest event of the sequence occurred just before 40th day as indicated by an arrow in Figure 3.11. Earthquakes then proceeded northeast again at around 50^{th} day, and finally diffused when 58 days after the first event. The final diffusion of epicenters can be observed in Figure 3.11(b).

Waldhauser et al. (1999) stated sources for linear alignment of epicenters. The possibilities are stress concentrations on the fault such

as at the edge of a rising screw dislocation, fluid pressure models (Hickman et al., 1995), the intersection of different rock strata, a wear process in which the host rock in contact with the fault zone core (Chester et al., 1993).

The largest event (M_w 3.3) in the Boryeong offshore earthquake sequence could be produced by a rupture of 250 m. This rupture length based on the study of Leonard (2010) is not much different from a length of the second segment estimated as shown by dashed lines in Figure 3.11a. The second segment is where the largest event occurred, and is where the concentrated events occurred before 30 days when the largest event occurred. The concentrated events of the second segment and the largest event are included in Cluster A based on high similarity (CC > 0.875) between their waveforms. The second segment would be a key for understanding the largest event of the Boryeong Offshore earthquake sequence.

Branches such as the segment formed by events of Cluster C, and the sub-segment of the second segment formed by events of Cluster A are visible in Figure 3.14 and 3.15b. The branches of the Boryeong sequence can be interpreted as a typical pattern observed spatially in growth strike-slip faults mentioned by Narteau (2007). Further studies are need for spatial patterns of the Boryeong sequence, and the waveform detection for unreported events has to be also applied for analysis of the temporal seismic patterns of the sequence.

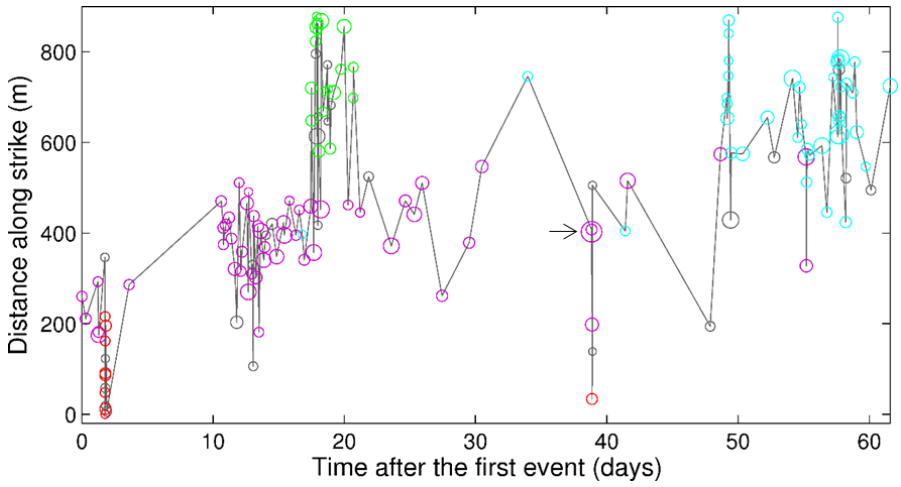

(a)

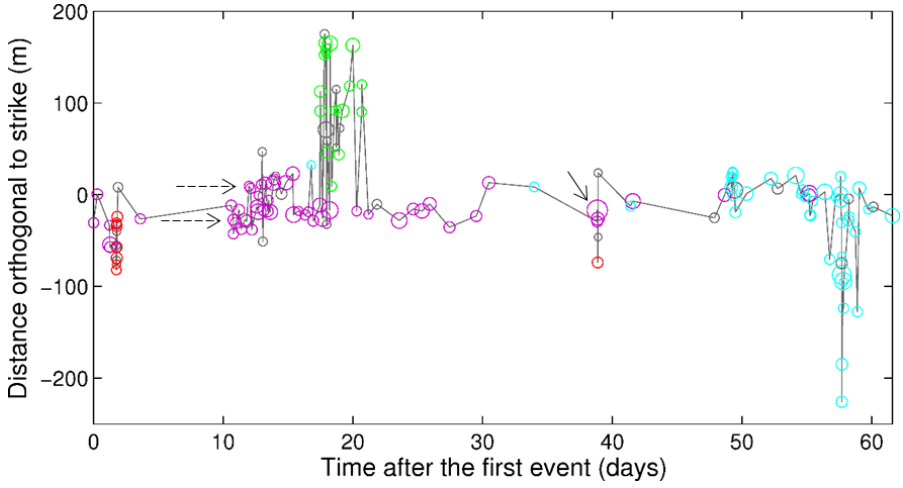

(b)

Figure 3.15. Spatiotemporal evolution for relocated epicenters of the Boryeong offshore earthquake sequence in the direction of (a) strike and (b) orthogonal to the strike with the four clusters shown in magenta for Cluster A, in cyan for Cluster B, in light green for Cluster C, and in red for Cluster D. The second segment (200 ~ 500 m) is where the largest event (arrows) occurred, and is where the concentrated events occurred 30 days before the largest event. The dashed arrows point sub-segments of the second segment.

3.3. Repeating earthquakes on the Yeonil tectonic line

The KIGAM catalogue reported 31 events that occurred around the city of Gyeongju (35.6 ~ 35.9°N, 129.3 ~ 129.5°E) in the south part of the Korean peninsula from January 2009 to October 2010. Figure 3.16 shows the epicenters of the 31 events and 14 seismic stations (HDB, MKL, WSN, WSB, WSC, DAG, YSB, KRA, KRB, KRN, CHS, CGD, BUS, and GKP1) used in epicenter relocation described in Chapter 5.3. All the 14 stations are located in the interior of the Korean Peninsula, and there is not any station in northeast area from the epicenters. Figure 3.17a shows the occurrence history of the 31 earthquakes with local magnitudes ranging from 0.7 to 2.2. No obvious mainshock was recorded during two years. Figure 3.17b is the histogram for depth reported by the catalogue. For 12 events, the catalogue failed to determine depth as shown by a dark grey bar in Figure 3.17b. Figure 3.18 shows normalized waveforms of the 31 events recorded at station HDB. The waveforms with sampling late of 100 Hz were band-pass filtered between 1.2 and 5 Hz. Events were ordered from earliest to latest, and the event number increases with the event origin time. Waveforms of Figure 3.18a were aligned by catalogued origin times. Waveforms of Figure 3.18b were aligned by cross-correlation for a time window including surface waves. More ten events with similar waveforms occurred at the study area as shown in Figure 3.18b.

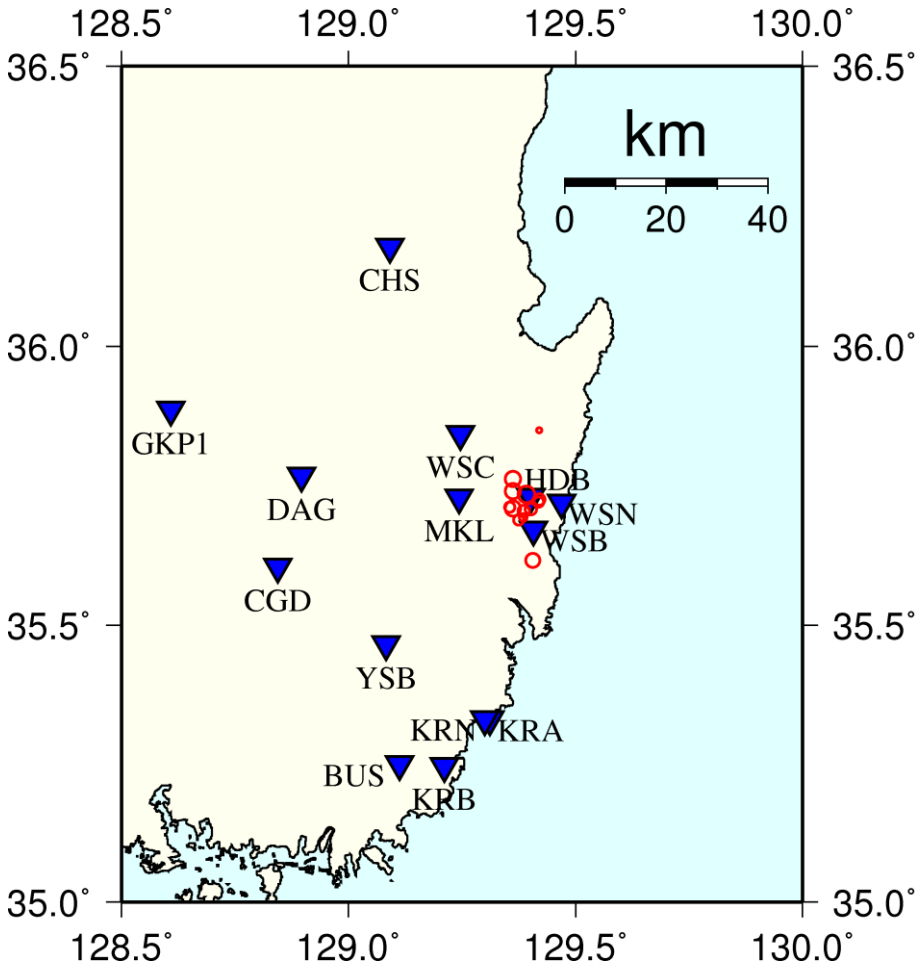

Figure 3.16. Map for 31 catalogued events that occurred around the city of Gyeongju. Circles represent the location of 31 epicenters from catalogue. Inverted triangles are seismic stations used in epicenter relocation.

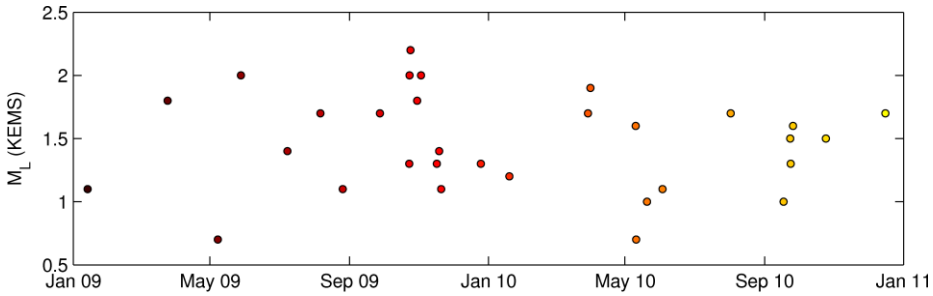

(a)

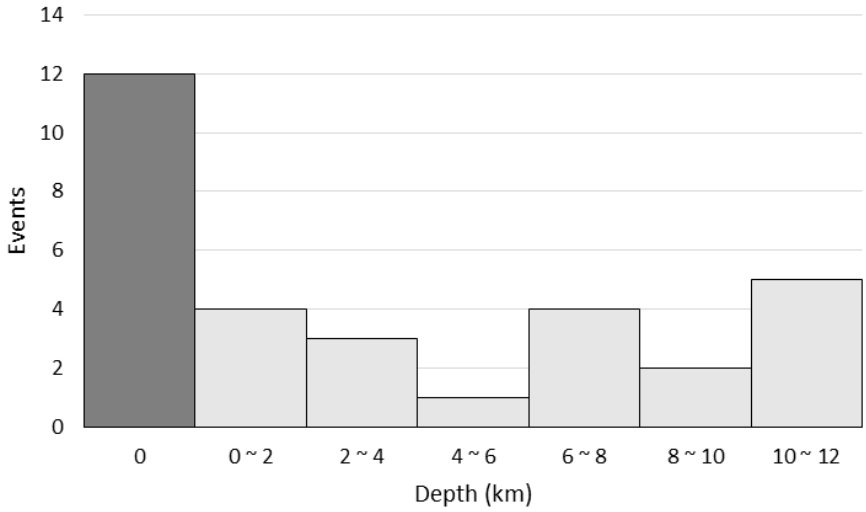

(b)

Figure 3.17. Statistics for the 31 events around Gyeongju: (a) occurrence history with their local magnitudes; (b) histogram for their depths from catalogue. Depths are distributed from 0 to 12 km, and the catalogue failed to define depths of 12 events depicted by a dark grey bar.

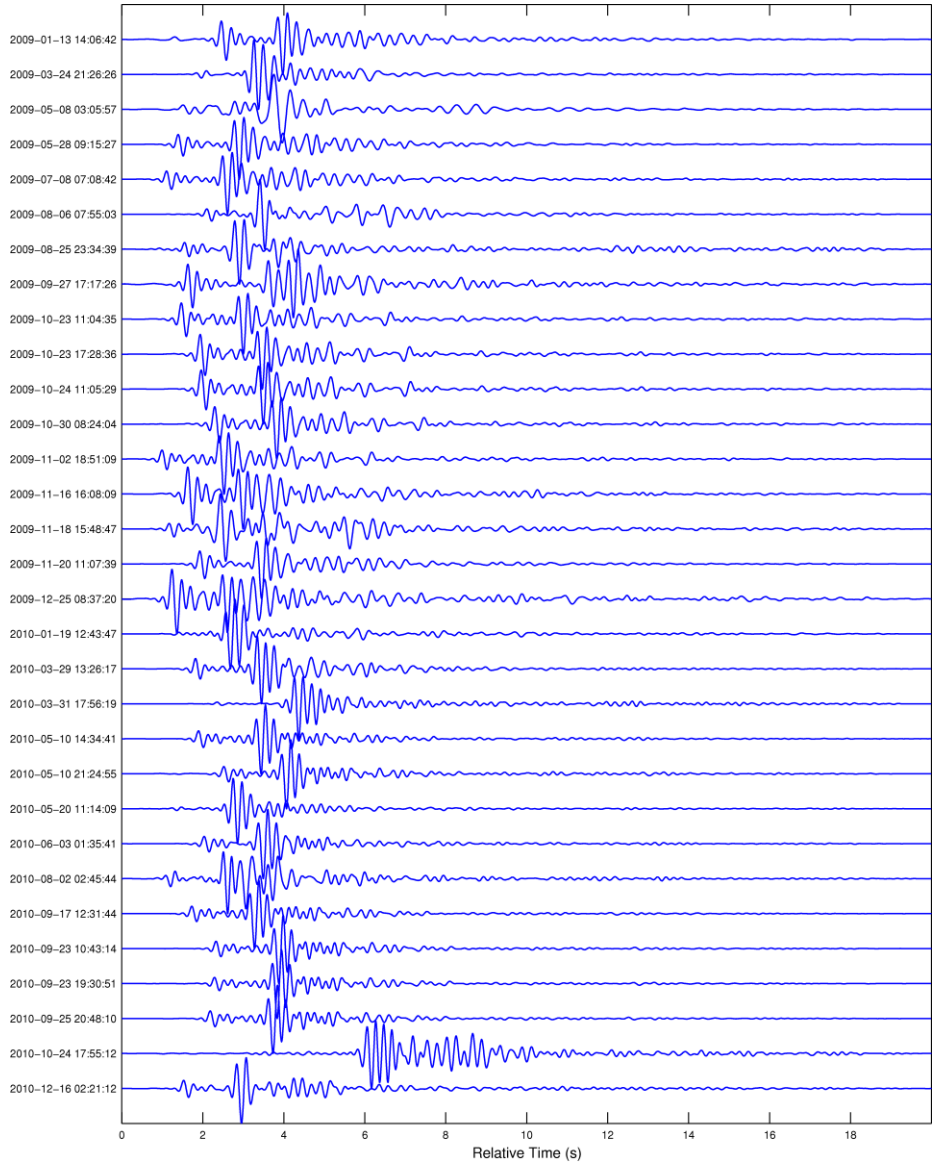
2009−01−13 14:06:42
2009−03−24 21:26:26
2009−05−08 03:05:57
2009−05−28 09:15:27
2009−07−08 07:08:42
2009−08−06 07:55:03
2009−08−25 23:34:39
2009−09−27 17:17:26
2009−10−23 11:04:35
2009−10−23 17:28:36
2009−10−24 11:05:29
2009−10−30 08:24:04
2009−11−02 18:51:09
2009−11−16 16:08:09
2009−11−18 15:48:47
2009−11−20 11:07:39
2009−12−25 08:37:20
2010−01−19 12:43:47
2010−03−29 13:26:17
2010−03−31 17:56:19
2010−05−10 14:34:41
2010−05−10 21:24:55
2010−05−20 11:14:09
2010−06−03 01:35:41
2010−08−02 02:45:44
2010−09−17 12:31:44
2010−09−23 10:43:14
2010−09−23 19:30:51
2010−09−25 20:48:10
2010−10−24 17:55:12
2010−12−16 02:21:12
0
2
4
6
8
10
12
14
16
18
Relative Time (s)

(a)

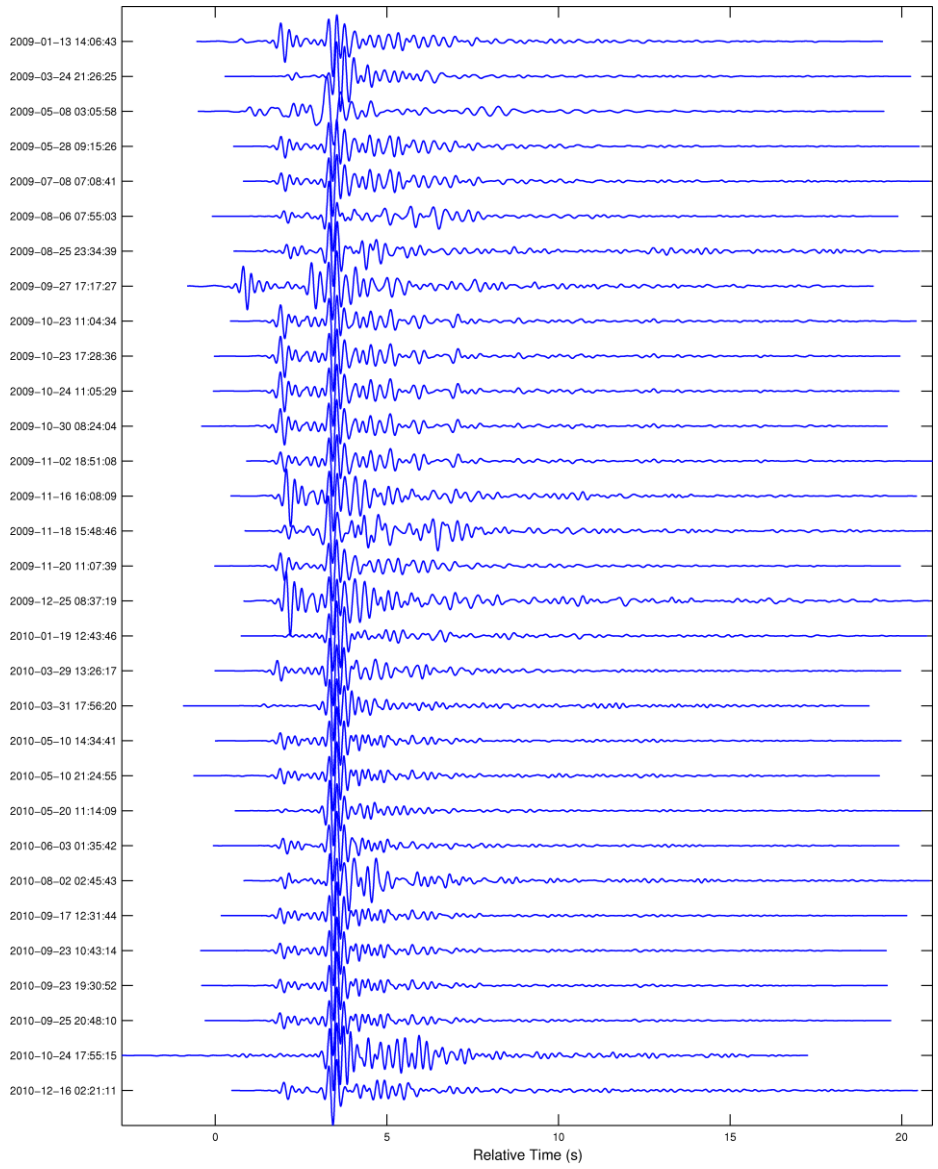

(b)

Figure 3.18. Waveforms of 31 events that occurred on the Yeonil tectonic line recorded at station HDB: aligned with catalogue origin time, and (b) aligned by cross-correlation for surface wave.

3.3.1. Detection of similar earthquakes

Waveform of the largest event (M_L 2.2) was employed as a template to detect new event that had not been catalogued. The template was cross-correlated with the continuous data of station HDB recorded from January in 2009 to October in 2010. All waveforms were from vertical velocity component with a sampling rate of 100 Hz and band-pass filtered between 1.2 and 5 Hz. With the cross-correlation coefficients of 0.9 as the detection criteria, 70 events were newly detected. Figure 3.19 is the occurrence histogram for catalogued events (white bars) and newly detected events (grey bars). There were five earthquake sequences: January, July, and October in 2009, May and October in 2010. In Figure 3.20, there are waveforms of the 70 events newly detected and the 14 events catalogued. Waveform similarity is clearly observed. After about the event number of 35, there is a little change in body-waves and coda of surface waves.

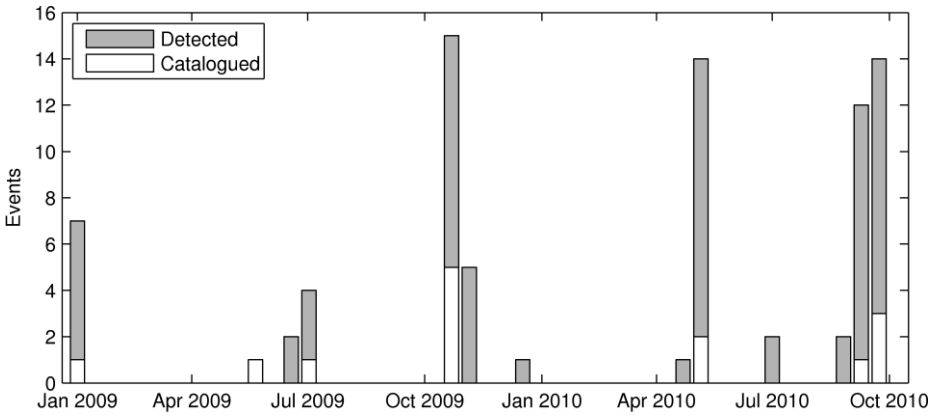

Figure 3.19. Occurrence histogram for 68 detected events (grey bar) and 13 catalogued events (white bar). The bin width is 14-day. Most of newly detected events occurred when the catalogued events were recorded.

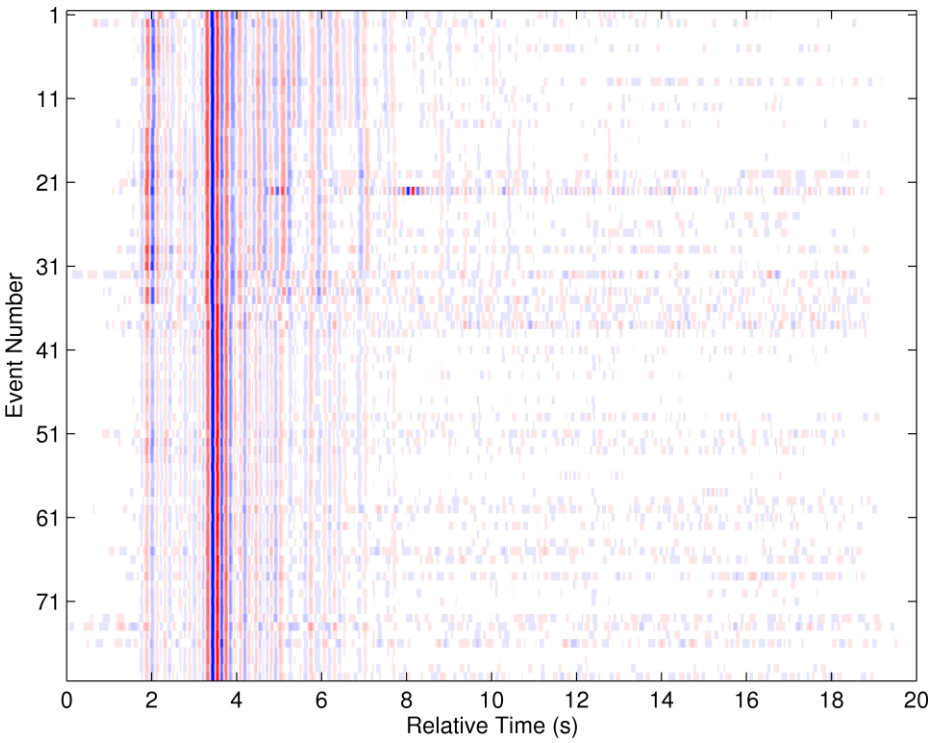

Figure 3.20. Waveforms of the 70 events newly detected by cross-correlation and the 14 events from catalogue: all the waveforms were from station HDB where the detection applied and were band-pass filtered between 1.2 and 5 Hz. Each trace was shaded with blue = -1 and red = +1 amplitude. Events are ordered from earliest to latest, and the event number increases with the origin time.

3.3.2. Hierarchical clustering of waveforms

The maximum cross-correlation coefficient matrix for surface wave of 83 events was computed after band-pass filtering between 1.2 and 5 Hz for waveforms of vertical acceleration component with sampling rate 100 Hz of station HDB. Figure 3.21 shows the CC matrix for 83 events in the city of Gyeongju. It is easily found in Figure 3.21 that all the events have high cross-correlation coefficients. Waveforms, however, slightly changed with the year 2010 starting. This waveform change is observed also in clustering results described below. The hierarchical clustering was carried out using the maximum correlation coefficients to define an event group with similar waveforms. Figure 3.22a presents the hierarchical tree (dendrogram) resulting from the maximum cross-correlation coefficients for surface wave of the 83 events. The height of the link among events represents the dissimilarity among waveforms. Waveforms of Figure 3.22b corresponding to the dendrogram of Figure 3.22a present high waveform similarity with clear alignment to surface wave. In addition, two clusters are observed in Figure 3.22 between 2009 and 2010. The change in waveforms especially for body-wave is obvious as shown in Figure 3.22b. It can be inferred that this change in waveform would result from the sensor replacement of station HDB in March 2010 – in borehole to on ground. The clustering technique succeeded to prove the high similarity in waveform of repeating earthquakes and could sense the depth change of station HDB.

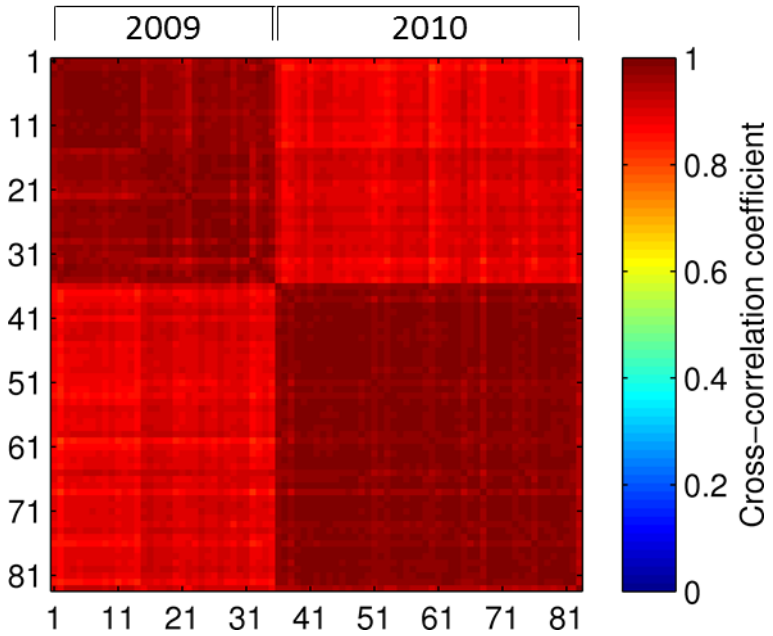

Figure 3.21. The maximum correlation coefficients matrix for surface waves of the83 events ordedred in their origin times. The coefficients are computed from waveform for vertical velocity component of station HDB after band-pass filtered between 1.2 and 5 Hz.

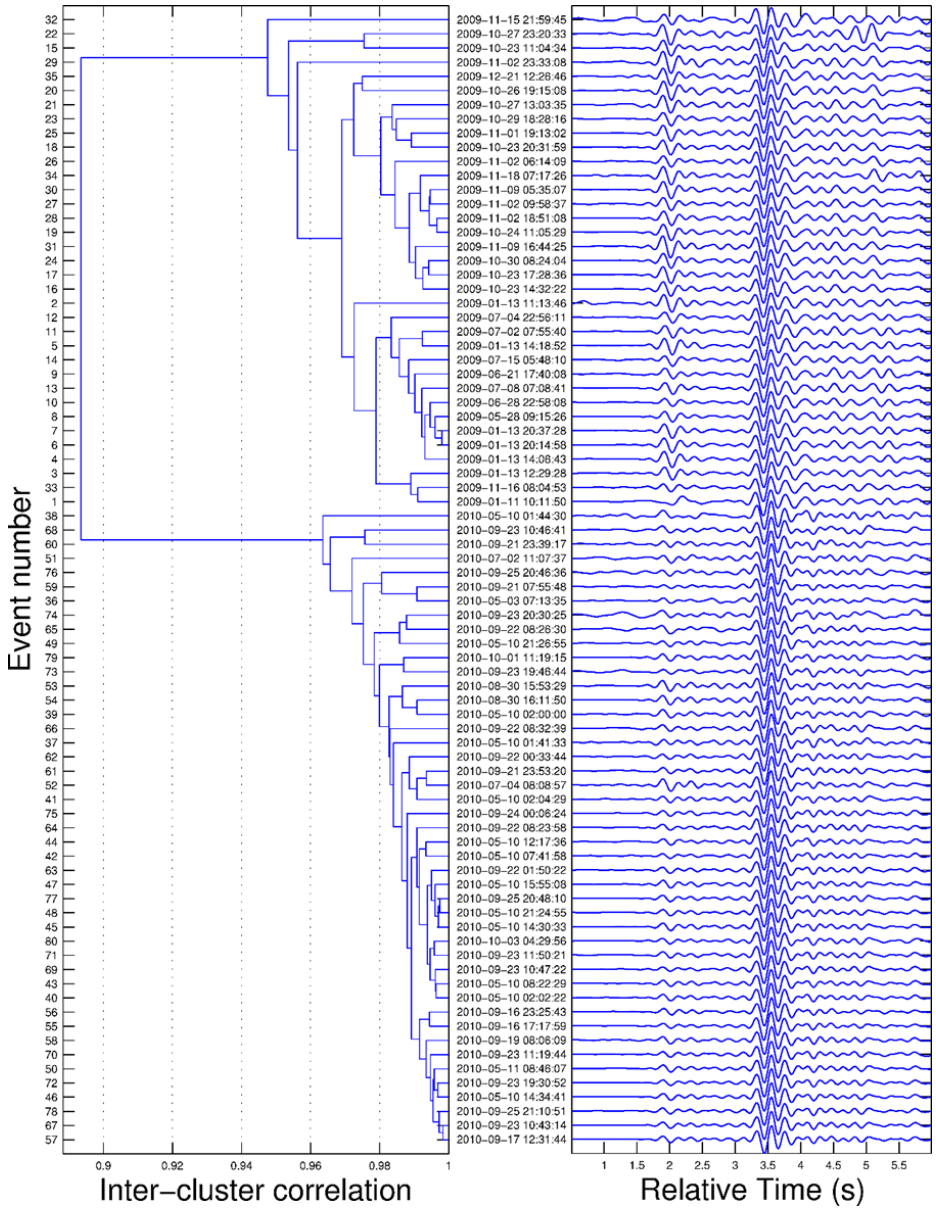

Figure 3.22. Hierarchical clustering result for micro-earthquake around Gyeongju: (a) dendrogram (hierarchical cluster tree) and (b) waveforms from data of station HDB after band-pass filtered between 1.2 and 5 Hz.

3.3.3. Epicenter relocation

Epicenters of 84 earthquakes was relocated by EpiDD based on the method of Schaff and Richards (2004a) using 14 station described in Figure 3.23. All the 14 stations are located in the interior of the Korean Peninsula, and there is not any station in north-east area from the epicenters. Epicenters relocated by EpiDD exhibited tighter spatial clustering of seismicity than did the catalogue as shown in Figure 3.23. Figure 3.23a shows epicenters of the 13 events from the KIGAM catalogue and the 70 detected events. To the newly detected events, randomly perturbed initial location within 0.05° in both latitude and longitude were assigned. Figure 3.23b shows relocated epicenters forming a linear pattern east of the Yeoinl Tectonic Line defined by Son et al. (2015b).

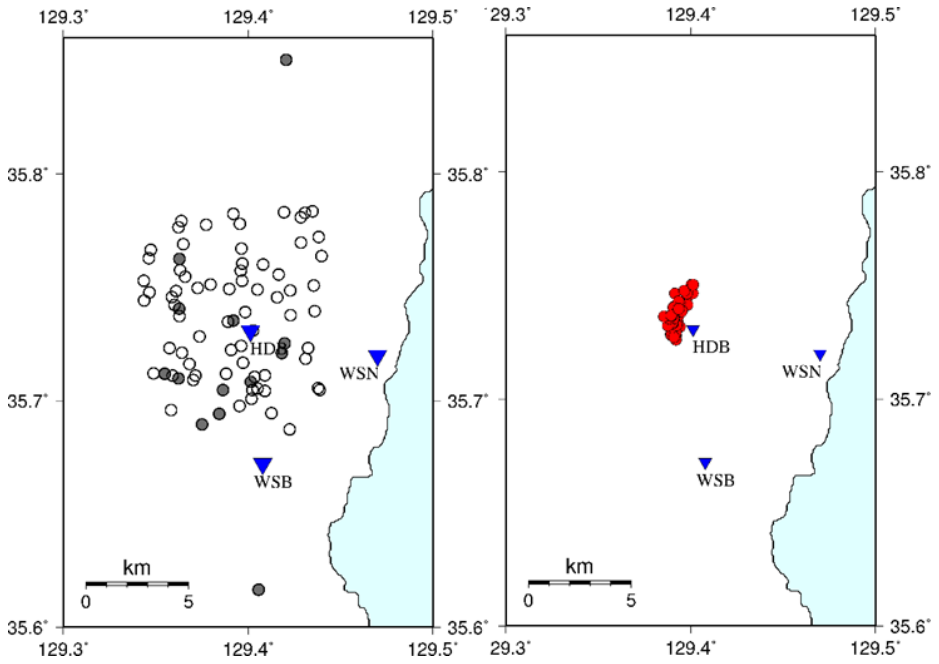

Figure 3.23. Epicenters of micro-earthquakes: (a) the catalogue for 13 events depicted as a grey circle, randomly perturbed locations for the 70 detected events depicted as an open circle, and the fault-plane solution of the largest event (M_L 2.2); (b) relocated epicenters for the 83 epicenters depicted as a solid circle.

3.3.4. Geological structures and fault plane solution

The southeastern Korean peninsula including is where the Quaternary faults are extensively observed along major fault zones such as the Yangsan fault system, Ulsan fault system, and Yeonil tectonic line (Cho et al., 2014). The epicentral region of relocated earthquakes is east of the Yeonil tectonic line defined by Son et al. (2015b). There are faults with strikes ranging from NS to NE-SW in east of the Yeonil tectonic line, which reminds the linear pattern consisting of the relocated epicenters shown in Figure 3.24. The fault solution for the largest event (M_L 2.2) of the relocated events were calculated using FOCMEC (Snoke, 2003), the grid search program for polarities. In calculation, the hypocenter depth was set to 9.3 km according to the catalogue that determined depths ranging from 6.6 to 11.8 km for seven of the thirteen events. The fault solution is shown in Figure 3.24: an open circle for compression (up polarity), an inverted triangle for dilatation (down polaity), a dash for emergent dilatation, a character ‘e’ for an emergent *P* arrival, and solid curves for possible fault planes. As shown in Figure 3.24, the inferred focal mechanism proposes a reverse fault striking NNW-SSE to NNE-SSW. Faults east of the Yeonil tectonic line strike from NS to NE-SW, and can be considered as an explanation for the estimated focal mechanism. Faults plane solutions of the 81 earthquakes, thus, would correspond to the solution of the largest event (M_L 2.2) striking NS because of their high waveform similarity confirmed previous chapters.

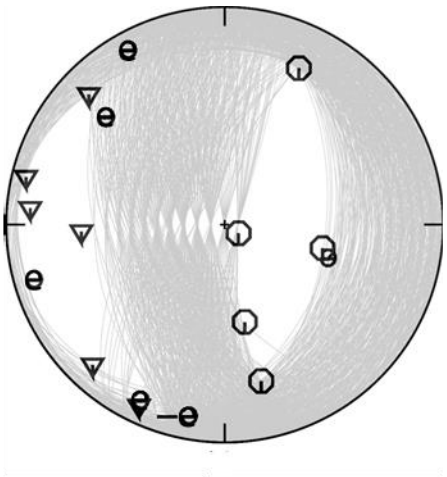

○ Compression

▽ Dilatation

– Emergent dilatation

e Emergent P arrival

Figure 3.24. Fault-plane solution showing reverse faults for the largest event (M_L 2.2) in the relocated 81events.The focal mechanism were computed by FOCMEC (Snoke, 2003) based on polarities: an open circle for compression (up polarity), an inverted triangle for dilatation (down polaity), a dash for emergent dilatation, a character ‘e’ for an emergent *P* arrival, and solid curves for possible solutions

3.4. Seismic events in the Dogye mining area

In the Dogye mining area (37.13 ~ 37.23°N, 129.00°E), the KIGAM catalogue reported that 223 events with local magnitudes ranging from 0.6 to 2.4 occurred from May 2009 to March 2014. There are four seismic stations close to epicentral area: TBA, GWL, and SND located 10 ~ 20 km west, and IMWB located about 20 km east. The data from station IMWB was available for only 31 events that occurred after the station installed at the end of 2012. Figure 3.25 shows epicenters of the 223 events, and 12 stations used in relocation described in the following Chapter 6.2. The grey box of Figure 3.25 denotes the area mapped with geological information as shown in Figure 3.26. Three mines – Dogye, Sangdeok, and Jangseong – are operated near the Taebaek and Dogye. On this area, Ko et al. (2000) reported subsidence but there is no early study about seismic events.

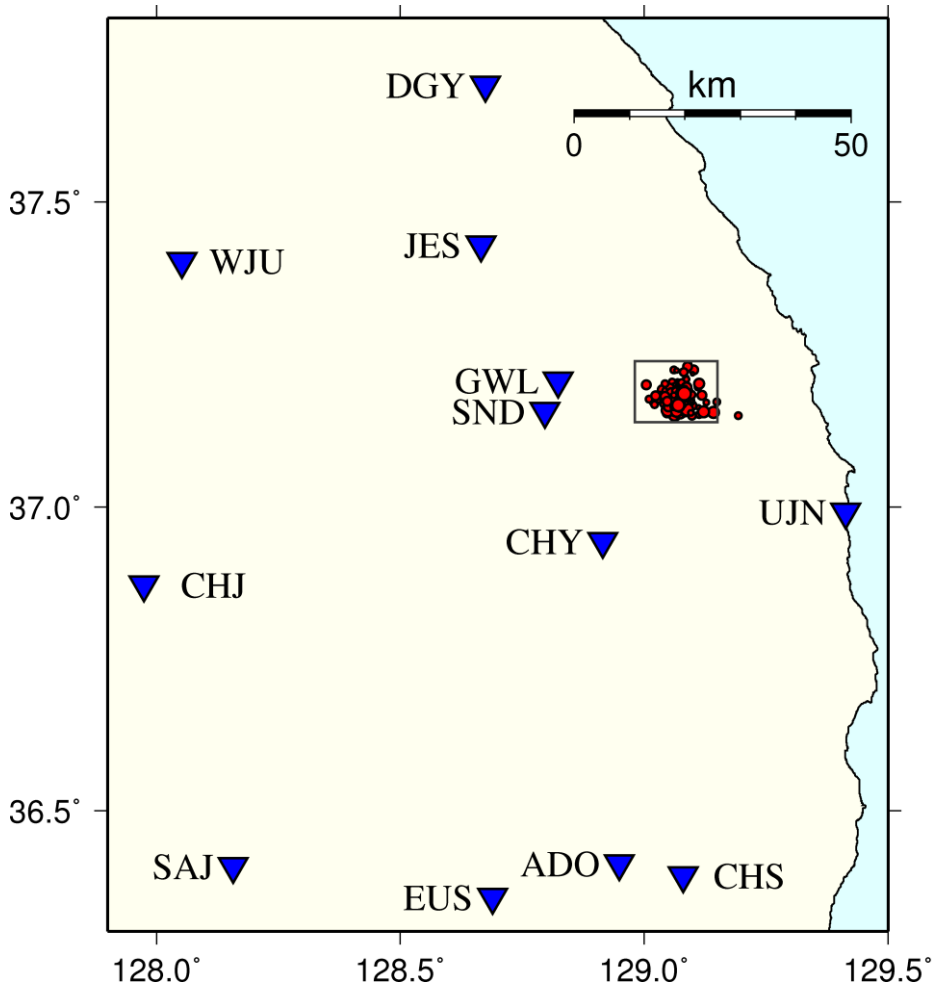

Figure 3.25. Map for epicenters (circles) of the 223 catalogued events in the Dogye mining area and stations used in relocation (inverted triangles). The grey box around epicenters represents the area mapped in Figure 3.26.

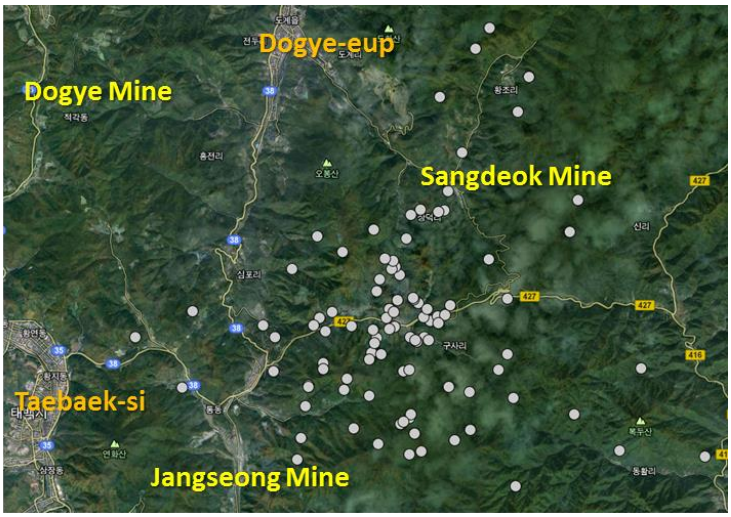

Figure 3.26. Map for 223 events of the Dogye mining area. There are three coalmines (Dogye, Jangseong, and Sangdeok) laying on the Taebaek-si and the Dogye-eup. The mapped area corresponds to the grey box in Figure 3.25.

3.4.1. Hierarchical clustering of waveforms

Waveform similarity of events was examined with data from the closest station SND. The station SND recorded 210 events of the 223 events. For the 210 events, the hierarchical tree (dendrogram) was computed from the maximum cross-correlation coefficient matrix for surface wave. Band-pass filtering between 1.4 and 6 Hz was applied to waveforms for vertical velocity component with sampling rate 100 Hz of station SND. Figure 3.27 presents the maximum cross-correlation coefficients matrix for waveforms from the closest station SND. The coefficients are ordered in origin time from the catalogue as shown in Figure 3.27a. After hierarchical clustering, it is observed that there are two event clusters with the branch cut of 0.4. Figure 3.27b presents the cross-correlation coefficients arranged by waveform similarity defined by hierarchical clustering. Two clusters (Cluster A with 124 events and Cluster B with 83 events) are visible in Figure 3.27b. It can be inferred that events composing Cluster B would be close together spatially from the fact Cluster B shows high cross-correlation coefficients.

:

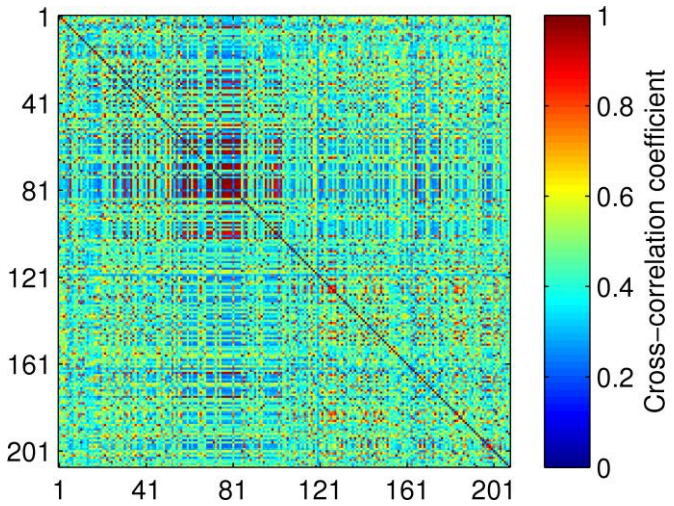

(a)

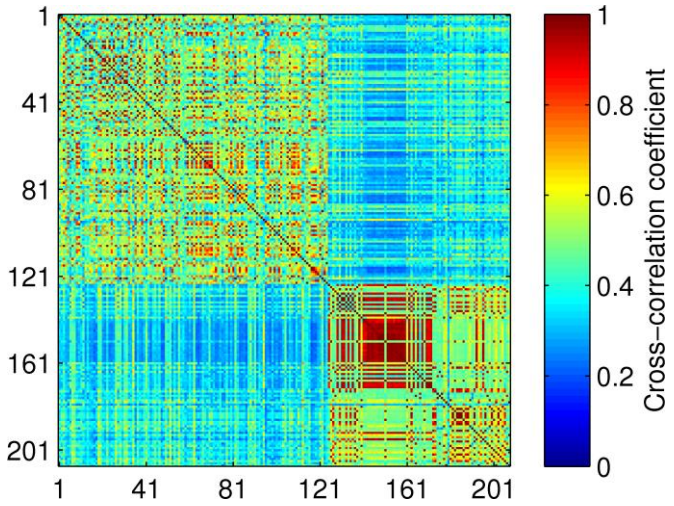

(b)

Figure 3.27. The maximum cross-correlation coefficients matrix for waveforms from the closest station SND of the 210 events ordered in (a) origin time and (b) waveform similarity after hierarchical clustering

Figure 3.28 shows waveforms of Cluster B consisting of 83 events. The band-pass filter between 1.4 ~ 6 Hz was applied to waveforms for vertical velocity component of station SND recording with sampling rate of 100 Hz. Events are ordered from earliest to latest, and the event number increases with the origin time. Waveforms in Figure 3.28a are aligned by cataloged origin times. Waveforms of Figure 3.28b are aligned using cross-correlation for a time window including surface wave. In Figure 3.28, waveform similarity is clearly observed on event numbers around 21, 61, and 81. The hierarchical clustering was performed for these 83 events using the procedure described above with waveforms of station SND. The dendrogram was obtained from the maximum cross-correlation matrix for surface wave. By the branch cut of 0.8 for the dendrogram, the 83 events were sorted into six groups: 34 events for G1, 19 events for G2, 8 events for G3, 7 events for G4, 5 events for G5, and 4 events for G6. Figure 3.29 displays occurrence histograms of the six groups in left panel and traces of relevant groups in right panel: Events G1 occupied 41 % of the total number of the Dogye events, and most of G1 is concentrated in the early part. Events of G2 to G6 occurred intermittently through the entire period. Figure 3.30 is the correlation matrix for each six groups. Waveform similarity in each group is clearly observed in Figure 3.30.

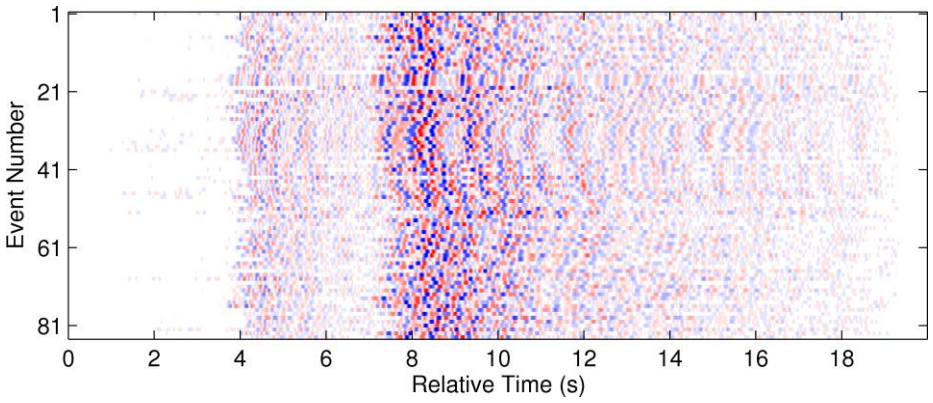

(a)

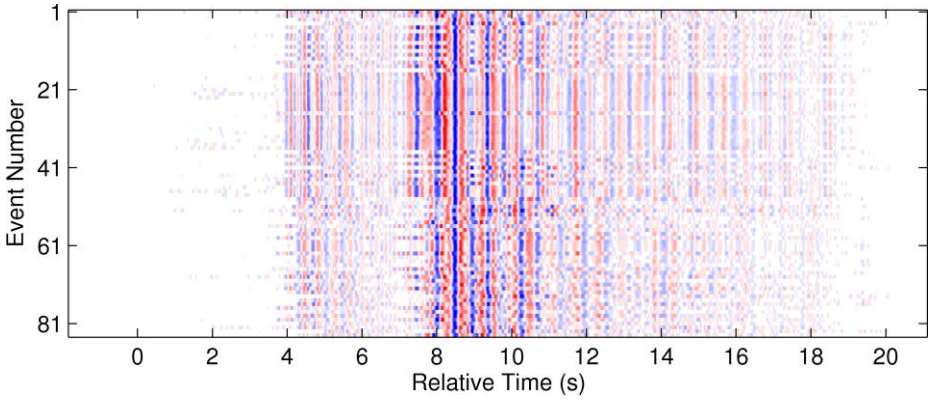

(b)

Figure 3.28. Waveforms for the 83 events of Cluster B recorded at station SND: (a) aligned by catalogue origin time, and (b) aligned by waveform cross- correlation for surface wave. Each trace was shaded with blue = -1 and red = +1 amplitude. Events are ordered from earliest to latest, and the event number increases with the origin time.

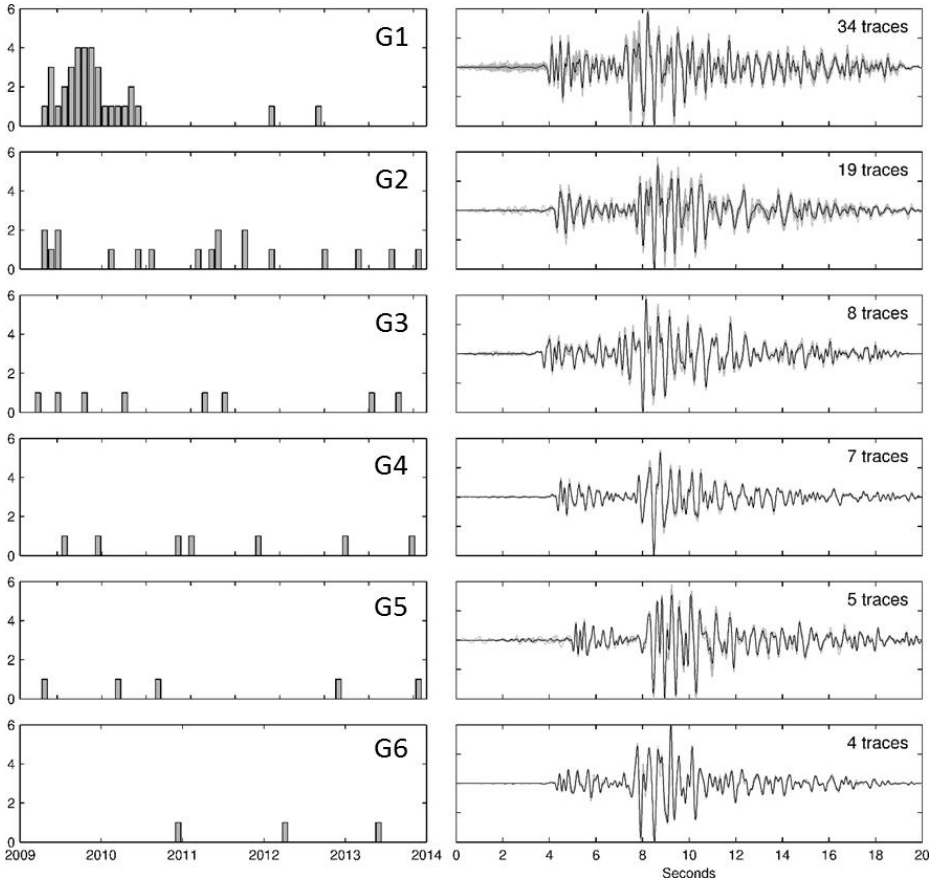

Figure 3.29. Occurrence histograms and traces of event clusters in the Doge events: G1 is concentrated in the early part, and most of the seismic events of Dogye mining area consists events of G1. Events of G2 to G6 occurred intermittently through the entire period.

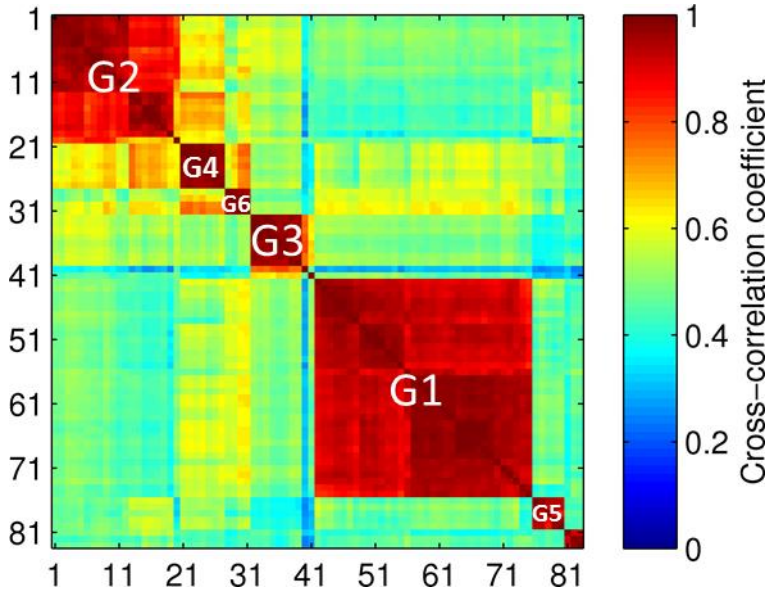

Figure 3.30. Correlation matrix for the 83 seismic events in the Dogye mining area. Over six event groups are clearly visible in red meaning high correlation coefficients between waveforms.

3.4.2. Epicenter relocation

Using EpiDD based on the method of Schaff and Richards (2004a), 71 events of the 83 events composing Cluster B were relocated. Seismic stations used in relocation are GWL, SND, CHY, UJN, JES, WJU, DGY, CHU, CHS, ADO, EUS, and SAJ. The locations of these 12 stations are shown in Figure 3.25. Stations are located west of the epicenters, except station UJN. The azimuthal gap reaches 160 ° . Epicenters are mapped in Cartesian coordinate as shown in Figure 3.31. Figures 3.31a and b show epicenters of the 71 events from the catalogue and relocation results, respectively. Color of circle indicates six event groups of Cluster B: yellow for 28 events of G1; red for 16 events of G2; cyan for 8 events of G3; magenta for 7 events of G4; light green for 4 events of G5; navy for 4 events of G6. Grey circles are the remains not included by six groups defined by hierarchical clustering. It is observed that events classified into the same group were clustered together after the relocation as shown in Figure 3.31b. Figure 3.31c shows relocation results on an enlarged map, and the gradation of black in the background presents the density of events. Events of Group 1 in red occupying over 30 % of Cluster B occurred on the concentrated area, one cell of 200 m × 200 m. The spatial distribution of relocated epicenters reflected the location of the six groups classified according to waveform similarity as shown in Figure 3.31c and Figure 3.32, which could validates the relocation results.

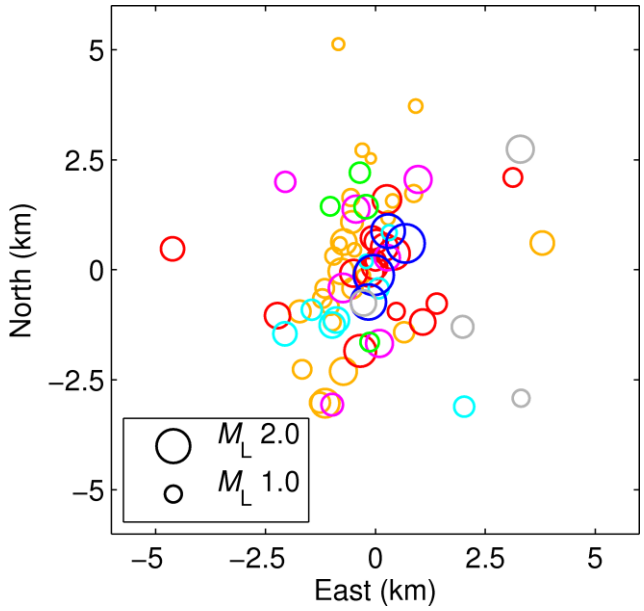
5
2.5
0
−2.5
−5
North (km)
−5
−2.5
0
2.5
5
East (km)
M_L 2.0
M_L 1.0

(a)

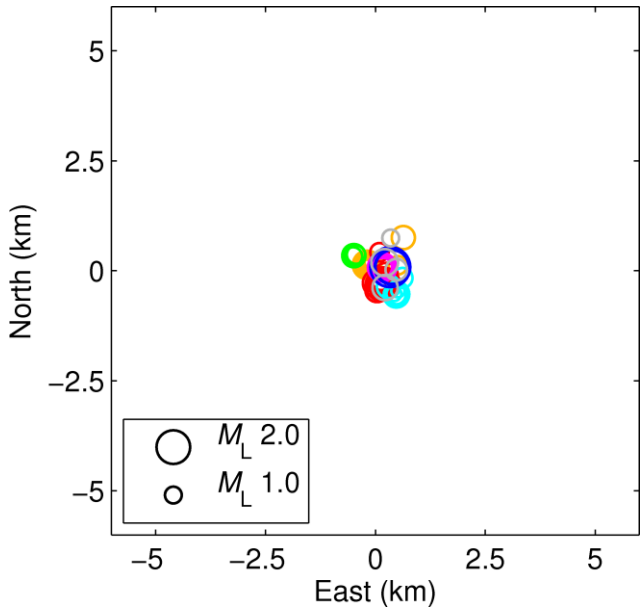
5
2.5
0
−2.5
−5
North (km)
−5
−2.5
0
2.5
5
East (km)
M_L 2.0
M_L 1.0

(b)

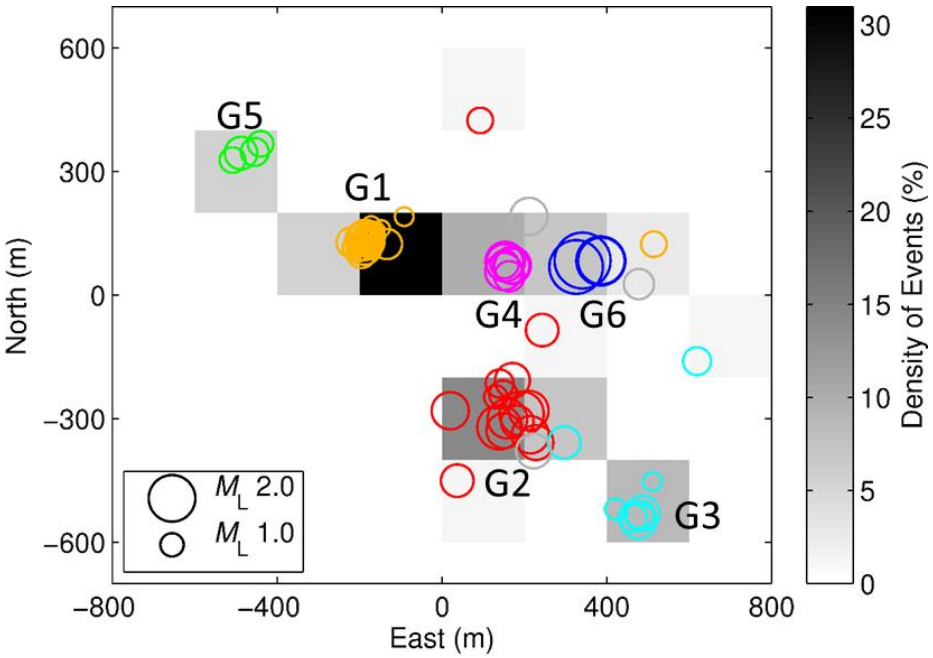

(c)

Figure 3.31. Epicenters of the 83 events: (a) the catalogue, (b) relocation results, and (c) results on an enlarged map. Six groups classified by waveform similarity are represented by colors: red for G1, pink for G2, blue for G3, light green for G4, cyan for G5, yellow for G6, and grey for the others.

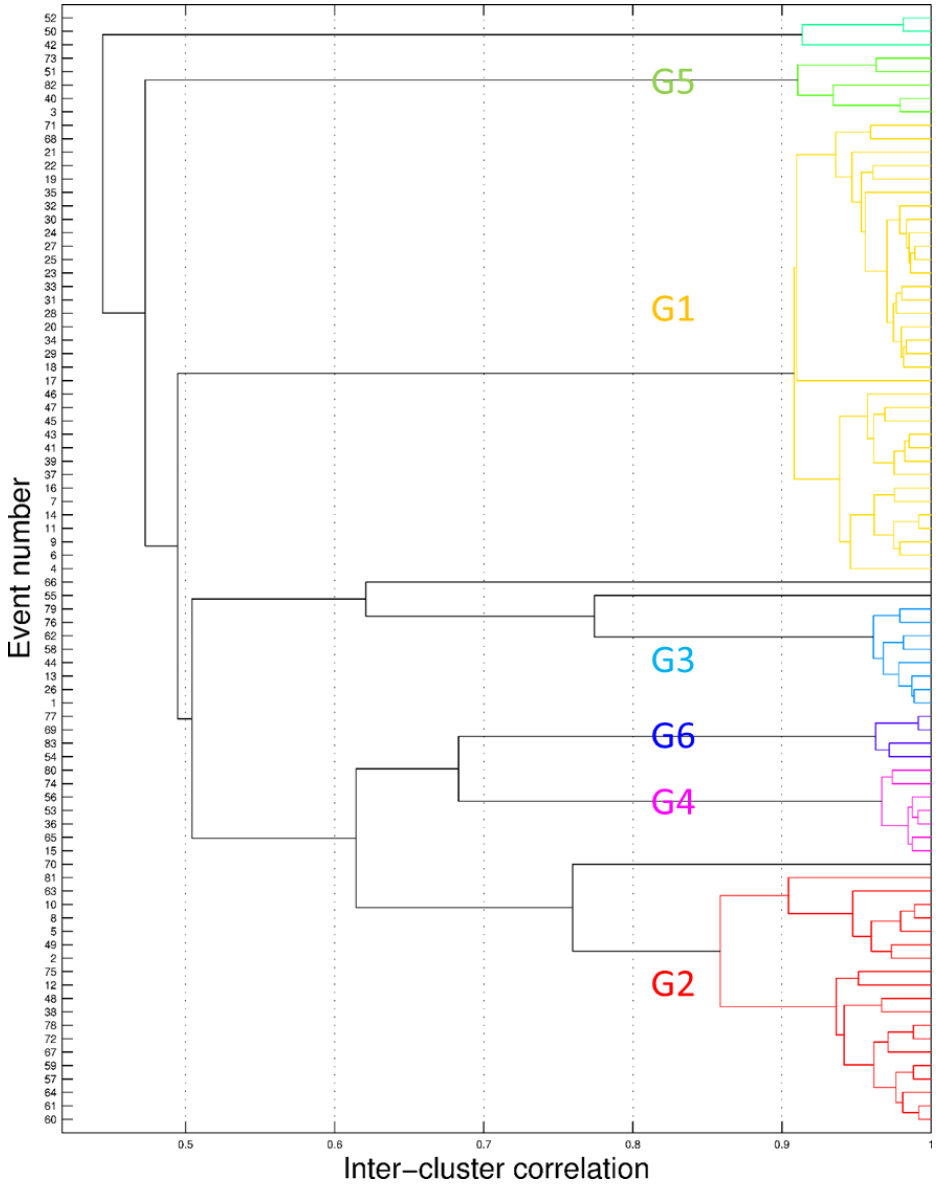

Figure 3.32. Hierarchical clustering result for the 83 seismic events in the Dogye mining area with branch cut of 0.8 shows seven clusters: G1 with 34 events in yellow, G2 with 19 events in red, G3 with 8 events in cyan, and G4 with 7 events in magenta, G5 with 5 events in light green, and G6 with 4 events in navy.

3.4.3. Detection of seismic events

Two seismic stations GDSG and KNUD were installed at the study area in May 2014. The KIGAM reported that 30 events occurred from June 2014 after installing the two stations in May 2015. Figure 3.33 presents epicenters of the 30 events with circle and two installed stations with inverted triangles. Using data of station GDSG newly installed in the Dogye mining area, unreported events were detected by the cross-correlation between waveforms of the 27 events that occurred in the study area after station GDSG installed and one-year continuous waveforms of station GDSG recorded from June 2014 to May 2015. All the waveforms were band-pass filtered between 1.2 and 5 Hz. Employing waveforms of the 30 events as a template; more than 44,000 events were detected from one-year continuous data with the cross-coefficient of 0.55 as a detection criterion. Events that occurred within 3 seconds after the other event occurring were considered as duplication in detection, and removed automatically. Of 44,000 detected events, it is found that about 13,000 detected events are comb-like waveform observed regularly. As shown in Figure 3.34a, the comb-like waveform with length of 30 to 60 minutes is a signal train composed of a blast every 30 seconds. Figure 3.34b and c display signal of one blast recorded by station GDSG and KNUD, respectively. The blast could not be recorded by station KNUD 5 km apart from station GDSG.

Figure 3.35 shows occurrence history of the 44,000 detected events. The comb-like waveform a series of blasts every 30 seconds was

computed and was plotted by grey bars. The remains 31,000 events are plotted with red line in Figure 3.35. It is obvious that the comb-like waveform appeared regularly in weekday colored by pain sky-blue from June to October in 2014. The number of detected events without blasts in red line increased whenever the comb-like waveform appeared in weekday as shown in Figure 3.35a. As the comb-like waveform suddenly disappeared after November in 2014, the number of events without blasts became small as shown in Figure 3.35b. The end of Figure 3.35c, however, displays that the number of events in red line increased temporarily in weekdays without the comb-like waveform.

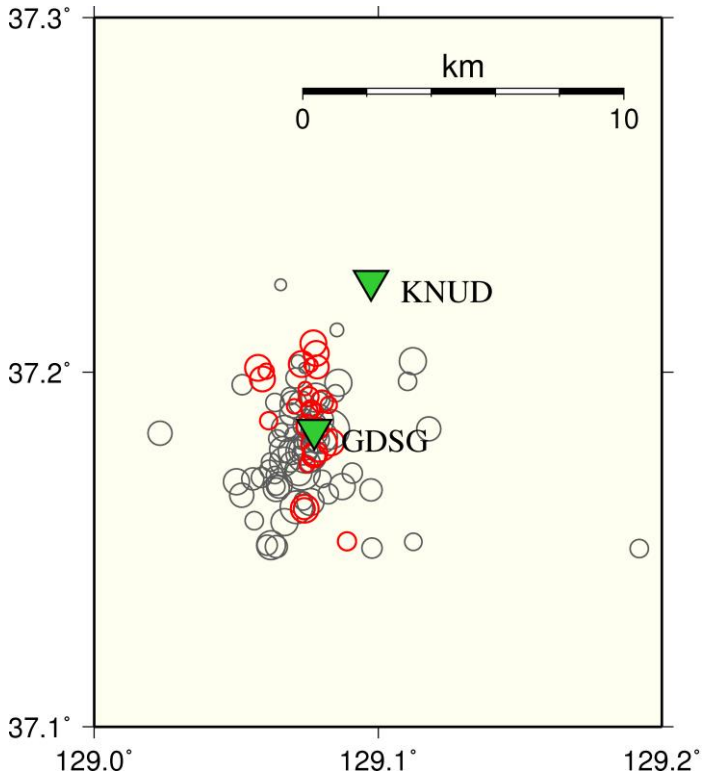

Figure 3.33. Locations of stations KNUD, GDSG (inverted triangles) installed in June 2014, the 223 events (grey circles) that occurred from May 2009 to March 2014, and 27 events (red circles) that occurred after the two station were installed.

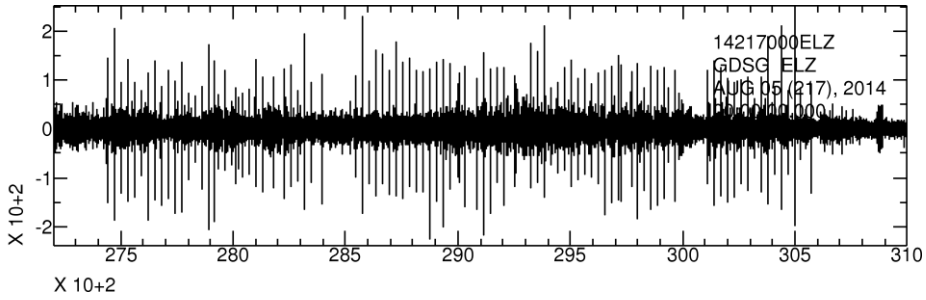

(a)

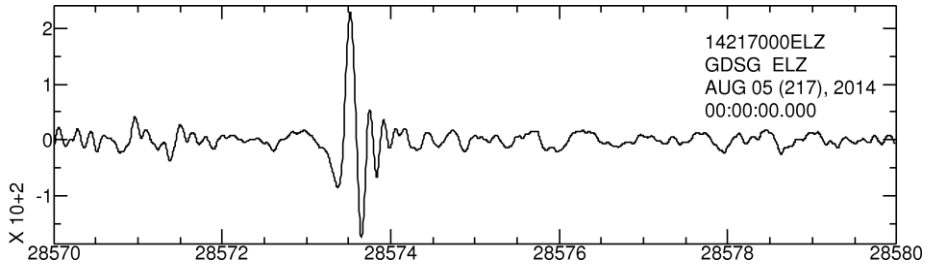

(b)

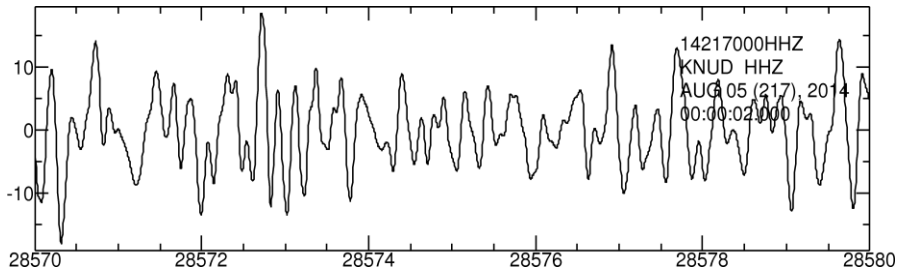

(c)

Figure 3.34. Seismic events from mine activities: (a) comb-like waveform with length of 30 to 60 minutes composed of a blast every 30 seconds; one blast signal recorded at (b) station GDSG to which detection was applied, and (c) station KNUD

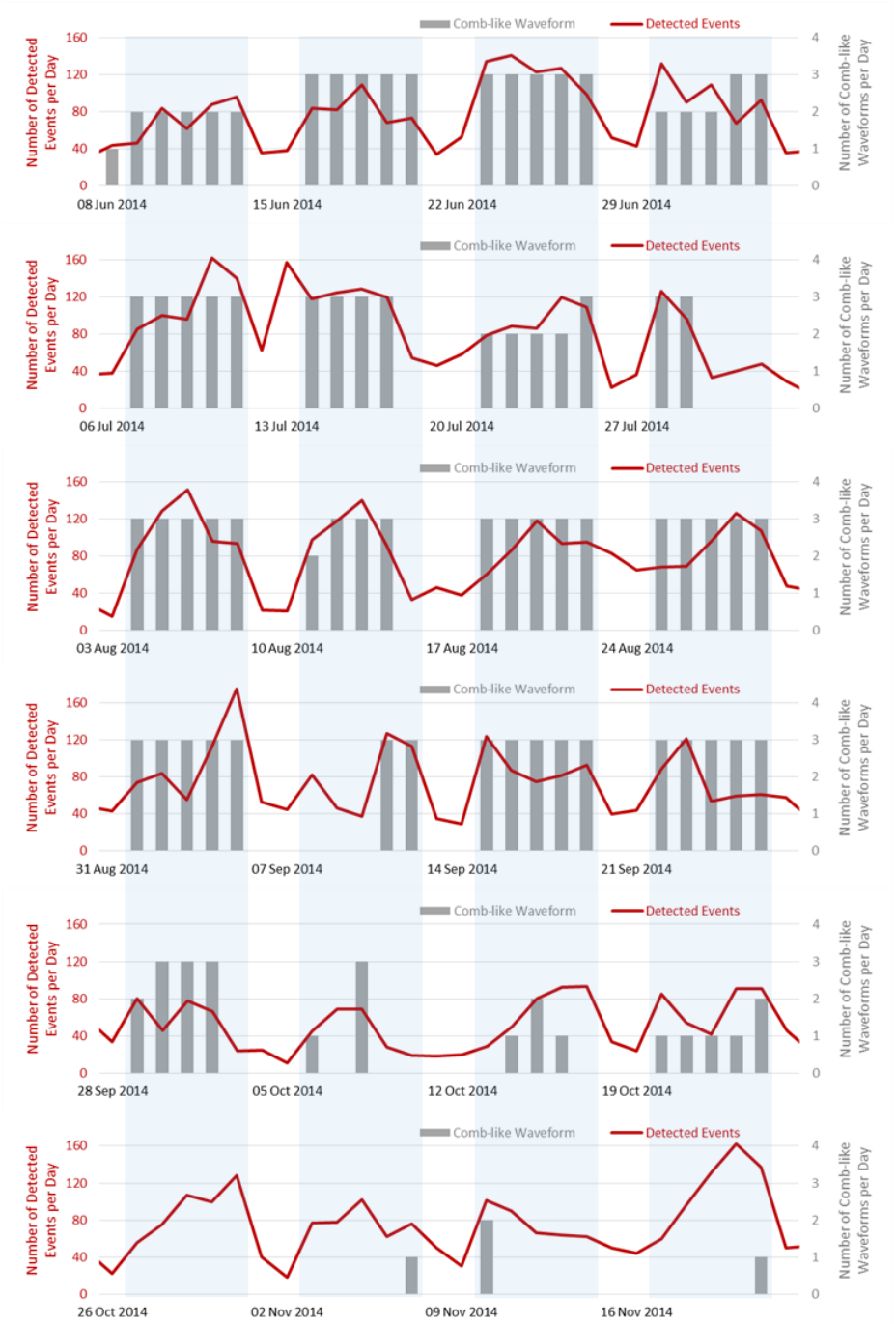
Comb-like Waveform
Detected Events
Number of Detected Events per Day
Number of Comb-like Waveforms per Day
08 Jun 2014
15 Jun 2014
22 Jun 2014
29 Jun 2014
06 Jul 2014
13 Jul 2014
20 Jul 2014
27 Jul 2014
03 Aug 2014
10 Aug 2014
17 Aug 2014
24 Aug 2014
31 Aug 2014
07 Sep 2014
14 Sep 2014
21 Sep 2014
28 Sep 2014
05 Oct 2014
12 Oct 2014
19 Oct 2014
26 Oct 2014
02 Nov 2014
09 Nov 2014
16 Nov 2014

(a)


Comb-like Waveform
Detected Events
Number of Detected Events per Day
Number of Comb-like Waveforms per Day
0
40
80
120
160
0
1
2
3
4
23 Nov 2014
30 Nov 2014
07 Dec 2014
14 Dec 2014
21 Dec 2014
28 Dec 2014
04 Jan 2015
11 Jan 2015
18 Jan 2015
25 Jan 2015
01 Feb 2015
08 Feb 2015
15 Feb 2015
22 Feb 2015
01 Mar 2015
08 Mar 2015
15 Mar 2015
22 Mar 2015
29 Mar 2015
05 Apr 2015
12 Apr 2015
19 Apr 2015
26 Apr 2015
03 May 2015

(b)

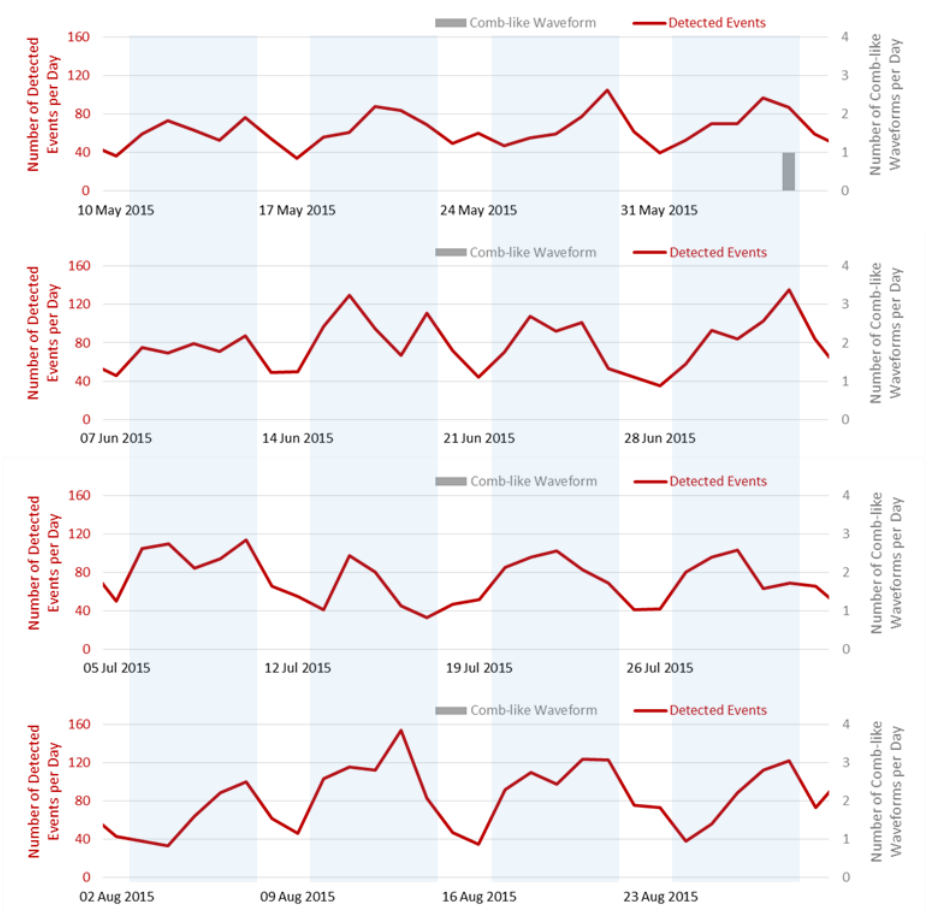

(c)

Figure 3.35. Occurrence plot for 44,000 detected events: grey bars and red line denote comb-like waveforms composed of blasts and the other events without blasts, respectively. The observation period of 64 weeks is segmented by 28 days with the period of (a) 2014.06.08 ~ 2014.11.22, (b) 2014.11.23 ~ 2015.05.09, and (c) 2015.05.10 ~ 2015.08.29.

3.4.4. Energy estimation for newly detected events

Ten logarithm of the maximum amplitude for each event was computed to estimate seismic energy of detected events. This process employed waveforms from station GDSG that was also used in detection. Figure 3.36 shows events with 10 logarithmic of the maximum amplitudes for each event. It was found that blasts composing comb-like waveform were expressed with even amplitude as shown in Figure 3.36a. Figure 3.36b has events scattered in amplitude and does not show events with even amplitude because comb-like waveform with even amplitude rarely appeared after November in 2014. Whole results were attached describing occurrence history of 44,000 detected events and their logarithmic amplitude during one-year in Figure 3.37. From the fact that the comb-like waveform appears regularly three to four times a day on weekdays and have monotonic amplitude, the comb-like waveform can be considered as a signal related directly by mining activities.

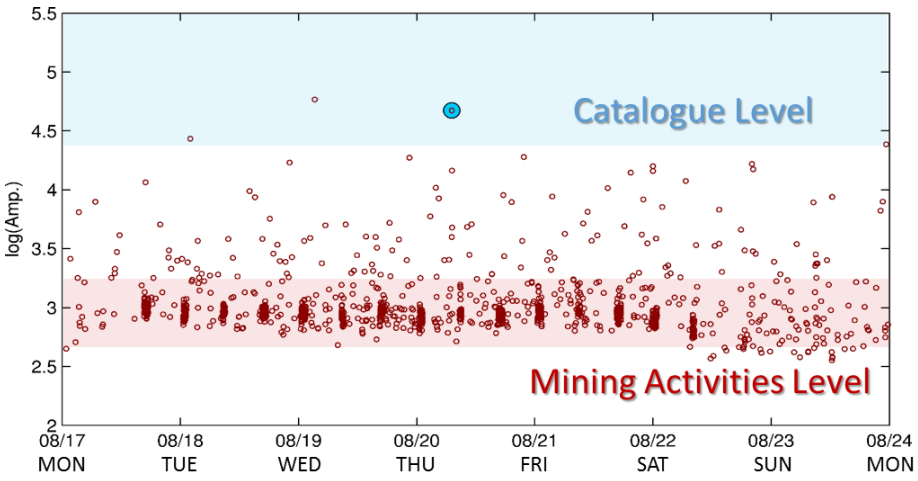

(a)

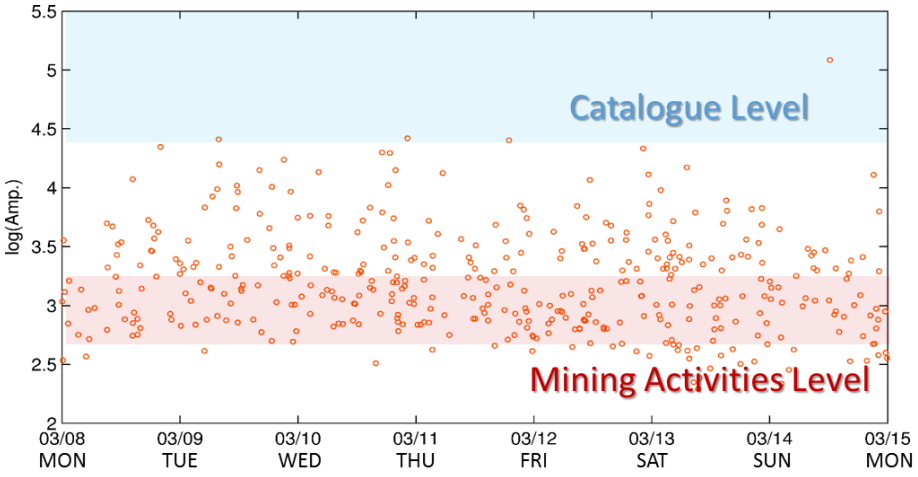

(b)

Figure 3.36. Logarithm of the maximum amplitude for each event: (a) with mining activities expressed by comb-like waveform consisting of blasts in August 2014, (b) without mining activities in March 2015

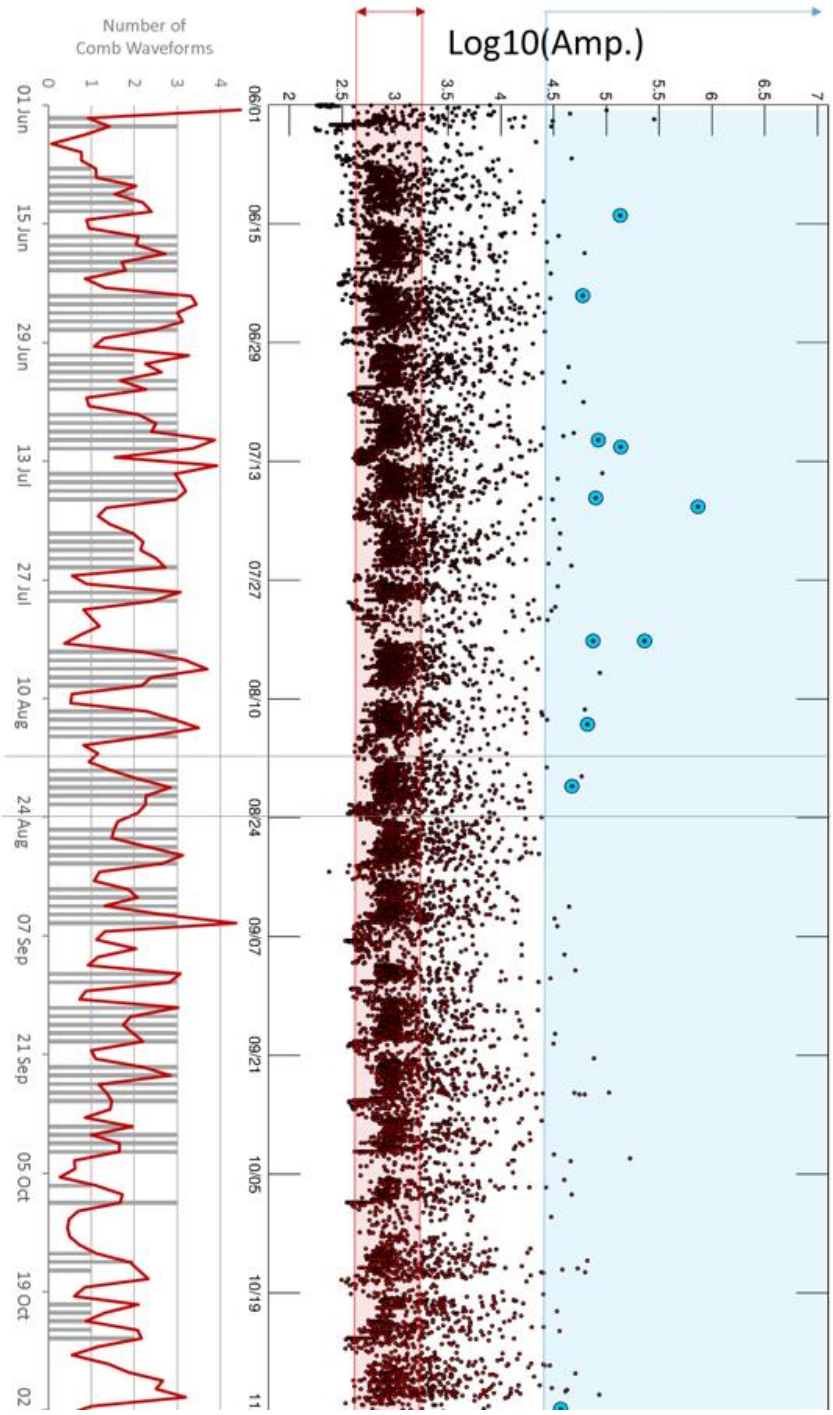
Number of
Comb Waveforms
Log10(Amp.)
01 Jun
15 Jun
29 Jun
13 Jul
27 Jul
10 Aug
24 Aug
07 Sep
21 Sep
05 Oct
19 Oct
02
06/01
06/15
06/29
07/13
07/27
08/10
08/24
09/07
09/21
10/05
10/19
11

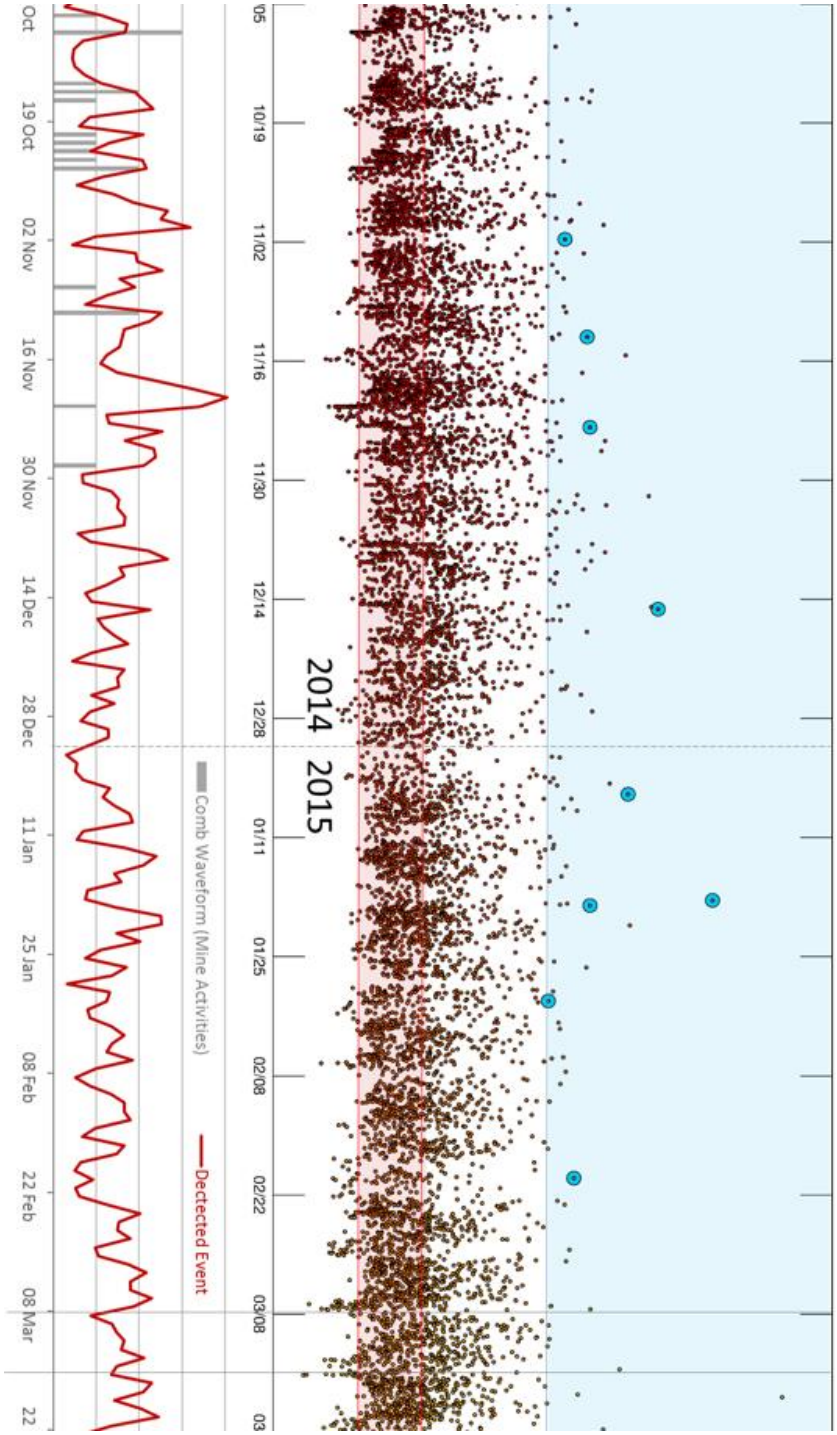
2014
2015
10/19
11/02
11/16
11/30
12/14
12/28
01/11
01/25
02/08
02/22
03/08
19 Oct
02 Nov
16 Nov
30 Nov
14 Dec
28 Dec
11 Jan
25 Jan
08 Feb
22 Feb
08 Mar
Comb Waveform (Mine Activities)
Dectected Event

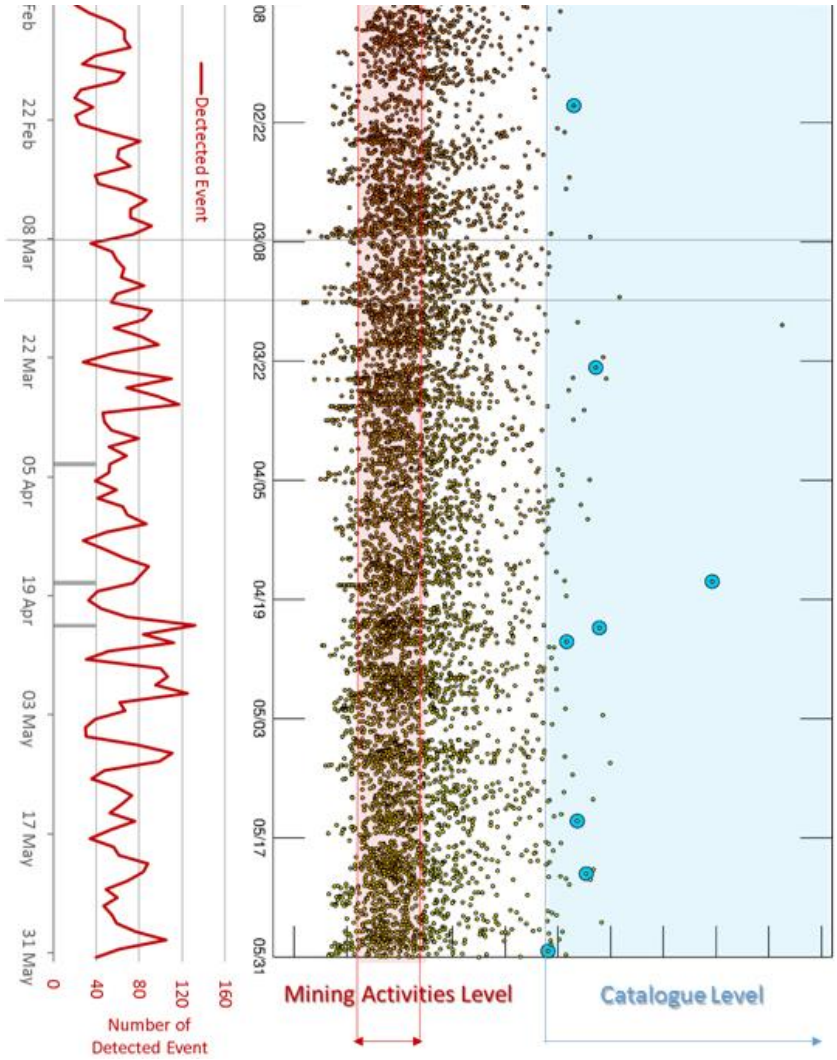

Figure 3.37. Seismicity of the Dogye mining area from June 2014 to May 2015. The left panel is the same with Figure 6.10, and the right panel is the entire result for energy estimation. The blue and red areas in the right panel represent energy level of events catalogued and events forming comb-like waveform directly induced by mining activities, respectively.

Most of the undefined events synchronized with the occurrence of comb-like waveform as show in Figures 3.35 to 37. Except blasts constituting comb-like waveform, however, most of detected events are unclear in their origin. It is possible that most of the undefined events would be formed from fracturing in response to stress-perturbation on an active mining face or represent slip in existing shear zones such as a fault or dike. Some of the remains appeared with their remarkable amplitude and were reported by the catalogue as shown in sky-blue shadow of Figures 3.35 to 37. More studies are necessary to discover sources of the undefined events and to organize the catalogue. Finally, Figure 3.38 was attached as additional information: a for the relocation result mapped on the satellite image map, and b for the pit map of the Sangdeok Mine corresponding the same area with a.

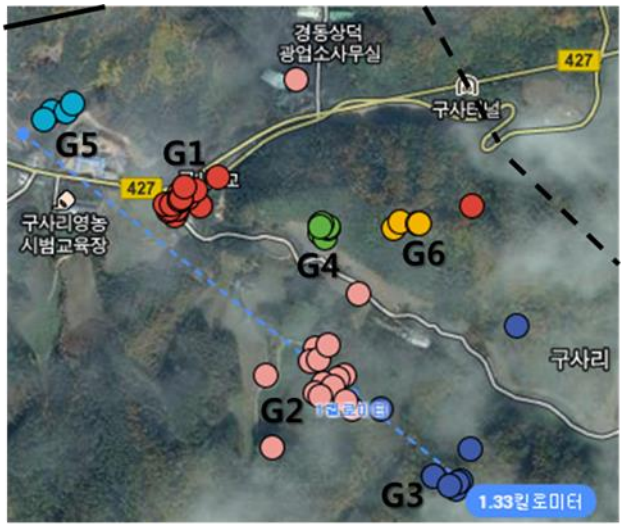

(a)

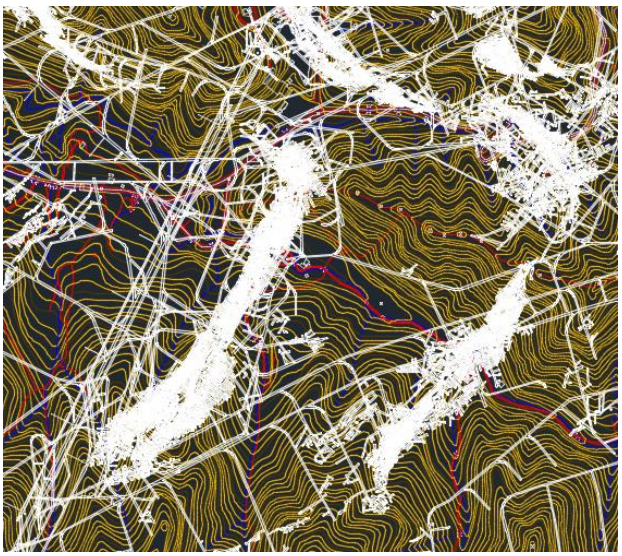

(b)

Figure 3.38. Maps for the epicentral area: (a) relocated epicenters with six groups on satellite image map, (b) mine pit map for the studied area (modified after receiving from Sangdeok mine)

4. Discussion

The double-difference technique for epicenter relocation EpiDD was applied to the four seismic clusters in and around of the Korean Peninsula in this study. On the Baekryeong Island earthquake sequence, the earthquakes swarm around Gyeongju, and the seismic events in the Dogye mining area, the seismic event detection using waveform cross-correlation succeeded to add new events. The performance of the detection is briefly reviewed before discussing relocation results.

Through all the four event groups, dramatic reduction in distances between epicenters was observed after relocation. The hypothesis test validated the reduction in distances between catalogued and relocated epicenters. The linearity made up of relocated epicenters was also examined especially for the Boryeong Offshore earthquake sequence. In addition, relative location of epicenters was displayed with varying velocity, and conditions affecting EpiDD results was considered in terms of waveform similarity

4.1. Performance of waveform detection

The detection for unreported event by waveform cross-correlation was applied to the Baekryeong Island earthquake sequence, the earthquakes swarm around Gyeongju, and the seismic events in the Dogye mining area. All the continuous records and templates employed in the detection are sampled with 100 Hz. Lengths of the continuous records vary with the period of observation: nine days for the Baekryeong Island earthquake sequence, 22 months for the earthquake swarm on the Yeonil tectonic line, 12 months for the seismic events in the Dogye mining area. Correlation coefficients (CC) as detection criteria are set to 0.7 for the Baekryeong sequence and 0.9 for the Yeonil events to search events that have similar waveform with a template. For the Dogye events, CC was set to 0.55 relatively low to find waveforms of 'triggers' seismically recorded. The detection succeeded to find all events reported in catalogue and to discover unreported events: 55 events detected including the 31 catalogued events for the Baekryoeng sequence, 68 events detected including the 13 catalogued events for the Yeonil events, and over 40,000 events detected including the 27 catalogued events for the Dogye events. The number of detected events is several times larger than the number of catalogued events. For the Dogye events when using to find waveforms displaying abrupt peaks, the number of the detected events is 1630 times larger than the number of catalogued events. The detection results described are summarized in Table 4.1.

Table 4.1. Statistics of waveform detection for each event group.

Index	Length	CC	Catalogue (A)	Detection (B)	B/A
Baekryeong Island earthquake sequence	9 days	0.7	31	55	1.77
Repeating earthquakes on the Yeonil tectonic line	22 months	0.9	13	81	6.23
Seismic events in the Dogye mining area	12 months	0.55	27	44000	1630

4.2. Hypothesis test for spatial pattern of epicenter distribution

Highly similar waveforms observed at each event group in previous chapters suggests that the true location of events are not scattered but concentrated. This section assumes that the source is actually at the centroid of the epicenters, and tests the hypothesis. The variable is distance from an epicenter to the centroid of epicenters as shown in Table 4.2. N is the number of distances equal to the number of events in Table 4.2. For the Baekryeong Island earthquake sequence and the seismic events in the Dogye mining area, N for the relocation is bigger than N for the catalogue because unreported events were added by the detection. Dramatic reduction on distances from each epicenter to the epicentroid is observed in both the average and standard deviation after relocation as shown in Table 4.2.

Table 4.2. Statistics of distances from each epicenter to the epicentroid.

Index	Catalogue			Relocation		
	N	Avg. (m)	Std. (m)	N	Avg. (m)	Std. (m)
Baekryeong Island earthquake sequence	31	4713	3101	55	664	309
Boryeong Offshore earthquake sequence	149	3184	2905	149	196	129
Earthquake swarm around Gyeongju	13	4466	4014	81	467	381
Seismic events in the Dogye mining area	71	1856	1615	71	355	176

Before inspecting the distance distribution of catalogue and that of relocation, normality of the distribution should be examined using the Kolmogorov-Smirnov test. The distance data was compared to the normal distribution with the average and standard deviation equal to those for the distance data. As shown in Table 4.3, the Kolmogorov-Smirnov test rejects the null hypothesis H_0 with extremely small p-value for every event group. Thus the two distance distributions have to be considered as non-normal distribution.

H_0: The data comes from a standard normal distribution.

H_1: The data does not come from a standard normal distribution.

Table 4.3.Normality test based on the Kolmogorov-Smirnov test.

Index	Catalogue			Relocation		
	H	p-value	data	H	p-value	data
Baekryeong Island earthquake sequence	1	~ 0	non-normal	1	~ 0	non-normal
Boryeong Offshore earthquake sequence	1	~ 0	non-normal	1	~ 0	non-normal
Earthquake swarm around Gyeongju	1	~ 0	non-normal	1	~ 0	non-normal
Seismic events in the Dogye mining area	1	~ 0	non-normal	1	~ 0	non-normal

To confirm existence of significant difference among two data sets that does not come from a normal distribution, the Kolmogorov-Smirnov test or Wilcoxon rank sum test can be employed. This study

performed the Wilcoxon rank sum test, because for large data sets the Wilcoxon rank sum test produces a z-value that can be an indicator showing how far two data sets are. Table 4.4 shows results of the Wilcoxon rank sum test for each event group. With extremely small p-value for all event group, the Wilcoxon rank sum test rejects the null hypothesis H_0, which means there is a significant difference in two data sets. In addition, the z-values quite far from -1.96 in Table 4.4 assure that the data set from relocation are much smaller than the data set from the catalogue. In other words, there is significant reduction in distances from each epicenter to the epicentroid after the relocation.

H_0: Two data sets are samples from continuous distributions with equal medians (There is no significant difference).

H_1: Two data sets are not samples from continuous distributions with equal medians (There is a significant difference).

Table 4.4. Results of Wilcoxon rank sum test for the distance data.

	H	p-value	z-value	Rank sum
Baekryeong Island earthquake sequence	1	2.82E-11	-6.66	1652
Boryeong Offshore earthquake sequence	1	7.49E-48	-14.5	11466
Earthquake swarm around Gyeongju	1	9.52E-09	-5.74	3323
Seismic events in the Dogye mining area	1	2.82E-17	-8.45	3004

In addition, it is observed that relocated epicenters seem to form linear pattern in the Baekryeong Isalnd earthquake sequence, the Boryeong Offshore earthquake sequence, and the earthquake swarm east of the Yeonil tectonic line. Linearity in locations of epicenters can be quantitatively estimated by computing correlation coefficients between coordinates of epicenters. The latitude and longitude for epicenters were changed into the Cartesian coordinate with x and y. The epicentroid was set to the origin. Correlation coefficients for x and y coordinates of the relocated epicenters are -0.60 (-0.70) for the Baekryeong sequence, 0.89 for the Boryeong sequence, 0.66 for the earthquake swarm around Gyeongju. The value in the bracket for the Baekryeoong sequence was computed after excluding the mainshock that has relatively low waveform similarity. For all the three event groups absolute values of the correlation coefficients are over 0.6. The minus value in correlation coefficients for the Baekryeong sequence corresponds to the ESE-WNW strike of fault plane solution as observed in the previous chapters.

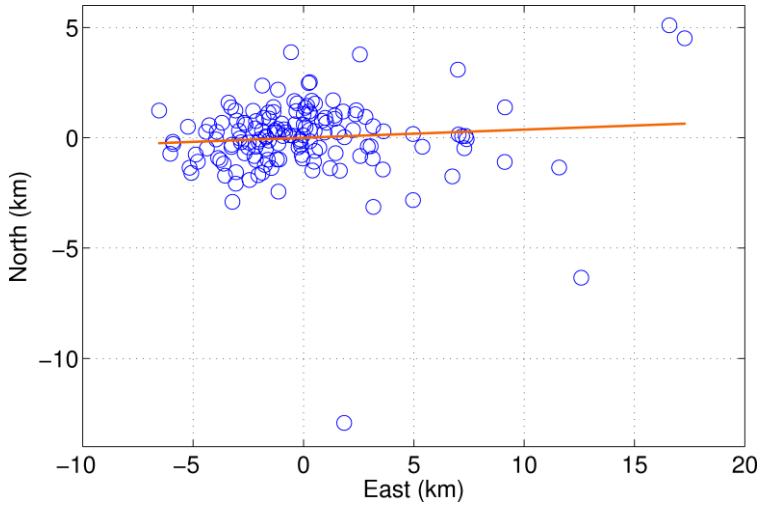

(a)

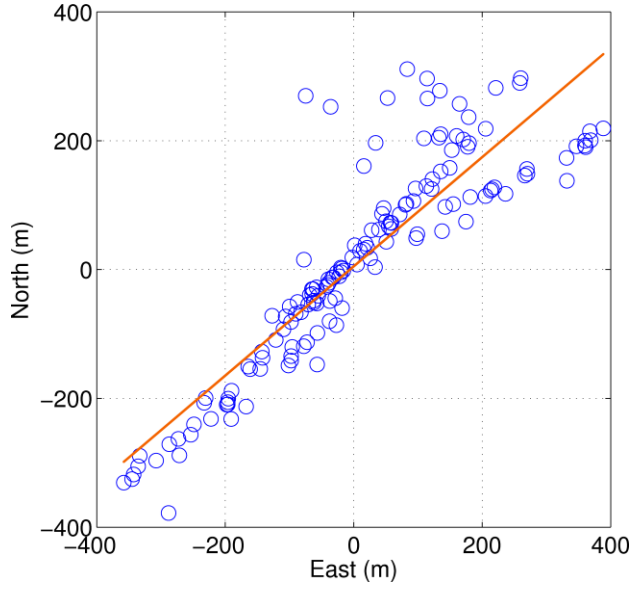

(b)

Figure 4.1. Linear regression for locations of epicenters: (a) catalogued events, (b) relocated events. Circles are locations of events, and a solid line presents estimated linear relationship. The relocated epicenters have a slope of 0.85 with p-value near zero, which ensures linearity in locations of epicenters.

Linear regression was performed on the Boryeong sequence that has the correlation coefficient between x and y about 0.9 for relocated epicenters. Figure 4.1 shows epicenters and estimated linear relationship depicted by circles and solid line, respectively. No obvious relationship is in the catalogued events as shown in Figure 4.1(a). In contrast to scattered epicenters of the catalogue, the x and y coordinates of relocated epicenters are aligned to the estimated linear relationship as shown in Figure 4.1(b). The slope (beta) for relocated epicenters is estimated at 0.85 with p-value close to zero, which ensure significant linearity for relocated epicenters as shown in Table 4.5. The catalogued events for the sequence has a slope of 0.03 with p-value of 0.32 that means rejection of the linearity in locations of the catalogued epicenters.

Table 4.5. Linear regression for epicenters of the Boryeong sequence.

Catalogue				Relocation			
R^2	Beta	p-value	t-value	R^2	Beta	p-value	t-value
0.01	0.03	0.32	1.00	0.79	0.85	0.00	23.4

4.3. Relocation results according to velocity change

The epicenter relocation using double-difference technique has different solution according to velocity change because partial derivatives include a term of surface wave velocity. This study employed a velocity of 3.5 km/s in epicenter relocation for all the four event group. Figure 4.2 displays the relocation results with a surface wave velocity of 3.0 km/s, 3.5 km/s and 4.0 km/s for all the four event groups. Figures 4.2a to c show epicenters relocated by EpiDD for the Baekryeong Island earthquake sequence with a surface-wave velocity of (a) 3.0 km/s, (b) 3.5 km/s, (c) 4.0 km/s. Figures 4.2d to f show relocated epicenter of the Boryeong Offshore earthquake sequence with a surface-wave velocity varying as described above. Figures 4.2g to i and Figure 4.2j to l are relocation results with varying velocities described above for the earthquake swarm of Gyeongju and the Dogye events, respectively. As shown in Figure 4.2, relative location of epicenters relocated by EpiDD does not change with varying velocity in all the four event groups. The inter-event distance, however, increases with increasing velocity because the travel-time differences are fixed as observed data.

(a)

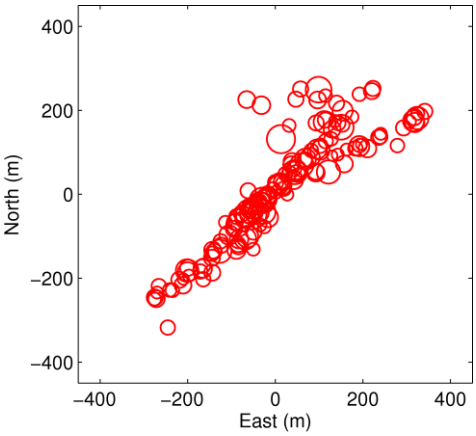
400
200
0
−200
−400
North (m)
−400
−200
0
200
400
East (m)

(b)

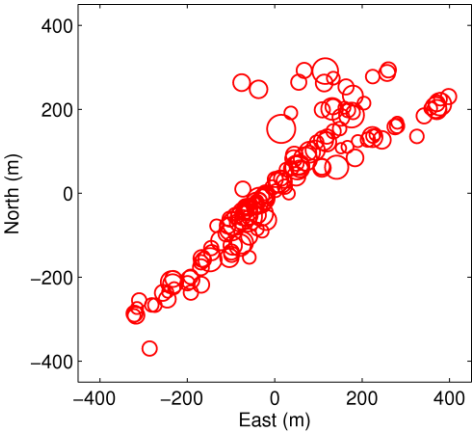
400
200
0
−200
−400
North (m)
−400
−200
0
200
400
East (m)

(c)

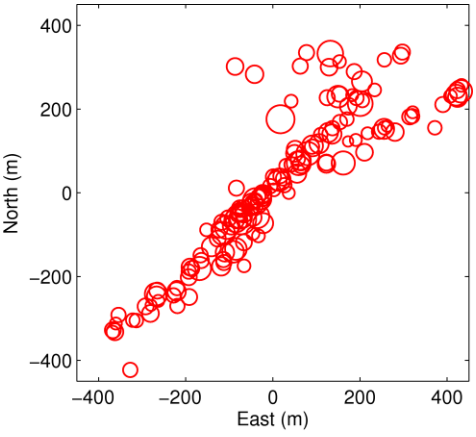
400
200
0
−200
−400
North (m)
−400
−200
0
200
400
East (m)

(d)

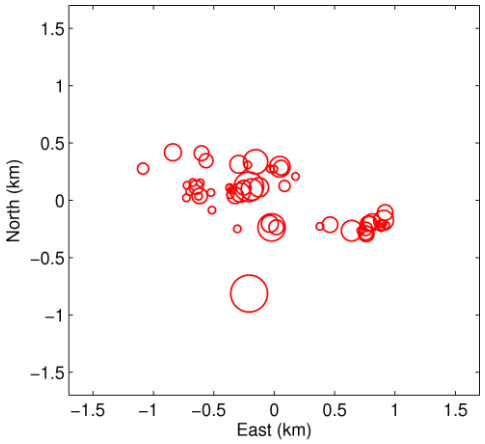
North (km)
East (km)
1.5
1
0.5
0
−0.5
−1
−1.5

(e)

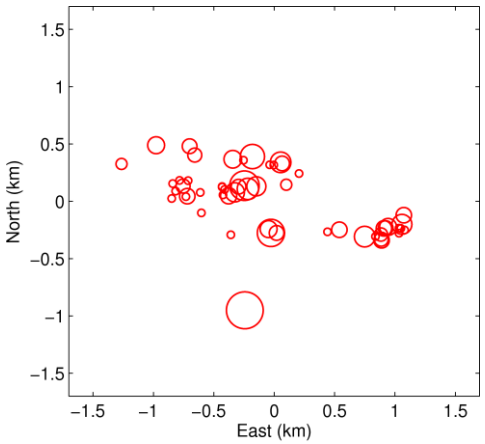
North (km)
East (km)
1.5
1
0.5
0
−0.5
−1
−1.5

(f)

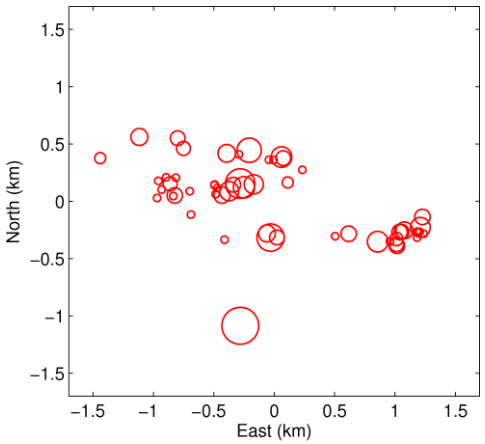
North (km)
East (km)
1.5
1
0.5
0
−0.5
−1
−1.5

(g)

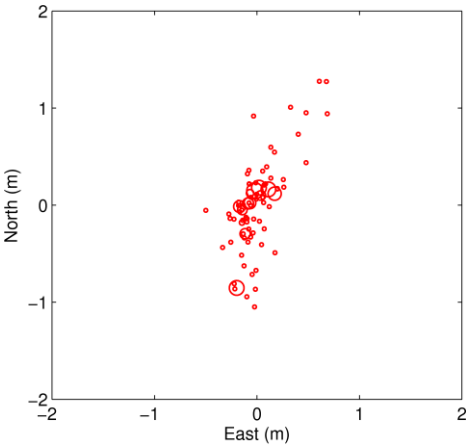
North (m)
East (m)
2
1
0
−1
−2
−2
−1
0
1
2

(h)

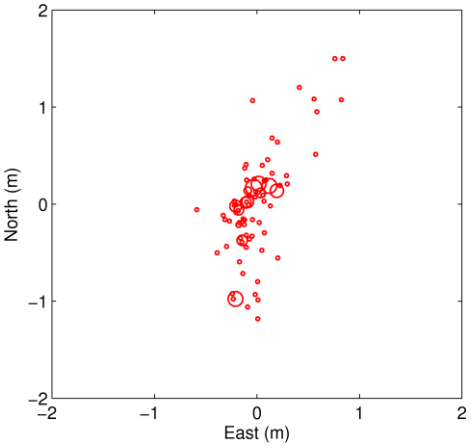
North (m)
East (m)
2
1
0
−1
−2
−2
−1
0
1
2

(i)

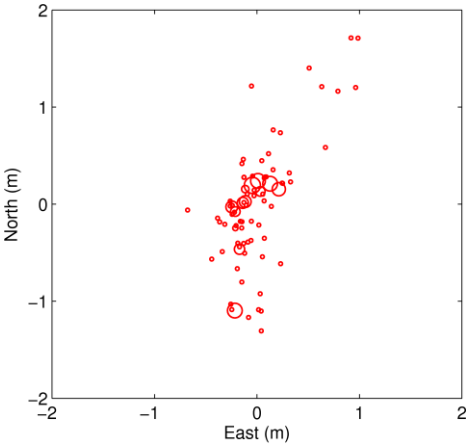
North (m)
East (m)
2
1
0
−1
−2
−2
−1
0
1
2

(j)

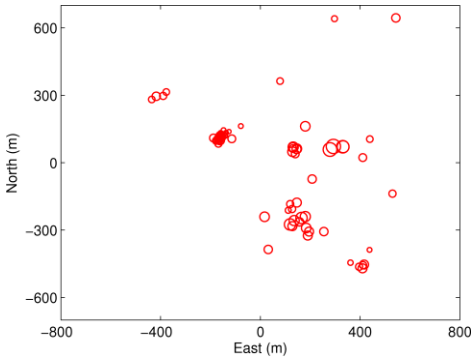

(k)

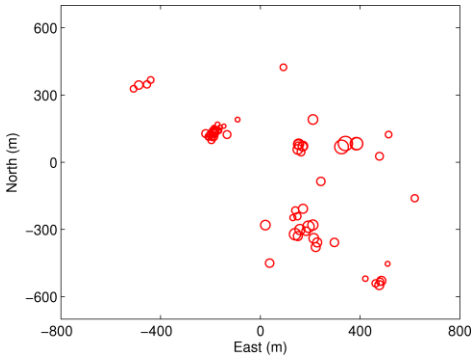

(l)

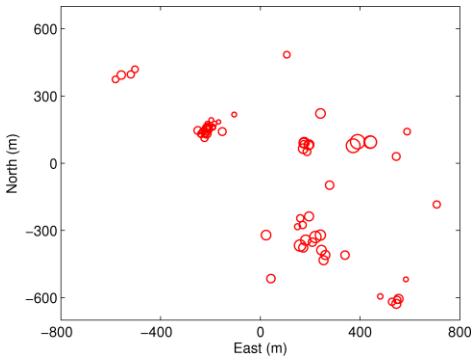

Figure 4.2. Relocated epicenters using varying surface wave velocity that are 3.0 km/s, 3.5 km/s, and 4.0 km/s: (a) to (c) for the Baekryoeng sequence; (d) to (f) for the Boryeong sequence; (g) to (i) for the earthquake swarm of Gyeongju; (j) and (l) for the Dogye event. Changes in velocity did not disturb relative locations of epicenters.

4.4. Conditions affecting epicenter relocation based on waveform similarity

Two 2013 earthquake sequences in the Yellow Sea of Korea was analyzed with the epicenter relocation algorithm using travel-time difference for surface wave. After the relocation of the Baekryeong Island earthquake sequence, tightly clustered epicenters were obtained. The longest line consisting of epicenters shrank in size by a factor of 10. In the Boryeong offshore earthquake sequence, relocated epicenters formed a significantly linear pattern, and the longest epicenter line shrank in size by a factor of ~30.

The Baekryeong and Boryeong sequences are different in terms of both the distribution of stations used in relocation and extent of similarity among waveforms. All 11 stations employed to relocate epicenters in the Boryeong offshore earthquake sequence are within an epicentral distance of 90 km. Of the six stations used to relocate epicenters of the Baekryeong Island earthquake sequence, only two stations are within 90 km of the epicenters. In addition, the azimuthal gap of the Baekryeong sequence exceeds 190 ° when the station with epicnetral distance reaching 210 km is ignored. The geometrical distribution of station affects setting of the minimum number of observations for travel-time differences to include only events well linked to other events (Waldhauser and Ellsworth, 2000; Waldhauser and Schaff, 2008; Kim et al., 2010), which could hinder EpiDD reduction of uncertainty in the Bakeryeong Island earthquake sequence.

The similarities among waveforms for two sequences was examined

and the waveform similarity among events regarding to spatial coordinates was shown in Figures 4.3. Figure 4.3 presents the percentage of events that have correlation coefficients $\geq$ 0.75 for surface waves with at least one other event. Figure 4.3a was computed from waveforms recorded at station DACB closest to the relocated epicenters of the Baekryeong Island earthquake sequence. Figure 4.3b was computed from waveforms recorded at station PORA, which is closest to the relocated epicenters of the Boryeong offshore earthquake sequence. Less similarity is found in Figure 4.3a for the Baekryeong Island earthquake sequence compared with Figure 4.3b for the Boryeong offshore sequence, which would produce less reliable travel-time differences.

Correlation coefficients representing waveform similarity decrease with increasing difference between the magnitudes of an event pair (Waldhauser and Schaff, 2008), and the pick for L_g wave composing surface wave is often magnitude dependent (Schaff and Richards, 2004a). Local magnitudes of the Boryeong offshore earthquake sequence range from 1.8 to 3.8. Local magnitude of the Baekryeong Island earthquake are in the range 1.5 to 4.9, which is more scattered than the distribution of local mgnitudes for the Boryeong sequence. In addition, Hauksson et al. (2012) mentioned that the waveform cross-correlation is more effective for small than large events. They observed that cross-correlation becomes less successful for events of magnitude up to 4.1. These facts suggest uncertainty in the travel-time differences measured by waveform cross-correlation for the Baekryeoeng Island earthquake sequence.

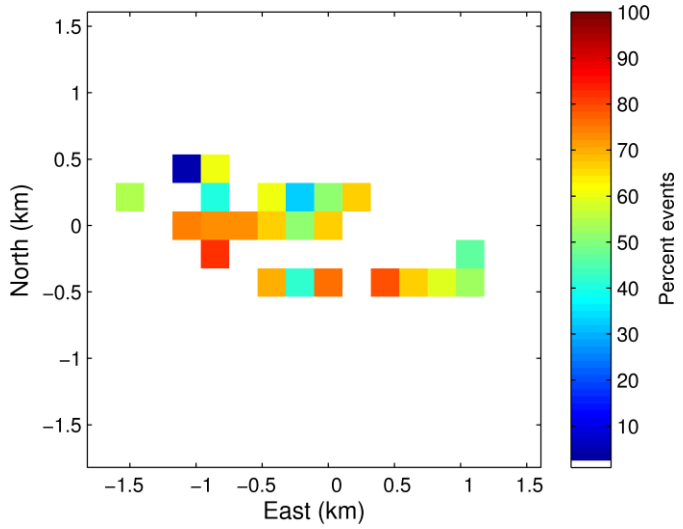

(a)

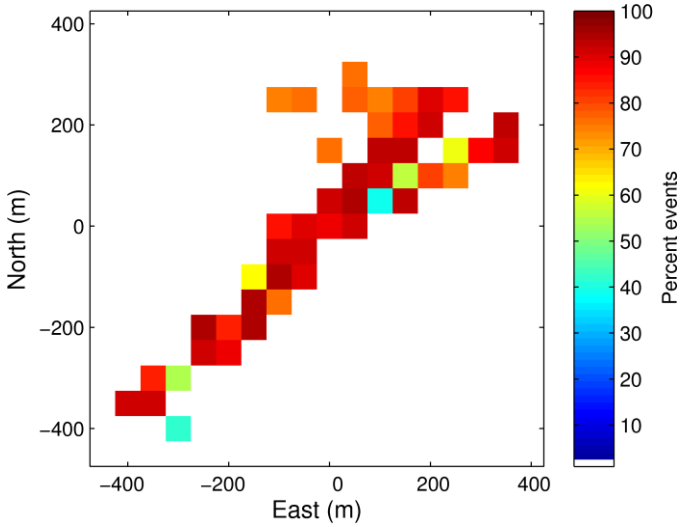

(b)

Figure 4.3. Percentage of correlated events with correlation coefficients ≥ 0.75 for surface wave with at least one other event: (a) recorded at station DACB for the Baekryeong Island earthquake sequence displayed within cells of 200 × 200 m, and (b) recorded at station PORA for the Boryeong offshore earthquake sequence displayed within cells of 50 × 50 m

5. Conclusion

Seismic events in and around the Korean Peninsula were relocated by using cross-correlation double-difference of travel time residual for surface wave. The analyzed events were from the Baekryeong Isalnd earthquake sequence, Boryeong offshore earthquake sequence, earthquake swarm around Gyeongju, and seismic events in the Dogye mining area. During the course of the analysis based on waveform similarity, unreported events were newly detected and waveforms were classified. Epicentral area shrank in size by a factor of hundreds after relocation, and the spatial distribution of relocated epicenters coincided with the location of clusters classified according to waveform similarity. When examing each of the four regions, for the Baekryeong Island earthquake sequence, unreported fore- and aftershocks of 24 were newly detected, and 55 relocated epicenters accorded with the result of waveform classification. On the Boryeong Offshore earthquake sequence, 149 relocated epicenters formed a clear lineament proceeding northeast during a two- months period. The estimated rupture length that can produce the largest event in the sequence corresponded to the length of the second segment where most of events occurred. The L_g-P_g time increase with increasing epicentral distance validated the relocation result. Around the city of Gyeongju, 70 earthquakes with similar waveforms were newly detected from the continuous data recorded during a two- year period. Relocated epicenters including catalogued and detected events were concentrated east of the Yeonil

Tectonic Line that strikes mainly from N- S to NE- SW. The fault solution derived from first motions displayed the same trend to the tectonic line. For seismic events in the Dogye mining area, six event groups were identified by the relocation and the waveform classification. Over 44,000 events were newly detected by waveform cross-correlation from the continuous data recorded during one year, and the signals produced by mining activities were distinguished. This study succeeded to detect and classify seismic events by using cross-correlation based on waveform similarity, and relocate their epicenters by the double-difference technique. Newly identified features would increase our understating of seismic clusters in the studied region.

References

Buurman, H., & West, M. E. (2010). Seismic precursors to volcanic explosions during the 2006 eruption of Augustine Volcano. In: Power, J.A., Coombs, M.L., Freymueller, J.T. (eds.), The 2006 eruption of Augustine Volcano. *U.S. Geological Survey Professional Paper*, 1769, 41-57.

Internal structure and weakening mechanisms of the San Andreas fault (1993). *International Journal of Rock Mechanics and Mining Sciences & Geomechanics Abstracts*, *30*(5), 270. doi:10.1016/0148-9062(93)92238-l

Deshon, H. R., Thurber, C. H., & Rowe, C. (2007). High-precision earthquake location and three-dimensional P wave velocity determination at Redoubt Volcano, Alaska. *Journa of Geophysical Research, 112*, B07312. doi:doi:10.1029/2006JB004751

Geiger, L. (1910). Herdbestimming bei Erdbeben aus den Ankunftszeiten, *K. Ges. Wiss. Go¨tt. 4*, 331–349.

Gibbons, S. J., & Ringdal, F. (2006). The detection of low magnitude seismic events using array-based waveform correlation. *Geophysical Journal International, 165*, 149-166.

doi:10.1111/j.1365-246x.2006.02865.x

Gibbons, S. J., Sørensen, M. B., Harris, D. B., & Ringdal, F. (2007). The detection and location of low magnitude earthquakes in northern Norway using multi-channel waveform correlation at regional distances. *Physics of the Earth and Planetary Interiors, 160*, 285-309. doi:10.1016/j.pepi.2006.11.008

Got, J. ., Fréchet, J., & Klein, F. W. (1994). Deep fault plane geometry inferred from multiplet relative relocation beneath the south flank of Kilauea. *Journal of Geophysical Research*, *99*, 15375. doi:10.1029/94jb00577

Harris, D. B. (1991). A waveform correlation method for identifying quarry explosions. *Bulletin of the Seismological Society of America*, *81*, 2395-2418.

Hauksson, E., & Shearer, P. (2005). Southern California Hypocenter Relocation with Waveform Cross-Correlation, Part 1: Results Using the Double-Difference Method. *Bulletin of the Seismological Society of America*, *95*, 896-903. doi:10.1785/0120040167

Hauksson, E., Yang, W., & Shearer, P. M. (2012). Waveform Relocated Earthquake Catalog for Southern California (1981 to June 2011). *Bulletin of the Seismological Society of America, 102*,

2239-2244. doi:10.1785/0120120010

Hickman, S., Sibson, R., & Bruhn, R. (1995). Introduction to special section: Mechanical involvement of fluids in faulting. *Journal of Geophysical Research: Solid Earth*, *100*(B7), 12831–12840. doi:10.1029/95jb01121

Jordan, T. H., & Sverdrup, K. A. (1981). Teleseismic location techniques and their application to earthquake clusters in the south-central Pacific. *Bulletin of the Seismological Society of America*, *71*, 1005-1130.

Julian, B. R., Foulger, G. R., Monastero, F. C., & Bjornstad, S. (2010). Imaging hydraulic fractures in a geothermal reservoir. *Geophysical Research Letters*, *37*, L07305. doi:10.1029/2009gl040933

Kang, T., & Shin, J. S. (2006a). Surface-wave tomography from ambient seismic noise of accelerograph networks in southern Korea. *Geophysical Research Letters*, *33*, L17303. doi:10.1029/2006gl027044

Kang, T., & Shin, J. S. (2006b). The offshore Uljin, Korea, earthquake sequence of April 2006: Seismogenesis in the western margin of the Ulleung Basin. *Geosciences Journal*, *10*, 159-164. doi:10.1007/bf02910360

Kasatkina, E., Koulakov, I., West, M., & Iabev, P. (2014). Seismic structure changes beneath Redoubt Volcano during the 2009 eruption inferred from local earthquake tomography. *Journal of Geophysical Research: Solid Earth, 119*, 4938-4954. doi:10.1002/2013JB010935

Kennett, B. L., & Engdahl, E. R. (1991). Traveltimes for global earthquake location and phase identification. *Geophysical Journal International, 105*, 429-465. doi:10.1111/j.1365-246x.1991.tb06724.x

Keranen, K. M., Weingarten, M., Abers, G. A., Bekins, B. A., & Ge, S. (2014). Sharp increase in central Oklahoma seismicity since 2008 induced by massive wastewater injection. *Science, 345*, 448-451. doi:10.1126/science.1255802

Kim, W. Y., Choi, H., & Noh, M. (2010). The 20 January 2007 Odaesan, Korea, Earthquake Sequence: Reactivation of a Buried Strike-Slip Fault? *Bulletin of the Seismological Society of America, 100*, 1120-1137. doi:10.1785/0120090069

Kim, W. (2013). Induced seismicity associated with fluid injection into a deep well in Youngstown, Ohio. *Journal of Geophysical Research: Solid Earth, 118*, 3506-3518. doi:10.1002/jgrb.50247

Ko, K. B., Gwak, S., & Lee, D. S. (2000). A filed parameter test for the design of near-surface seismic survey in an area of ground subsidence. *Geosystem Engineering, 3.*

Lahr, J., Chouet, B., Stephens, C., Power, J., & Page, R. (1994). Earthquake classification, location, and error analysis in a volcanic environment: Implications for the magmatic system of the 1989–1990 eruptions at redoubt volcano, Alaska. *Journal of Volcanology and Geothermal Research, 62,* 137-151. doi:10.1016/0377-0273(94)90031-0

Lee, K., & Yang, W. (2006). Historical Seismicity of Korea. *Bulletin of the Seismological Society of America, 96,* 846-855. doi:10.1785/0120050050

Leonard, M. (2010). Earthquake fault scaling: Self-consistent relating of rupture length, width, average displacement, and moment release. *Bulletin of the Seismological Society of America, 100,* 1971-1988. doi: 10.1785/0120090189

Lienert, B. R., Berg, E., & Frazer, L. N. (1986). HYPOCENTER: An earthquake location method using centered, scaled, and adaptively damped least squares. *Bulletin of the Seismological Society of America, 76,* 771-783.

Lin, G., Shearer, P. M., & Hauksson, E. (2007). Applying a three-dimensional velocity model, waveform cross correlation, and cluster analysis to locate southern California seismicity from 1981 to 2005. *Journal of Geophysical Research*, *112*, . doi:10.1029/2007jb004986

Miller, S. A., Collettini, C., Chiaraluce, L., Cocco, M., Barchi, M., & Kaus, B. J. (2004). Aftershocks driven by a high-pressure CO2 source at depth. *Nature*, *427*, 724-727. doi:10.1038/nature02251

Narteau, C. (2007). Formation and evolution of a population of strike-slip faults in a multiscale cellular automaton model. *Geophysical Journal International*, *168*(2), 723–744. doi:10.1111/j.1365-246x.2006.03213.x

Obara, K. (2002). Nonvolcanic Deep Tremor Associated with Subduction in Southwest Japan. *Science, 296*, 1679-1681. doi:10.1126/science.1070378

Paige, C. C., & Saunders, M. A. (1982). LSQR: Spare linear equations and least squares problems. *ACM Transactions on Mathematical Software, 8/2,* 195-209.

Poupinet, G., Ellsworth, W. L., & Frechet, J. (1984). Monitoring velocity variations in the crust using earthquake doublets: An

application to the Calaveras Fault, California. *Journal of Geophysical Research: Solid Earth, 89*, 5719-5731. doi:10.1029/jb089ib07p05719

Richards, P. G., Waldhauser, F., Schaff, D., & Kim, W. (2006). The Applicability of Modern Methods of Earthquake Location. *Pure and Applied Geophysics, 163*, 351-372. doi:10.1007/s00024-005-0019-5

Riviere-Brbier, F., & Grant, L. T. (1993). Identification and location of closely spaced mining events. *Bulletin of the Seismological Society of America, 83*, 1527-1546.

Rowe, C. A., Aster, R. C., Borcers, B., & Yong, C. J. (2002). An Automatic, Adaptive Algorithm for Refining Phase Picks in Large Seismic Data Sets. *Bulletin of the Seismological Society of America, 92*, 1660-1674. doi:10.1785/0120010224

Rubin, A. M., Gillard, D., & Got, J.-L. (1998). A reinterpretation of seismicity associated with the January 1983 dike intrusion at Kilauea volcano, Hawaii. *Journal of Geophysical Research: Solid Earth, 103*, 10003–10015. doi:10.1029/97jb03513

Schaff, D. P., & Richards, P. G. (2004a). L_g-wave Cross Correlation and Double-Difference Location: Application to the 1999 Xiuyan, China, Sequence. *Bulletin of the Seismological Society of*

America, *94*, 867-879. doi:10.1785/0120030136

Schaff, D. P., & Richards, P. G. (2004b). Repeating Seismic Events in China. *Science*, *303*(5661), 1176-1178. doi:10.1126/science.1093422

Schaff, D. P., & Waldhauser, F. (2010). One magnitude unit reduction in detection threshold by cross correlation applied to Parkfield (California) and China Seismicity. *Bulletin of the Seismological Society of America*, *100*, 3224–3238. doi:10.1785/0120100042

Segall, P., Desmarais, E. K., Shelly, D., Miklius, A., & Cervelli, P. (2006). Earthquakes triggered by silent slip events on Kīlauea volcano, Hawaii. *Nature*, *442*, 71–74. doi:10.1038/nature04938

Shearer, P. M. (1997). Improving local earthquake locations using the L1 norm and waveform cross correlation: Application to the Whittier narrows, California, aftershock sequence. *Journal of Geophysical Research: Solid Earth*, *102*, 8269–8283. doi:10.1029/96jb03228

Shearer, P. M. (1998). Evidence from a cluster of small earthquakes for a fault at 18 km depth beneath Oak Ridge, southern California. *Bulletin of the Seismological Society of America,*

88, 1327-1336.

Shelly, D. R., Beroza, G. C., Ide, S., & Nakamula, S. (2006). Low-frequency earthquakes in Shikoku, Japan, and their relationship to episodic tremor and slip. *Nature*, *442*, 188–191. doi:10.1038/nature04931

Shelly, D. R., Beroza, G. C., & Ide, S. (2007). Non-volcanic tremor and low-frequency earthquake swarms. *Nature, 446*, 305-307. doi:10.1038/nature05666

Shelly, D. R., Hill, D. P., Massin, F., Farrell, J., Smith, R. B., & Taira, T. (2013). A fluid-driven earthquake swarm on the margin of the Yellowstone caldera. *Journal of Geophysical Research: Solid Earth, 118*, 4872-4886. doi:10.1002/jgrb.50362

Snoke, J. A. (2003). FOCMEC: FOCal MEChanism determinations. In: Lee et al. (Eds.) International handbook of earthquake and engineering seismology. IASPEI, Academic Press, New York, 81A, 823-825.

Son, M., Shin, J. S., Kim, G., & Cho, C. S. (2015a). Epicenter relocation of two 2013 earthquake sequences in the yellow sea, Korea, using travel-time double-differences and Lg-wave cross-correlation. *Geosciences Journal*, *19*, 295–303. doi:10.1007/s12303-014-0038-2

Son, M., Song, C. W., Kim, M., Cheon, Y., Cho, H., & Sohn, Y. K. (2015b). Miocene tectonic evolution of the basins and fault systems, SE Korea: Dextral, simple shear during the East Sea (Sea of Japan) opening. *Journal of the Geological Society, 172*, 664-680. doi:10.1144/jgs2014-079

Waldhauser, F. (2001). HypoDD: A program to compute double-difference hypocenter locations. *U.S. Geological Survey, Open File Report*, 1-113, 13 p.

Waldhauser, F., & Ellsworth, W. L. (2000). A Double-Difference Earthquake Location Algorithm: Method and Application to the Northern Hayward Fault, California. *Bulletin of the Seismological Society of America, 90*, 1353-1368. doi:10.1785/0120000006

Waldhauser, F., Ellsworth, W. L., & Cole, A. (1999). Slip-parallel seismic lineations on the northern Hayward fault, California. *Geophysical Research Letters, 26*, 3525–3528. doi:10.1029/1999gl010462

Waldhauser, F., & Schaff, D. P. (2008). Large-scale relocation of two decades of Northern California seismicity using cross-correlation and double-difference methods. *Journal of Geophysical Research, 113*, B08311.

doi:10.1029/2007jb005479

West, M. E. (2013). Recent eruptions at Bezymianny volcano—A seismological comparison. *Journal of Volcanology and Geothermal Research, 263*, 42-57. doi:10.1016/j.jvolgeores.2012.12.015

Wolfe, C. J., Okubo, P. G., Ekström, G., Nettles, M., & Shearer, P. M. (2004). Characteristics of deep (≥13 km) Hawaiian earthquakes and Hawaiian earthquakes west of 155.55°W. *Geochemistry, Geophysics, Geosystems, 5*. doi:10.1029/2003gc000618

초 록

이중차기법과 상호상관을 이용한 한반도 군집지진 발생 위치 재결정

서울대학교 대학원
협동과정 계산과학전공
손 민 경

지진 연구에 있어 가장 기초적이며 필수적인 정보인 지진의 발생 위치를 주시이중차와 파형상호상관을 이용하여 정밀히 계산하였다. 2009 년 이후의 군집하여 발생한 것으로 관측된 백령도 연속지진, 보령해역 연속지진, 경주 부근 군발지진, 그리고 도계 광산 지역의 군발지진을 연구 대상으로 하였다. 진앙은 표면파 주시이중차 기법을 이용하여 재결정되었고, 파형 상호상관을 기반으로 유사파형이벤트가 분류되고 보고되지 않았던 지진이 추가 식별되었다. 주시 오차의 이중차 기법을 이용하여 재결정된 진앙은 기존 진앙분포에 대하여 수 백 분의 일에 해당하는 영역에 집중 되었다. 재결정된 진앙분포는 파형유사성을 이용한 계층적 클러스터링 결과와 부합하는 모습을 보였다. 각 연구 지역별로 살펴보면, 백령도 연속지진의 보고되지 않았던 전진 및 여진을 새로이 식별하였고, 재결정된 진앙 위치가 파형분류 결과를 뚜렷이 반영하는 것을 확인했다. 보령해역 연속지진의 재결정된 진앙은 뚜렷한 선형을 이루며 2

개월 간 북동 방향으로 이동했음이 확인되었으며, 가장 큰 규모의 지진을 일으킨 단층 분절이 특정되었다. 재결정 결과는 L_g-P_g 시간의 증가의 관찰을 통하여 검증되었다. 경주 부근에서는 높은 파형 유사성을 보이는 십 여건 이상의 지진을 확인하고, 상호상관을 통하여 2 년 간의 연속파형 기록에서 반복하여 발생한 70 건의 유사파형 이벤트를 추가 탐지하였다. 새로이 식별된 지진을 포함하여 진앙 재결정을 수행하였고, 재결정된 진앙은 남북 주향의 단층으로 이루어진 연일구조선의 동쪽에 집중하여 분포함을 확인하고, 초동 극성을 이용하여 계산된 단층해와 비교하였다. 마지막으로, 강원도 도계 광산 지역에서는 기존 지진관측망 자료를 이용하여 규칙성 없이 흩어져있던 이벤트의 발생 위치를 여섯 곳으로 특정하였고, 재결정 결과를 지지하는 파형유사성에 기반한 계층적 클러스터링 결과를 얻었다. 또한, 진앙영역에 추가적으로 설치된 관측소로부터 1 년 간 기록된 파형으로부터 보고된 200 여건의 이벤트 외에 도계지역에서 4만 건 이상의 이벤트가 발생하고 있음을 확인했고, 새로 식별된 이벤트에서 일정한 진폭을 갖고 규칙적으로 발생하는 광산활동 신호를 분리했다.

주요어: 지진 위치 재결정, 주시 이중차, 보령, 백령도, 경주, 도계 광산

학 번: 2011-30135